

**INVESTIGATION OF WINDSHIELD DEFOGGING  
AND DEFROSTING DESIGNS TO DECREASE  
ENERGY CONSUMPTION IN VEHICLES**

**Thesis Submitted to  
The Graduate School of  
İzmir Institute of Technology  
in Partial Fulfillment of the Requirements for the Degree of  
MASTER OF SCIENCE  
in Mechanical Engineering**

**by  
Fatih EDİZ**

**December 2023  
İZMİR**

We approve the thesis of **Fatih EDİZ**

Examining Committee Members:

---

**Prof. Dr. Erdal ÇETKİN**

Department of Mechanical Engineering/İzmir Institute of Technology

---

**Assoc. Prof. Dr. Mehmet Akif EZAN**

Department of Mechanical Engineering/ Dokuz Eylül University

---

**Assist. Prof. Dr. Kasım TOPRAK**

Department of Mechanical Engineering/İzmir Institute of Technology

**05 December 2023**

---

**Prof. Dr. Erdal ÇETKİN**

Supervisor, Department of Mechanical  
Engineering/ İzmir Institute of Technology

---

**Prof. Dr. M.İ. Can DEDE**

Head of the Department of  
Mechanical Engineering

---

**Prof. Dr. Mehtap EANES**

Dean of the Graduate School

## **ACKNOWLEDGEMENTS**

I would like to express my sincere thanks to my thesis supervisor, Prof. Dr. Erdal Çetkin, for his invaluable guidance, knowledge, and experience throughout my research. His support and insights have been instrumental in shaping the direction of my study.

I would also like to extend my gratitude to BMC Otomotiv San Tic A.Ş., who supported my master's thesis study by providing me with access to experimental data and company resources. Their contributions have been essential to the successful completion of my research.

Finally, I am deeply grateful to my family, who have always been there to support me financially and emotionally throughout my life. Their love and encouragement have been a constant source of inspiration and motivation for me.

# ABSTRACT

## INVESTIGATION OF WINDSHIELD DEFOGGING AND DEFROSTING DESIGNS TO DECREASE ENERGY CONSUMPTION IN VEHICLES

Fogging and icing of windshields are general problems that affect driving safety and energy consumption. The aim of this study is to improve the truck windshield defogging system and reduce energy consumption.

Firstly, we investigated the effects of vent position and width relative to the glass. In the first stage, we performed analysis on the truck xz plane (2D). We preferred this method to quickly see the effect of vent changes. In the second stage, we applied the modification parameters to the 3D duct model. In both studies, we determined that the independent variables had a statistically significant effect on the dependent variable and determined the parameters with the highest desirability value by using the Analysis of Variance method. Secondly, we added various separators to the duct model. We investigated the total mass flow rate coming to the driver's side with total pressure drop.

In this thesis, we used the Eulerian Wall Film (EWF) Model to model the defogging phenomenon on windshields. In the EWF model, the wall film is treated as a separate fluid phase, and the conservation equations for mass, momentum, and energy are solved separately for each fluid phase.

As a result, we applied the obtained data to the current design. Windshield defogging performance has improved in the optimization model. The average film thickness in region A decreased by 8.2% compared to the current model, while the average film thickness in region B decreased by 48.1%.

**Keywords and Phrases:** Fogging and Icing of Windshields, Defogging System, Analysis of Variance Method, Eulerian Wall Film (EWF), Average Film Thickness.

## ÖZET

### ARAÇLARDA ENERJİ TÜKETİMİNİ AZALTMAK İÇİN ÖN CAM BUĞU ÇÖZME VE BUZ ÇÖZME TASARIMLARININ İNCELENMESİ

Ön camların buğulanması ve buzlanması sürüş güvenliğini ve enerji tüketimini etkileyen genel sorunlardandır. Bu çalışmanın amacı kamyon ön camı buğu giderme sistemini iyileştirmek ve enerji tüketimini azaltmaktır.

İlk olarak, üfleç konumunun ve genişliğinin cama göre etkilerini araştırdık. İlk aşamada kamyon xz düzlemi (2D) üzerinde analiz gerçekleştirdik. Üfleç değişikliklerinin etkisini hızlı bir şekilde görmek için bu yöntemi tercih ettik. İkinci aşamada değişiklik parametrelerini 3 boyutlu kanal modeline uyguladık. Her iki çalışmada da Varyans Analizi yöntemini kullanarak, bağımsız değişkenlerin bağımlı değişken üzerinde istatistiksel olarak anlamlı bir etkiye sahip olduğunu tespit ettik ve istenilirlik değeri en yüksek olan parametreleri belirledik. İkinci olarak kanal modeline çeşitli separatörler ekledik. Toplam basınç kaybıyla birlikte sürücü tarafına gelen toplam kütleli debiyi araştırdık.

Bu tezde, ön camlardaki buğu çözmeyi modellemek için Eulerian Wall Film (EWF) Modelini kullandık. EWF modelinde duvar filmi ayrı bir akışkan fazı olarak ele alınır ve kütle, momentum ve enerjinin korunumu denklemleri her akışkan faz için ayrı ayrı çözülür.

Sonuç olarak elde edilen verileri mevcut tasarıma uyguladık. Optimizasyon modelde ön cam buğu giderme performansı iyileşti. A bölgesindeki ortalama film kalınlığı mevcut modele göre % 8.2 oranında azalırken, B bölgesindeki ortalama film kalınlığı % 48.1 oranında azaldı.

**Anahtar Kelimeler ve İfadeler:** Ön Camların Buğulanması ve Buzlanması, Buğu Giderme Sistemi, Varyans Analizi Yöntemi, Eulerian Wall Film (EWF), Ortalama Film Kalınlığı.

# TABLE OF CONTENTS

ACKNOWLEDGEMENTS .....	iii
TABLE OF CONTENTS .....	vi
LIST OF FIGURES .....	viii
LIST OF TABLES .....	xi
LIST OF SYMBOLS .....	xiii
CHAPTER 1. INTRODUCTION .....	15
1.1. Important of Defogging and Deicing Systems.....	16
1.2. System Performance Measurement Methods.....	16
1.3. Condensation and Icing on the Windshield .....	17
1.4. Defogging and Deicing System .....	19
1.4.1. Defroster .....	20
1.4.2. Air Conditioning and Dehumidification .....	21
1.4.3. Electrical Heating Elements.....	22
1.4.4. Recirculation Button .....	23
CHAPTER 2. LITERATURE VIEW .....	24
2.1. International Windscreen Defrosting and Demisting Standards.....	29
2.1.1. 78/317/EEC.....	29
2.1.2. SAE Standard J902a.....	30
2.1.3. SAE Standard J381 .....	31
CHAPTER 3. WINDSHIELD DEFOGGING TEST .....	32
3.1. Acceptance Criteria.....	32
3.2. Test Requirements .....	33
3.3. Test Methods.....	34
CHAPTER 4. COMPUTATIONAL FLUID DYNAMICS.....	35
4.1. Approaches to Multiphase Modeling .....	36
4.1.1. Euler-Lagrange Approach.....	36
4.1.2. Euler-Euler Approach .....	37
4.1.2.1. Volume of Fluid Model .....	38
4.1.2.2. Mixture Model .....	38
4.1.2.3. Eulerian Model.....	39

CHAPTER 5. NUMERICAL MODEL AND METHOD .....	40
5.1. Governing Equation .....	41
5.1.1. Continuity, Momentum and Energy Equation .....	42
5.1.2. Eulerian Wall Film Model .....	46
5.2. Design of Experiment .....	48
5.2.1. Full Factorial Design.....	49
5.3. Boundary Condition .....	50
CHAPTER 6. MODEL AND NUMERICAL ANALYSIS .....	53
6.1. Cabin Geometry .....	53
6.2. Defrost Duct Geometry .....	54
6.3. CFD Analysis .....	55
6.3.1. Pre-Processing.....	57
6.3.2. Solver .....	58
6.3.3. Post-Processing .....	58
6.3.4. Model Validation .....	60
CHAPTER 7. MODEL OPTIMIZATION .....	64
7.1. The Effect of Vent Position Parameters.....	64
7.1.1. Cabin Model Geometry and Analysis of Variance .....	65
7.1.1.1. Hypothesis for Models.....	65
7.1.1.2. Design Layout for Models .....	69
7.1.1.3. Half Normal Plot for Models .....	70
7.1.1.4. Analysis of Variance (ANOVA).....	77
7.1.1.5. Optimization Results.....	80
7.1.1.6. Model Cube Graph and Desirability .....	81
7.2. The Effect of Defroster Duct Shape.....	84
7.2.1. Optimization Results.....	86
CHAPTER 8. RESULTS AND DISCUSSIONS .....	92
CHAPTER 9. CONCLUSIONS .....	96
APENDIX A .....	98
REFERENCES .....	100

# LIST OF FIGURES

<b><u>Figure</u></b>	<b><u>Page</u></b>
Figure 1. The phase diagram of water Source: (Mao, et al. 2016) .....	18
Figure 2. Graph of the dew point Source: (Ko, et al. 2018) .....	18
Figure 3. Phase Change of Water Source: (Hermes, et al. 2021) .....	19
Figure 4. HVAC System Source: (TestingAutos 2020) .....	20
Figure 5. System Fan Curve Source: (ASHRAE® HANDBOOK 2008).....	21
Figure 6. HVAC system Source: (Fojtlína, et al. 2016) .....	22
Figure 7. Grid of wires of the windshield Source: (Pinnacle Auto Glass 2023) .....	23
Figure 8. Recirculation Button Source: (Goreham 2020).....	23
Figure 9. SAE 381 Deicing Windshield Zones Source: (Link and Pohlman 2018) .....	26
Figure 10. Windshield Area Source: (78/317/EEC 1978) .....	30
Figure 11. Windshield Area Source: (SAE Standard J902A 1967).....	30
Figure 12. Windshield Area Source: (SAE J381 2000).....	31
Figure 13. Windshield Area.....	32
Figure 14. Temperature Control- Flow Control- Humidity Control.....	33
Figure 15. CFD Modelling Source: (Ariyaratne, et al. 2016).....	36
Figure 16. Eulerian and Lagrangian Derivative Source: (Qiu, Henke and Grab 2011) .	37
Figure 17. Transfer of Temperature Source: (Davis, Dage and Hoeschele 2001).....	40
Figure 18. Condensation on Windshield Surface Source: (Hassan, et al. 1999) .....	41
Figure 19. Design Expert Software- Type of Full Factorial Design.....	49
Figure 20. Truck Cabin (3D Model).....	52
Figure 21. Truck Cabin (a. 3D Model and b. 2D Model) .....	52
Figure 22. Defroster Duct Model.....	52
Figure 23. Truck Cabin Model (a. 3D Model and b. 2D Model).....	54
Figure 24. Defroster Duct Model (Isometric View) .....	54
Figure 25. Defroster Duct Model (Top View).....	55
Figure 26. ANSYS Analysis Steps Source: (ANSYS Inc. 2011) .....	56
Figure 27. Mesh Domain (3D Model) .....	57
Figure 28. Film Thickness on the Windshield (Current Model).....	59
Figure 29. Film Thickness of Area A and B (Current Model) (t: 600 s) .....	60



<b><u>Figure</u></b>	<b><u>Page</u></b>
Figure 30. Film Temperature on the Windshield (Current Model) .....	60
Figure 31. Comparison of Results (a. Current Model; b. Test Cabin) (t: 0 s) .....	61
Figure 32. Comparison of Results (a. Current Model; b. Test Cabin) (t: 300 s) .....	61
Figure 33. Comparison of Results (a. Current Model; b. Test Cabin) (t: 600 s) .....	62
Figure 34. Comparison of Results (a. Current Model; b. Test Cabin) (t: 900 s) .....	62
Figure 35. Comparison of Results (a. Current Model; b. Test Cabin) (t: 1200 s) .....	63
Figure 36. Truck Cabin (2D Model) .....	66
Figure 37. Parameters for 2D Model .....	66
Figure 38. Truck Cabin (3D Model) .....	67
Figure 39. Parameters for 3D Model (xz Section View) .....	67
Figure 40. Temperature Gradient - Half Normal Plot .....	71
Figure 41. Pressure Drop- Half Normal Plot .....	72
Figure 42. Average Film Thickness on A Windshield (t: 600 s) .....	74
Figure 43. Average Film Thickness on B Windshield (t: 600 s) .....	75
Figure 44. Average Film Thickness on C Windshield (t: 600 s) .....	76
Figure 45. Cube Desirability for 2D Model .....	82
Figure 46. Cube Desirability for 3D Model .....	83
Figure 47. Defroster Duct Model-1 (DF-1) .....	86
Figure 48. Defroster Duct Model-1 .....	86
Figure 49. Defroster Duct Model-2 (DF-2) .....	87
Figure 50. Defroster Duct Model-2 .....	87
Figure 51. Defroster Duct Model-3 (DF-3) .....	87
Figure 52. Defroster Duct Model-3 .....	88
Figure 53. Defroster Duct Model-4 (DF-4) .....	88
Figure 54. Defroster Duct Model-4 .....	88
Figure 55. Defroster Duct Model-5 (DF-5) .....	89
Figure 56. Defroster Duct Model-5 .....	89
Figure 57. Comparison of Results (a. Current Model; b. Optimized Model) (t: 0 s) .....	92
Figure 58. Comparison of Results (a. Current Model; b. Optimized Model) (t: 300 s) .	93
Figure 59. Comparison of Results (a. Current Model; b. Optimized Model) (t: 600 s) .	93
Figure 60. Comparison of Results (a. Current Model; b. Optimized Model) (t: 900 s) .	94

**Figure**

**Page**

Figure 61. Comparison of Results (a. Current Model; b. Optimized Model) (t: 1200 s) 94  
Figure 62. Comparison of Results (a. Current Model; b. Optimized Model) (t: 600 s) . 94  
Figure 63. Psychometrics chart Source: (Shamshiri 2014)..... 99

## LIST OF TABLES

<b><u>Table</u></b>	<b><u>Page</u></b>
Table 1. Analysis Steps Source: (Sadananda 2016) .....	24
Table 2. Boundary Condition Source: (Sadananda 2016) .....	25
Table 3. Analysis Steps Source: (He, et al. 2020) .....	25
Table 4. Boundary Condition Source: (He, et al. 2020) .....	25
Table 5. Analysis Steps Source: (Link and Pohlman 2018) .....	27
Table 6. Analysis Steps Source: (Hassan, et al. 1999) .....	28
Table 7. Boundary Condition Source: (Hassan, et al. 1999) .....	29
Table 8. Test Equipment .....	33
Table 9. Significant Level Source: (Schmidt and Osebold 2017) .....	49
Table 10. Boundary Conditions .....	51
Table 11. Analysis Steps.....	55
Table 12. Material Properties.....	58
Table 13. The Percentages of Defogged Area .....	59
Table 14. The percentages of defogged areas on the windshield .....	63
Table 15. Factors for Models .....	68
Table 16. Responses for 2D Model .....	68
Table 17. Responses of 3D Model.....	68
Table 18. Design Layout for 2D Model.....	69
Table 19. Design Layout for 3D Model.....	69
Table 20. Model Effects of Temperature Gradient.....	70
Table 21. Model Effects of Pressure Drop .....	70
Table 22. Model Effects of Average Film Thickness on A Windshield.....	73
Table 23. Model Effects of Average Film Thickness on B Windshield.....	73
Table 24. Model Effects of Average Film Thickness on C Windshield.....	73
Table 25. Temperature Gradient -ANOVA .....	77
Table 26. Pressure Drop -ANOVA.....	78
Table 27. Average Film Thickness on A Windshield -ANOVA.....	78
Table 28. Average Film Thickness on B Windshield -ANOVA .....	79

**Table****Page**

Table 29. Average Film Thickness on C Windshield -ANOVA .....	80
Table 30. Constraints for Models .....	80
Table 31. Selected Solution Table for 2D Model .....	81
Table 32. Selected Solution Table for 3D Model .....	81
Table 33. Defroster Duct Models .....	85
Table 34. Percentage of Total Mass Flow Rate of Vents (%) .....	90
Table 35. The Total Pressure Drop of Duct Models.....	90
Table 36. The Percentages of Defogged Area .....	95
Table 37. Average Film Thickness of Windshield .....	95

## LIST OF SYMBOLS

### Nomenclature

Symbol	Meaning	Unit
P	Pressure	Pa
t	Time	s
x, y, z	Spatial coordinates	
h	Specific Enthalpy	J/kg
V	Volume	m <sup>3</sup>
v	Velocity	m/s
F	Force	N
w	Specific dissipation rate	W/kg
h	Film height	m
$\dot{m}$	Mass flow rate	kg/s
k	Turbulence kinetic energy	J/kg
$Y_K$	Dissipation of k	
$T_s$	Temperature at the film–gas interface	K
$D_w$	Cross-diffusion	
$S_k$	Source of k	

### Greek Letters

Symbol	Meaning	Unit
$\nabla \cdot \tilde{\tau}$	Viscous force per unit volume	Pa/m
$\rho g$	Gravity force per unit volume	Pa/m
$\rho$	Density	kg/m <sup>3</sup>
$\nabla p$	Pressure force per unit volume	Pa/m
$\mu$	Viscosity	Pa · s
$\beta$	Coefficient of destruction term	
$\sigma_k$	Prandtl numbers for k	
$\Gamma_k$	Effective diffusivity of k	

$\nabla_s$	Surface gradient operator	
$\Delta$	Nabla operator	
$\Delta T$	Temperature difference	K
$\Delta P$	Pressure difference	Pa

### Subscripts and Superscripts

Symbol	Meaning	Unit
HVAC	Heating, Ventilation and Air Conditioning	
DF	Defroster duct model	
df	Design of freedom	
Min	Minimum	
Max	Maximum	
AFT	Average film thickness	m
ANOVA	Analysis of variance	
RANS	Reynolds-averaged Navier–Stokes equations	

# CHAPTER 1

## INTRODUCTION

Cold and humid weather can cause fog and ice formation on the windshield, which can significantly reduce transparency and visibility while driving. When the temperature inside the car is warmer than the temperature outside, moisture in the air can condense on the windshield, causing fog to form. The condensation process is a phase transition where water vapor from the air undergoes a transformation into liquid, accompanied by the release of heat. This occurrence can occur within the fluid itself, referred to as homogeneous condensation, or on a solid surface, known as heterogeneous condensation. (Ene and Teodosiu 2021) Foggy windows can reduce visibility and make it difficult to see obstacles, other vehicles, or pedestrians. In very low temperatures, any moisture on the windshield can freeze and form ice. This can create a dangerous situation where the windshield is completely obscured, making it impossible to see the road ahead. There are two major sources of moisture. These are respectively:

- Respiration
- Weather Conditions (A.Bhatia 2023)

**Respiration:** When people or animals breathe inside a car, they exhale moisture in the form of water vapor. This can contribute significantly to the humidity inside the car, especially if there are multiple occupants or the windows are closed.

**Weather Conditions:** If the outside air is humid, it can also contribute to the humidity inside the car, especially if the windows are open or if air is circulating through the car's ventilation system. When the temperature of the windshield surface drops below the dew point temperature of the air inside the car, moisture in the air can condense onto the windshield. This is because the colder surface of the windshield causes the water vapor in the air to lose its energy and form droplets on the surface.

This is commonly seen in situations such as when the car is parked outside on a cold night, or when the air conditioning is turned on in a warm and humid car. The moisture that collects on the windshield can impair visibility and make driving unsafe.

## **1.1. Important of Defogging and Deicing Systems**

The effectiveness of a vehicle's windshield defogging system significantly impacts driver safety. In challenging conditions, such as when a vehicle lacks air conditioning and is fully occupied, the defroster system must efficiently channel the airflow to clear specific areas on the windshield. This operation needs to be prompt, ensuring a minimal fog-free zone to enhance the driver's visibility. (Zolet, et al. 2010)

- Safety
- Comfort
- Energy efficiency
- Environmental effect

**Safety:** A clear windshield is essential for safe driving, as it provides unobstructed visibility of the road and surrounding environment. Fogged or iced windshields can impair visibility and increase the risk of accidents.

**Comfort:** Defogging and deicing systems improve the comfort of the occupants by providing a clear and comfortable driving environment. A fogged or iced windshield can be uncomfortable and distracting for drivers.

**Energy efficiency:** Efficient defogging and deicing systems can save energy by reducing the need for manual scraping or wiping of the windshield. This can also reduce wear and tear on the windshield and wipers.

**Environmental effect:** Efficient defogging and deicing systems can reduce the use of chemical deicers or other environmentally harmful methods of removing ice and fog from windshields.

## **1.2. System Performance Measurement Methods**

In this era focused on developing vehicles powered by alternative fuels due to depleting petroleum reserves, it is essential to design high-efficiency systems. This involves optimizing product performance through computer-aided engineering analysis and testing. This approach ensures that the vehicles are not only environmentally friendly but also operate at peak efficiency, addressing the challenges posed by the limited



availability of traditional petroleum resources. (Unverdi, et al. 2010) Performance of defogging and deicing systems can be measured using a variety of methods. Some of the common methods are:

- Time
- Energy consumption
- Effectiveness
- Durability

**Time:** This metric involves quantifying the time required for the system to effectively remove fog or ice from the windshield, thereby assessing its performance in swiftly clearing the driver's line of sight (Ono, et al. 2019). To measure this, a stopwatch is initiated upon system activation and stopped once the windshield has been cleared.

**Energy consumption:** This measures the amount of energy that is consumed by the system to clear the fog or ice from the windshield. This can be measured using a power meter or by calculating the electrical current and voltage used by the system.

**Effectiveness:** These measures how effectively the system clears the fog or ice from the windshield. This can be evaluated by measuring the percentage of the windshield that is cleared, or by assessing the clarity of the windshield after the system has been activated.

**Durability:** These measures show how long the system remains effective over time. This can be assessed by repeatedly testing the system over a period to determine if its performance declines or if it continues to operate consistently.

### **1.3. Condensation and Icing on the Windshield**

The phase of water on a car windshield depends on the temperature and humidity of the surrounding air. If the temperature of the windshield is below freezing ( $0^{\circ}\text{C}$ ), any moisture on the surface of the windshield will freeze and form ice. If the temperature of the windshield is above freezing but the air around it is very humid, water vapor in the air can condense onto the cooler surface of the windshield and form droplets of liquid water. Figure 1 shows the phase diagram of water.

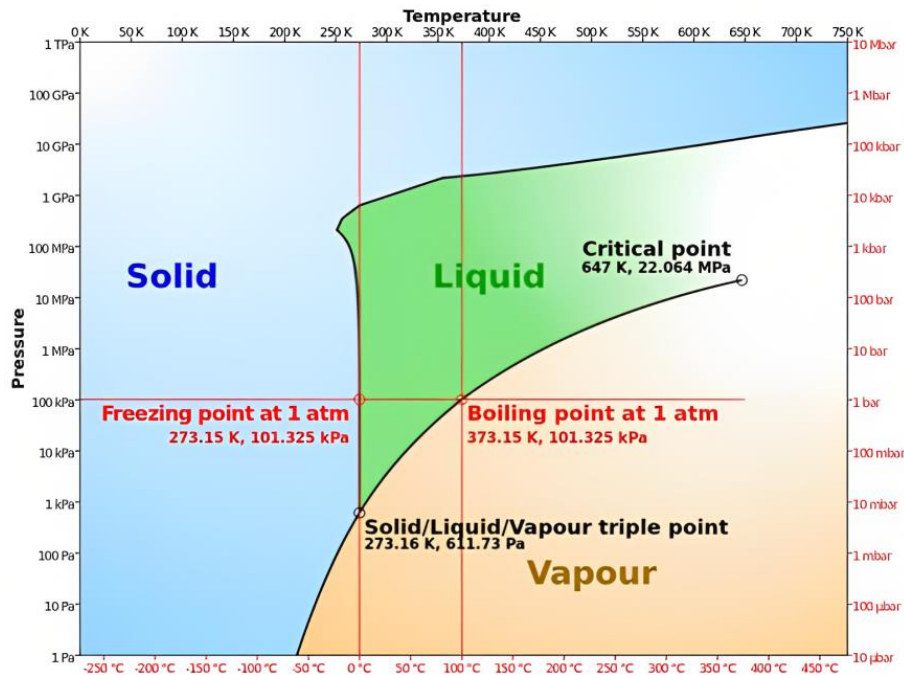


Figure 1. The phase diagram of water Source: (Mao, et al. 2016)

The phase of water on a car windshield and the dew point are closely related. The dew point temperature is the temperature at which the air is saturated with water vapor and the relative humidity reaches 100%. When the temperature of the glass drops below the dew point of the indoor air, leading to the condensation of moisture on the windshield surface. (Guzej and Zachar 2019) Figure 2 shows the graph of the dew point against air temperature for various values of relative humidity.

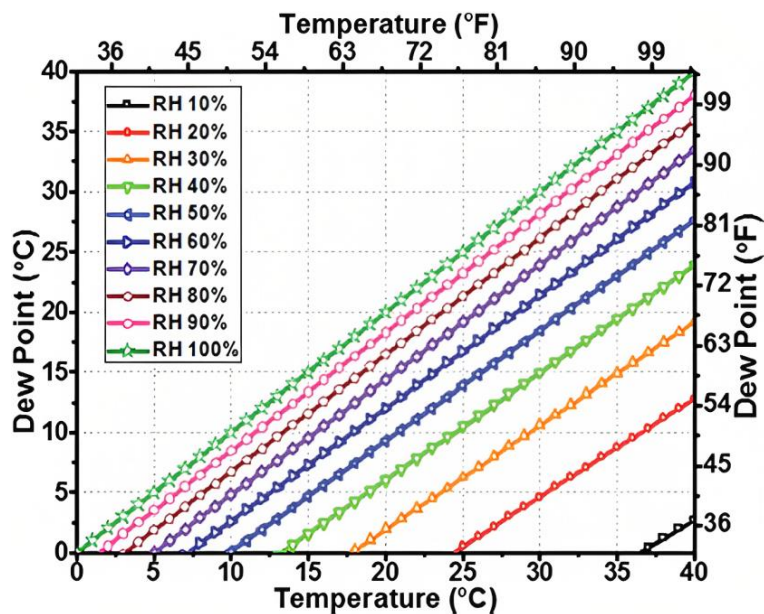


Figure 2. Graph of the dew point Source: (Ko, et al. 2018)

Freezing occurs when liquid water is cooled below its freezing point, which is  $0^{\circ}\text{C}$  ( $32^{\circ}\text{F}$ ) at standard atmospheric pressure. As water cools, its molecules slow down and become less chaotic. At the freezing point, the water molecules form a crystalline structure, and the liquid water becomes solid ice. Figure 3 shows the phase change of water for different psychrometric and surface conditions.

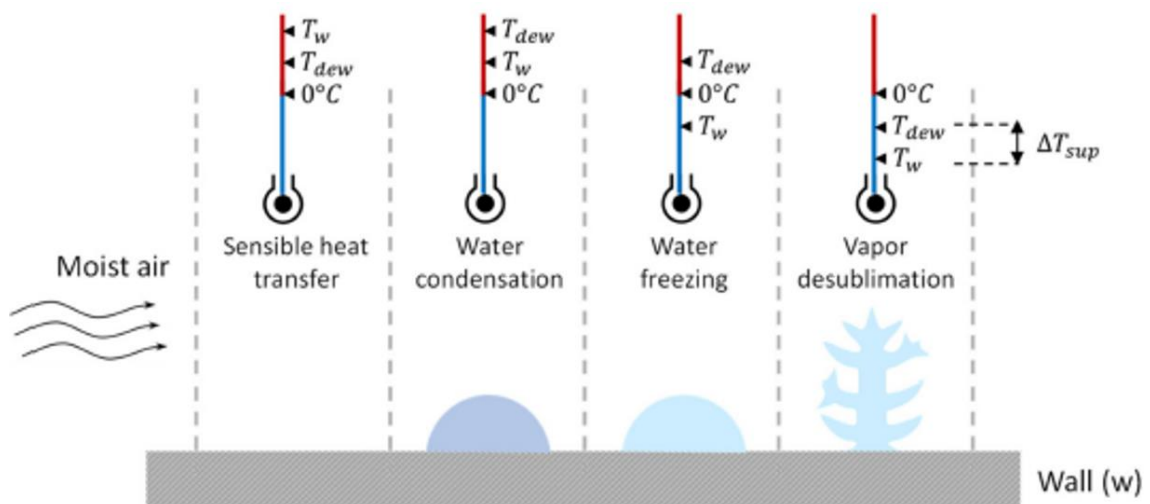


Figure 3. Phase Change of Water Source: (Hermes, et al. 2021)

#### 1.4. Defogging and Deicing System

Most modern cars come equipped with defogging and deicing systems to help clear the windshield and improve visibility in cold and humid weather conditions. There are a few steps that drivers can take to prevent fog and ice formation on the windshield.

- Defroster
- Air Conditioning
- Electrical Heating Elements
- Recirculation

The steps mentioned are detailed below. One additional precautionary measure is to park your car in a garage whenever possible, as this not only shields it from extreme weather but also minimizes the need for frequent defogging or deicing treatments.

### 1.4.1. Defroster

A defroster is a system in a vehicle that helps clear fog, ice, or frost from the windshield or other windows. It typically works by blowing warm air onto the inside of the window, which helps to melt or evaporate the ice or condensation that has formed on the glass. This allows the driver to have a clear view of the road, which is essential for safe driving in cold or wet conditions. Defrosters can be manually or automatically activated by the driver, and they may be part of a larger climate control system in the vehicle. Turning on the defroster will help to warm up the windshield and prevent moisture from condensing on the glass. It is important to make sure that the defroster is working properly and is set to the correct temperature. Figure 4 shows the HVAC (Heating, Ventilation and Air Conditioning) system.

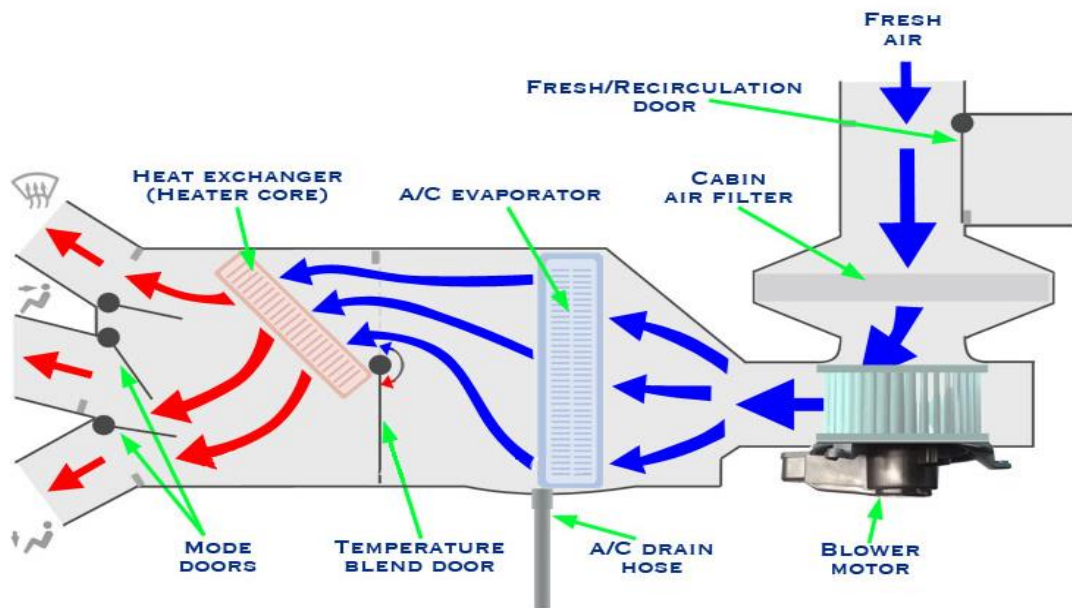


Figure 4. HVAC System Source: (TestingAutos 2020)

A blower in a HVAC (Heating, Ventilation and Air Conditioning) system is a mechanical device that moves air through the system by creating a pressure difference between the inlet and outlet of the blower. The blower is typically driven by an electric motor and consists of a housing, an impeller, and a motor. The blower is responsible for moving air through the ductwork and delivering it to the conditioned space. The blower creates the necessary airflow to distribute conditioned air throughout the building and maintain the desired temperature and humidity levels.

The performance of the blower in an HVAC system is typically characterized by its airflow rate, static pressure, and power consumption. The defroster unit's pressure rise is measured by varying the flow restriction using outlets on a plate in the test chamber, while the blower operates at maximum speed. The resulting pressure rise is then recorded as a function of the air flow rate. The air flow rate is determined by finding the intersection point of the duct subsystem air pressure drop characteristic curve (which shows the variation of the total pressure drop across the inlet and outlet ducts with air flow rate) and the defroster unit's measured air pressure rise versus air flow rate characteristic curve (Unverdi, et al. 2010). Figure 5 shows how we can generate the system fan curve.

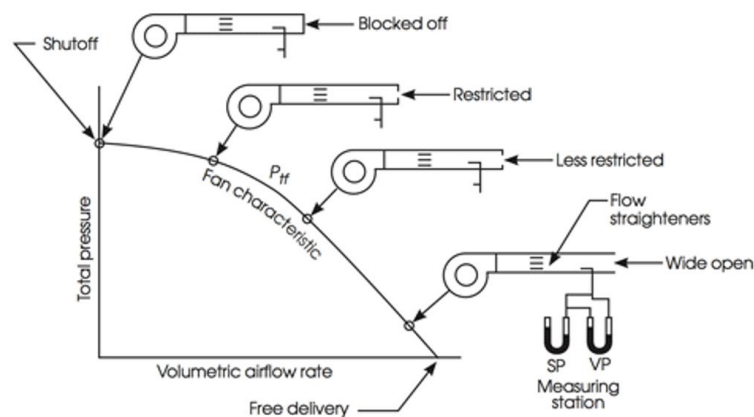


Figure 5. System Fan Curve Source: (ASHRAE® HANDBOOK 2008)

### 1.4.2. Air Conditioning and Dehumidification

In air conditioning (AC) is a system that is used to cool and dehumidify the air inside a vehicle. The AC system works by removing heat and moisture from the air, and then circulating the cooled and dehumidified air back into the space. The basic components of an AC system include a compressor, condenser, evaporator, and expansion valve. (Santos, et al. 2014)

The AC system typically operates by drawing in outside air, which is then cooled and circulated inside the passenger compartment. This can be done using a variety of methods, such as a belt-driven compressor that is powered by the engine, or an electric compressor that is powered by the vehicle's electrical system. Some modern vehicles also include features such as dual-zone climate control, which allows the driver and passengers to set different temperature and airflow settings for their respective areas.

Turning on the air conditioning in the car can help to remove moisture from the air as it passes over the cooling coils, which can help to reduce the humidity inside the car and prevent fog from forming on the windshield. When the air conditioning is turned on, the compressor pumps refrigerant through the cooling coils, which cools the air passing over them and causes moisture to condense into water droplets. The water droplets are then drained away from the car's interior, reducing the humidity, and preventing fog from forming on the windshield. It is important to note that running the air conditioning continuously for extended periods of time can place additional strain on the car's battery and engine, which can reduce fuel efficiency and increase wear and tear on the car. Drivers should use the air conditioning judiciously and avoid leaving it on when it is not necessary, to maximize fuel efficiency and reduce wear and tear on the car's components.

A vehicle's air conditioning system may also include a defrost function, which allows the system to blow warm air onto the windshield or other windows to help clear any condensation or ice.

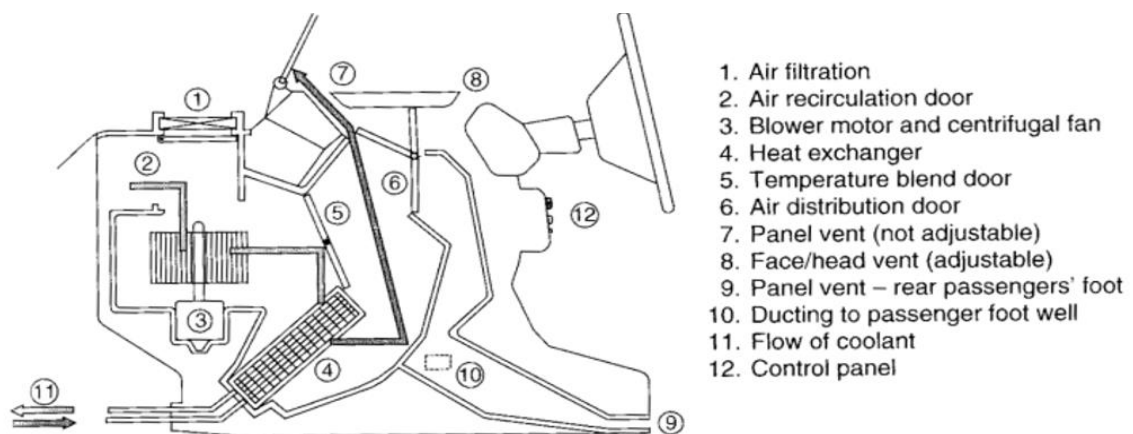


Figure 6. HVAC system Source: (Fojtlína, et al. 2016)

### 1.4.3. Electrical Heating Elements

Electrical heating elements used to defrost car windshields are typically thin wires embedded in the windshield. These wires are often made of a conductive material, such as silver or copper, and they are designed to generate heat when an electrical current is passed through them (Nagano, et al. 2016). The heating elements are usually arranged in a grid pattern that covers the entire windshield or a specific portion of it. In some cases, the heating elements may be laminated between two layers of glass, while in other cases,



they may be attached to the surface of the glass using a special adhesive. When the heating system is activated, an electrical current is sent through the heating elements, which generates heat and melts any ice or snow that has accumulated on the windshield. This technology allows windshields to remove ice or frost three to five times quicker than those with traditional defrosters. (Nasr ve AbdulNour 2000). The system may be controlled by a switch or a timer, and it may also be equipped with sensors that detect the presence of ice or snow on the windshield and activate the heating elements automatically. Figure 7 shows the grid of wires at the surface of the windshield.

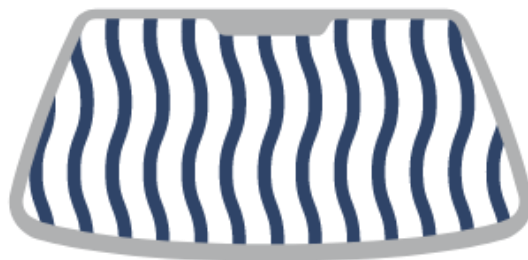


Figure 7. Grid of wires of the windshield Source: (Pinnacle Auto Glass 2023)

#### 1.4.4. Recirculation Button

The activation of the air recirculation button effectively causes the circulation of air within the cabin, ensuring that the air conditioning system cools the already-chilled interior air rather than continuously cooling incoming hot air. (Leasca 2022) An elevated recirculation ratio results in a concentrated amount of water vapor inside the cabin, consequently leading to fogging on the glass surfaces (Nagano, et al. 2016).

By turning off the recirculation button, the car's air conditioning system will bring in fresh, outside air that is typically cooler and dryer, helping to reduce the humidity inside the car and prevent fog from forming on the windshield.

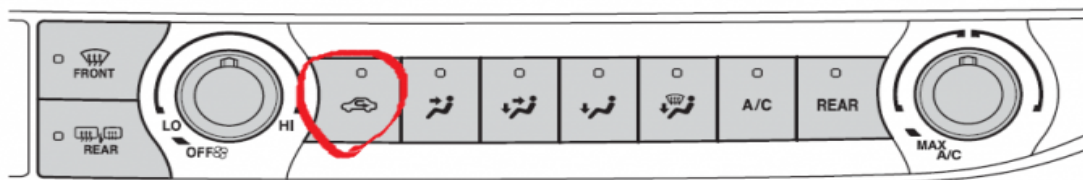


Figure 8. Recirculation Button Source: (Goreham 2020)

## CHAPTER 2

### LITERATURE VIEW

Defrosting and demisting are essential for clear vision and safe driving in cold and humid weather conditions. Effective windshield defrosting and defrosting involves removing ice and moisture from the windshield surface, which can significantly impair visibility and increase the risk of an accident. Despite the importance of these processes, there are significant differences in the methods and techniques used to ensure their effectiveness under different environmental conditions. In this chapter will review current knowledge on defrosting and demisting windshields, focusing on factors affecting performance and possible solutions to related challenges.

Table 1. Analysis Steps Source: (Sadananda 2016)

<b>Method</b>	Computational Fluid Dynamic
<b>Geometry Modelling</b>	Volvo V40 (3D Model)
<b>Meshing</b>	ANSA meshing software (Surface Meshing- Volume Meshing)
<b>First Analysis</b>	Steady state-Turbulent Flow (Realizable k-e and k- $\omega$ SST turbulence model) (Note: To predict distributed flow -Realizable k-e model is better than k-w SST model)
<b>Second Analysis</b>	Transient-Turbulent Flow (Solidification and Melting model) (To improvement in the performance of the transient CFD model)
<b>Assumption</b>	Radiation Effect (No have any influence on simulation)
<b>Solver</b>	Unsteady first order discretization scheme and unsteady second order scheme (Note: Unsteady first order discretization scheme predicts the melting quicker)

Thejeshwar S. (2016) aims to enhance the accuracy of the current computational fluid dynamics (CFD) approach in forecasting the melting behavior of ice on a vehicle's windshield. Table 1 shows the analysis steps and some recommendations and Table 2 shows the boundary conditions in this article. The ice melting pattern was evaluated over



the liquid fraction values on the windshield. The test time is 20 minutes in the defrosting and defogging standards. Therefore, the results of CFD analysis and experimental tests are examined according to 20 minutes.

Table 2. Boundary Condition Source: (Sadananda 2016)

<b>Boundary conditions</b>	<b>Setting</b>	<b>Value</b>
Inlet	Mass Flow inlet	Mass Flow Rate: 100 l/s
Outlet	Pressure outlet	101325 Pa
Windshield surface	Stationary Wall	
Computational domain	Air Temperature	- 18 °C

Table 3. Analysis Steps Source: (He, et al. 2020)

<b>Method</b>	Computational Fluid Dynamic
<b>Geometry Modelling</b>	N800 Truck (3D Model)
<b>Meshing</b>	Meshing (Surface Meshing-Volume Meshing)
<b>Analysis</b>	Transient -Turbulent Flow ( $k-\omega$ SST turbulence model) (To predict distributed flow)
<b>Assumption</b>	1) The total energy and the heat of melting (When (The total energy) = (The heat of melting), the melting begins) 2) Radiation Effect (No have any influence on simulation)

Table 4. Boundary Condition Source: (He, et al. 2020)

<b>Boundary conditions</b>	<b>Setting</b>	<b>Value</b>
Inlet	Velocity inlet	-
	Temperature	HVAC heating curve
Outlet	Pressure outlet	101325 Pa
Windshield surface	Stationary wall	
	Temperature	255 K
Computational domain	Air temperature	253 K

He, Qu, Ji, Wu, and Wang (2020) also performed defrost analysis optimization on the model N800 truck window. The data from the analysis were compared with the

physical test results. In the study, the effect of the guide plate and defroster duct position on performance was determined. Defrosting time was reduced with guide plate and duct optimization, respectively. Table 3 shows the analysis steps and some recommendations, Table 4 shows the boundary conditions in this article. As a result, defroster efficiency increased, and defroster performance improved by 99 %.

Link and Pohlman (2018) investigated CFD ice melting simulations for commercial vehicle applications. The standards regulate windshield defrosting and demisting requirements. The SAE J381 shows the required test procedure for the windshield. Figure 9 shows the deicing windshield zones.

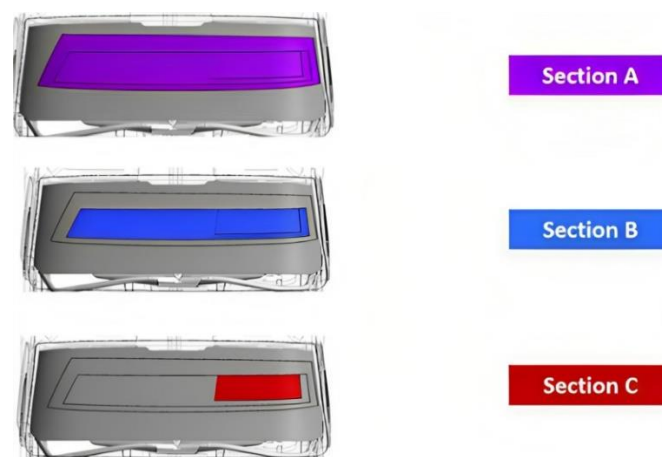


Figure 9. SAE 381 Deicing Windshield Zones Source: (Link and Pohlman 2018)

The SAE J381 test procedure specifies that Zones A and C are to be tested, while Zone B is an intermediate area that is generated as per the request of the HVAC design engineer. Among these zones, Section C, which is related to the driver's visibility, is the most critical. According to the procedure, Section C of the windshield must be clear of ice within 30 minutes, while 80% of Section A must be clear of ice within the same time frame. Within 45 minutes, Zone A needs to be 95% free of ice, whereas 85% clearance is required after 30 minutes.

The pressure drop along the duct from the HVAC module to the vehicle instrument panel (IP) must be optimized to be successful in test regulation. The CFD analysis method helps to achieve the improvement in a short time. Table 5 shows the analysis steps and some recommendations.

In terms of flow simulation, tetrahedral elements provide more accurate results by default, while hexahedral elements are used to reduce the mesh count in model areas that either exhibit simple flow behavior or are not significant to the computational results.

Table 5. Analysis Steps Source: (Link and Pohlman 2018)

<b>Method</b>	Computational Fluid Dynamic
<b>Geometry Modelling</b>	Cabin (Shell Modelling Method (1-D glass-ice) took 40% less CPU time than Solid Modelling Method (3-D glass-ice))
<b>Meshing</b>	1) Meshing (Surface Meshing) 2) Mesh Type (Tetrahedral, hexahedral) 3) Element Size (1.5 mm)
<b>First Analysis</b>	Steady (Incompressible-Viscous-Newtonian-Isotropic) Turbulent Flow (RNG k-e turbulence model) (Turbulence-Continuity) (To optimize the cold flow directional aspect of the airflow)
<b>Second Analysis</b>	Transient (Incompressible-Viscous-Newtonian-Isotropic) Turbulent Flow (RNG k-e turbulence model) (Turbulence-Continuity- Heat Transfer) (The ice melting process on the windshield)
<b>Assumption</b>	Radiation Effect (No have any influence on simulation)
<b>Solver</b>	First order upwind convection differencing scheme (second order discretization scheme could be utilized in some analysis)

Moulay Bel Hassan, Christophe Petitjean, Jean C. Deffieux and Philippe Gilotte investigate the windshield defogging simulation in this study. The objective of this study is basically to develop and validate the necessary techniques for computational analysis of windshield defogging problems.

They constructed a numerical model of a simplified test vehicle setup incorporating the passenger compartment, windshield, and the condensed vapor layer film. They conducted transient analysis to simulate the conditions present during cold room tests, where data was available. The results of the numerical simulation demonstrate a high level of agreement with the test data, indicating the model's reliability and accuracy (Hassan, et al. 1999).

Table 6 shows the analysis steps and some recommendations, Table 7 shows the boundary conditions in this study. Analysis consists of two cases, steady state, and transient state. This study has two different inlet temperature conditions. When the thickness exceeds  $1.5 \times 10^{-5}$  m, runoff becomes visible on the windshield. This value represents an asymptotic threshold derived from experimental conditions.

The thickness of the runoff film is determined by dividing the mass flow rate from the vapor generator over a five-minute period by the surface area of the windshield. The windshield is considered transparent if the thickness of the film is less than  $5 \times 10^{-6}$  m. This specific value is based on experimental data (Hassan, et al. 1999).

Table 6. Analysis Steps Source: (Hassan, et al. 1999)

<b>Method</b>	Computational Fluid Dynamic (Star- CD Software)
<b>Geometry Modelling</b>	Defroster Nozzle-Internal Structure (3D Model)
<b>Meshing</b>	The entire model: 100 000 cells
<b>First Analysis</b>	Steady state-Turbulent Flow (Realizable k-e turbulence model) – Isothermal Condition (Solve the temperature field variations)
<b>Second Analysis</b>	Transient-Turbulent Flow (Realizable k-e turbulence model) (To improve the performance of the transient CFD model)
<b>Assumption</b>	Radiation Effect (No have any influence on simulation)
<b>Solver</b>	Unsteady first order discretization scheme and unsteady second order scheme (Unsteady first order discretization scheme predicts the melting quicker)

Table 7. Boundary Condition Source: (Hassan, et al. 1999)

Boundary conditions	Setting	Value
Inlet	Mass Flow Rate	0.063 kg/s
	Humidity	94%
	Temperature	- 3 °C (or 10 °C)
Outlet	Pressure outlet	101325 Pa
Windshield surface	Initial Condensed Film	$1.5 \times 10^{-5}$ m
	Stationary Wall	
Wall Thermal	Adiabatic	
Computational domain	Air Temperature	- 3 °C (or 10 °C)

## 2.1. International Windscreen Defrosting and Demisting Standards

In the automotive industry, Ice and mist formed on the windshields of vehicles pose a significant safety risk for driving. Automotive manufacturers have developed standards for defogging, which is the process of removing condensation and frost from vehicle surfaces to improve visibility and enhance safety. These standards include specifications for defrosting and defogging systems, such as time to clear fogged or iced-over surfaces, required temperature and airflow rate, and other related factors. Compliance with these standards is crucial for manufacturers to ensure their vehicles meet minimum safety requirements and regulatory standards for road safety.

- Windscreen Defrosting and Demisting: 78/317/EEC
- Passenger Car Windshield Defrosting Systems: SAE Standard J902
- Windshield Defrosting Systems Test Procedure and Performance Requirements Trucks, Buses, and Multipurpose Vehicles: SAE Standard J381

### 2.1.1. 78/317/EEC

In the European standard 78/317/EEC, area A indicates the driver's area, and area B indicates the passenger area. The defrost system is started and after 20 minutes, %80 of area A should be defrosted. After 25 minutes, 80% of the B area should be defrosted. After 40 minutes, this rate should increase to 95%.

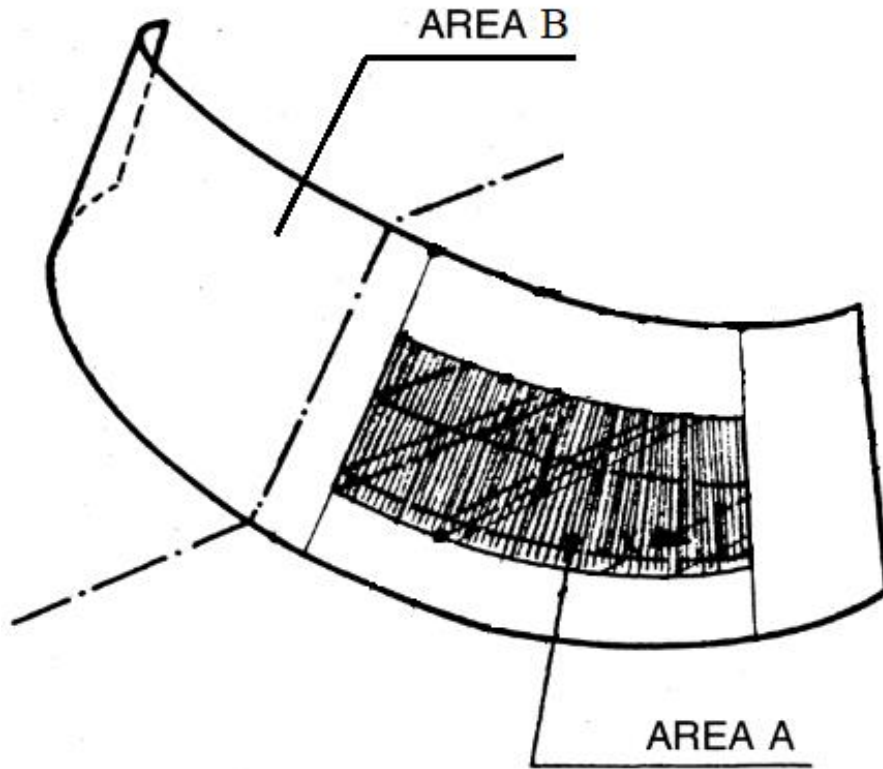


Figure 10. Windshield Area Source: (78/317/EEC 1978)

### 2.1.2. SAE Standard J902a

In the ABD standard SAE J 902, area C indicates the driver's area, and area B indicates the passenger area. The defrost system is started and after 30 minutes, minimum 80% of area A, minimum 95% of area B and minimum 100% of area C should be defrosted.

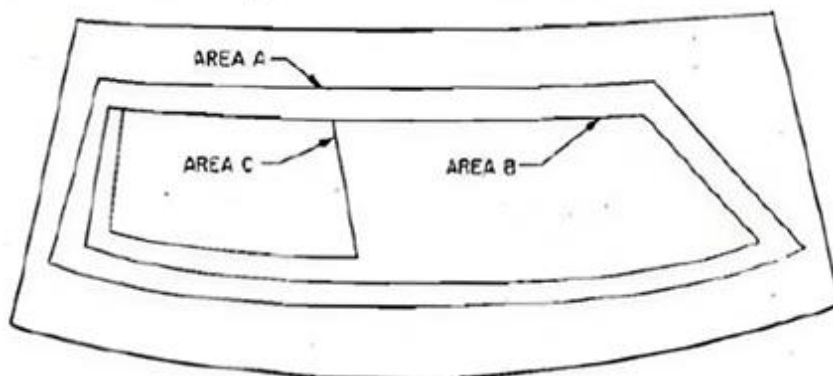


Figure 11. Windshield Area Source: (SAE Standard J902A 1967)

### 2.1.3. SAE Standard J381

In the ABD standard SAE J 381, area C indicates the driver's area, and area A indicates the passenger area. The defrost system is started and after 30 minutes, minimum 99% of area C and minimum 80% of area A should be defrosted for the single glass. The defrost system is started and after 30 minutes, minimum 84% of area C and minimum 65% of area A should be defrosted for the double glass.

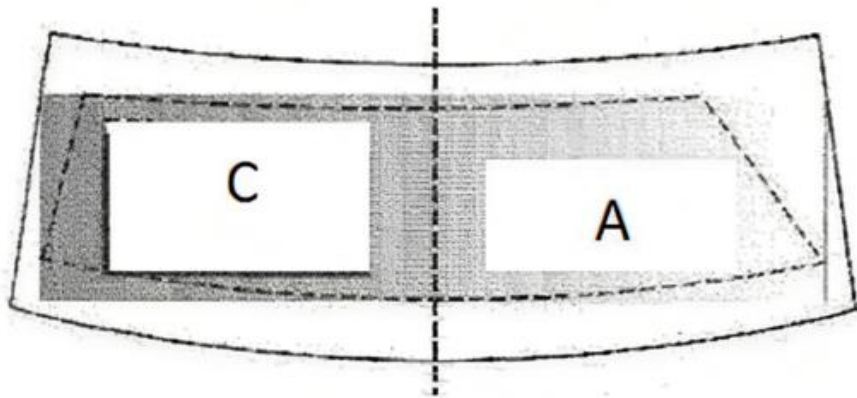


Figure 12. Windshield Area Source: (SAE J381 2000)

## CHAPTER 3

### WINDSHIELD DEFOGGING TEST

This methodology encompasses essential testing procedures aimed at assessing the defogging performance of the vehicle defroster system in specific environmental conditions, specifically focusing on clearing fog on the front windshield. The primary objective of defogging test studies is to evaluate the defogging efficacy at a temperature of  $-3^{\circ}\text{C}$ . The designated areas for assessment are denoted as A for the driver's section and B for the passenger's section. The examination seeks to gauge the system's ability to effectively eliminate fog, ensuring optimal visibility in critical cold weather scenarios. Figure 13 shows that windshield area. A is the driver's area and B is passenger's area.

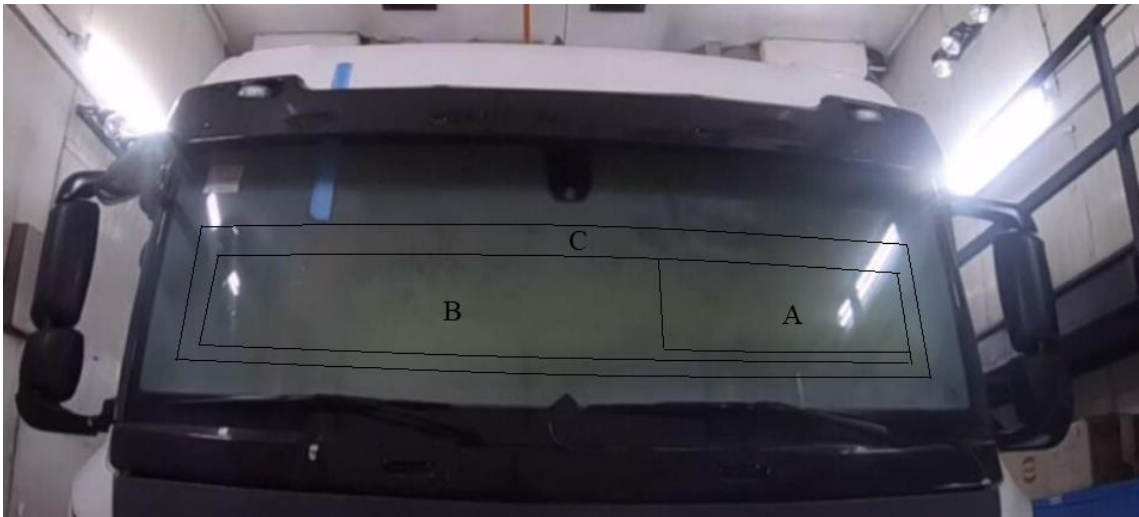


Figure 13. Windshield Area

#### 3.1. Acceptance Criteria

The defrost system is started and after 10 minutes, minimum 90% of area A, minimum 80% of area B should be defogging. After 20 minutes, 100% of area A+B should be defogged.



### 3.2. Test Requirements

Initially, we employ specialized devices to measure the airflow properties of the HVAC duct. The instrumentation utilized for this purpose is detailed in Table 8, providing a comprehensive overview of the equipment involved in capturing relevant airflow data.

Table 8. Test Equipment

Equipment	Model	Recording Frequency
Temperature Control	TESTO	5 s
Flow Control	CEM DT-619	Momentary
Humidity Control	TESTO	5 s

Figure 14 visually presents an image of the measuring devices employed in the airflow property assessments of the HVAC duct.



Figure 14. Temperature Control- Flow Control- Humidity Control

We do the defogging test in the climatic room. The environment should be conditioned to  $-3 \pm 1$  °C with sensitivity.

We use the steam generator to produce humid air. There should be sufficient water to provide humidity of  $70 \pm 5$  g/h per person. Finally, we use strip printing paper with contrast colors (e.g., black-yellow) for displaying the defrosted area.

### 3.3. Test Methods

Test stages are listed below in order.

- It should be ensured that the temperature of the test room (-3 °C) is stable.
- All doors, windows and hoods must be closed.
- There should be enough water in the steam machine chamber to provide humidity of  $70 \pm 5$  g/h per person.
- There should be a maximum of 2 observers in the vehicle (this value should be deducted from the total number of people when creating humidity).
- Steam machine 5 min. should be run throughout. Then it should be turned off.
- On the inner surfaces of the windshield and side glass, the demisting area that dissolves every 5 minutes (must be the completely dry area) should be marked with a board marker pen.
- The test should be terminated after 20 minutes. If the mist is completely removed before 20 minutes, the test can be terminated.

## CHAPTER 4

### COMPUTATIONAL FLUID DYNAMICS

Computational Fluid Dynamics (CFD) is a powerful tool that can help engineers and scientists understand and optimize the behavior of fluids in a wide range of applications, from aerospace and automotive engineering to medical devices and environmental systems.

CFD models are typically based on the Navier-Stokes equations, which describe the motion of fluids. These equations are solved numerically using a variety of techniques, including finite difference, finite volume, and finite element methods.

Finite Difference Method (FDM), Finite Volume Method (FVM), and Finite Element Method (FEM) are all numerical techniques for solving partial differential equations that describe physical systems. FDM, FVM, and FEM are all numerical methods used to approximate solutions to partial differential equations, but they differ in the way they discretize the domain and approximate the solution. FDM is used for simple geometries, FVM is particularly suited for simulating fluid flows, and FEM is useful for problems with irregular geometries. (Sjodin 2016)

The FDM discretizes the domain into a grid of points, and the differential equations are approximated using finite differences between the values of the solution at neighboring grid points. FDM is typically used for problems with regular geometric shapes and uniform meshes, such as heat transfer and fluid flow in simple geometries.

The FVM discretizes the domain into a set of control volumes, which are volumes in the physical domain that enclose a single grid point or a group of grid points. The differential equations are approximated using the fluxes of the solution across the boundaries of the control volumes. FVM is particularly suited for simulating fluid flows and combustion, as it conserves mass, momentum, and energy in the control volumes.

The FEM discretizes the domain into a mesh of elements, which are geometric shapes that make up the physical domain. The differential equations are approximated using basis functions that are defined on each element of the mesh. FEM is particularly suited for problems with irregular geometries, as it allows for the use of non-uniform meshes and can handle complex boundary conditions. (Sjodin 2016)

## 4.1. Approaches to Multiphase Modeling

Multiphase modeling is the mathematical representation of the behavior of multiple phases in a physical system. It is a useful tool in many engineering and scientific fields, such as fluid dynamics, chemical engineering, and materials science. There are several approaches to multiphase (gas-solid flows) modeling, including. (Chen and Wang 2014)

- The Euler- Lagrange Approach
- The Euler-Euler Approach

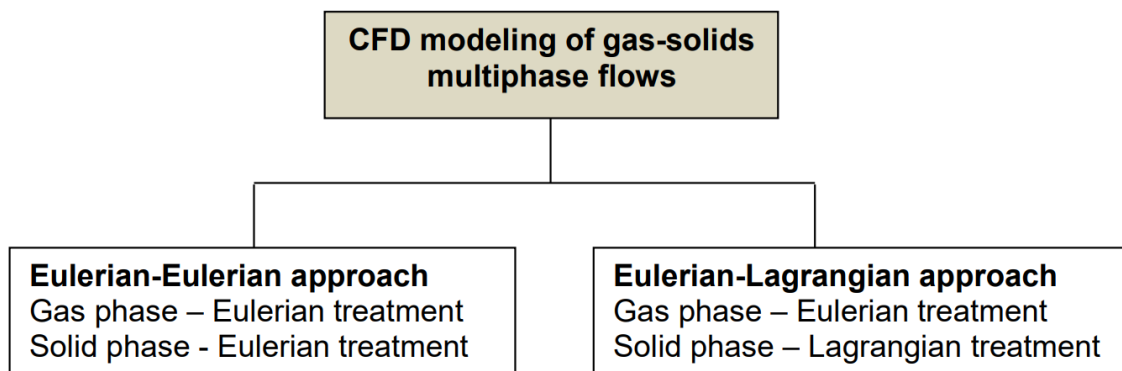


Figure 15. CFD Modelling Source: (Ariyaratne, et al. 2016)

### 4.1.1. Euler-Lagrange Approach

The Eulerian approach is a method of studying fluid motion in which we observe the flow of fluid at a fixed point in space. This approach considers the properties of the fluid, such as pressure, velocity, and density, at a specific point in space and time. This approach is commonly used in numerical simulations of fluid dynamics. The Lagrangian approach is a method of studying fluid motion in which we follow individual particles of fluid as they move through space. This approach considers the trajectory of a particle, its velocity, and its acceleration as it moves through the fluid. The Lagrangian approach is commonly used in experiments to measure the motion of fluid particles. Euler-Lagrange approach is a method of modeling multiphase flows in which one phase is treated as a continuous fluid, while the other phase is considered as a set of discrete particles. In this approach, the fluid phase is modeled using the Eulerian, while the discrete particles are

modeled using the Lagrangian. Euler-Lagrange approach is typically used for modeling particle-laden flows with low particle volume fractions and strong particle-fluid interactions.

The fluid phase is characterized by the utilization of time-averaged Navier-Stokes equations and other conservation equations, while the discrete phase is modeled by tracking the motion and interactions of individual particles using Newton's laws of motion. (Yin, et al. 2014)

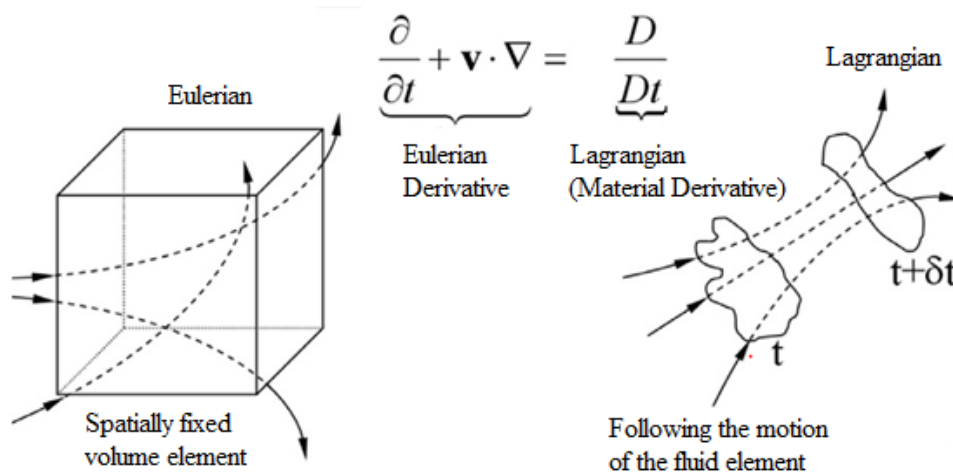


Figure 16. Eulerian and Lagrangian Derivative Source: (Qiu, Henke and Grab 2011)

#### 4.1.2. Euler-Euler Approach

Euler-Euler approach is a method of modeling multiphase flows in which both phases are treated as interpenetrating continuum (Zhang, Lan and Gao 2012).

In this approach, the fluid and particle phases are modeled using separate sets of conservation equations, and the interfacial momentum and energy exchange are accounted for using suitable interfacial conditions. Euler-Euler approach assumes that the volume fractions of both phases are well defined, and that the interfacial area is calculated using the volume-averaged phase variables.

Euler-Euler approach is preferred for modeling dispersed multiphase flows with high particle volume fractions and weak particle-fluid interactions. Euler-Euler approach normally requires less computational resources compared to Euler-Lagrange approaches (Chen and Wang 2014). Three different Euler-Euler multiphase models are available (ANSYS Inc. 2011).

- The volume of fluid (VOF) model
- The mixture model
- Eulerian model

#### **4.1.2.1. Volume of Fluid Model**

The Volume of Fluid (VOF) model is a numerical method used in computational fluid dynamics (CFD) to simulate fluid flows. It is a widely used method for modeling the behavior of free surfaces, such as the interface between two immiscible fluids or the surface of a liquid in contact with air (Mulbah, et al. 2022). The VOF method is based on the concept of tracking the volume fraction of one fluid (e.g., air) within a mixture of two or more fluids (e.g., air and water). The VOF model solves a set of partial differential equations that describe the conservation of mass, momentum, and energy for each fluid in the mixture (Ghani and Farid 2006). The VOF model tracks the interface between the two fluids by using a marker function that assigns a value of 0 or 1 to each point in the computational domain, depending on whether it is occupied by one fluid or the other. The marker function is updated at each time step based on the computed velocities and pressures, and the position of the interface is determined by the location of the points where the marker function transitions from 0 to 1 (or vice versa).

#### **4.1.2.2. Mixture Model**

The Mixture Model is a numerical method used in computational fluid dynamics (CFD) to simulate flows involving two or more immiscible fluids. It is a popular method for simulating two-phase flow, such as air-water or oil-water flows. The model solves the conservation equations for mass, momentum, and energy for the mixture. The model also includes additional terms to account for interfacial forces between the two fluids, such as surface tension and drag. The Mixture Model is characterized using a volume fraction function, which is defined as the ratio of the volume occupied by one fluid to the total volume of the mixture. The volume fraction function varies between 0 and 1 and is used to determine the location of the interface between the two fluids. One advantage of the Mixture Model is that it is computationally efficient compared to other methods such as the Volume of Fluid (VOF) method. It is also more suitable for simulating flows with

large variations in volume fraction, such as bubbly or slug flow. However, the Mixture Model has some limitations. It assumes that the two fluids are perfectly mixed and that their properties are constant across the interface. This may not be true in some situations, such as for flows with large density or viscosity differences between the two fluids. Additionally, the model may not accurately capture the dynamics of the interface between the two fluids, which can lead to errors in the simulation results.

#### **4.1.2.3. Eulerian Model**

The Eulerian model is a numerical method used in computational fluid dynamics (CFD) to simulate fluid flows. It treats the fluid as a continuum and solves the equations of motion at fixed points in space. Eulerian methods involve the discretization of the spatial domain through which the material flows. (Matthias, et al. 2007)

The model represents fluid flow using partial differential equations that describe the conservation of mass, momentum, and energy at each point in space. These equations are solved numerically, using methods like finite volume or finite element, to generate a solution that describes the flow field at each point. The Eulerian Model's strength lies in its ability to handle complex fluid flows, including turbulent flows, multiphase flows, and flows with heat and mass transfer. It is also well-suited for simulating fluid flows in complex geometries, such as flows through porous media or around obstacles. The Eulerian Model is often used in combination with other methods, such as the Volume of Fluid (VOF) method or the Mixture Model, to simulate flows involving multiple fluids or phases. In such cases, the Eulerian Model solves the equations of motion for each fluid or phase separately. The interface between them is tracked using a marker function or volume fraction function. However, the Eulerian Model has some limitations. It requires high numerical accuracy and stability, which can make it computationally expensive for large-scale simulations or complex geometries. It may also require the use of turbulence models or other sub-models to accurately capture the physics of the flow.

## CHAPTER 5

### NUMERICAL MODEL AND METHOD

The scope of this thesis is on the occurrence of fogging on the inner surface of a vehicle's windshield caused by the condensation of water vapor from the vehicle's interior air. Figure 17 shows the transfer of temperature from the exterior of a vehicle (ambient temperature) through the windshield to the interior of the cabin (interior temperature).

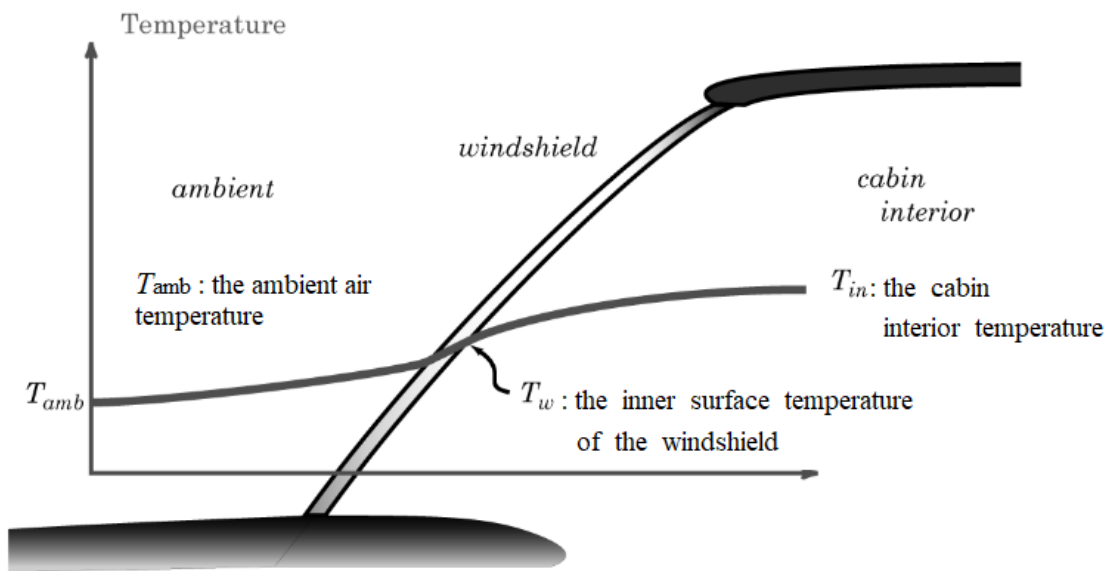


Figure 17. Transfer of Temperature Source: (Davis, Dage and Hoeschele 2001)

If the temperature of inner surface is the same as or lower than the dew point temperature of the surrounding cabin air, the moisture present in the air will condense and cause the windshield to become foggy (Davis, Dage and Hoeschele 2001). Figure 18 shows the condensation on the windshield surface. The condensation depends on pressure, temperature, and humidity. The primary objective of defogging the windshield is to simulate the transfer of mass at the boundary between the layer of liquid on the windshield and the surrounding air. We can divide the transfer process into two steps. The first step involves the motion of water molecules in the gas phase, which is caused by the partial pressure gradient. This is a diffusion phenomenon that occurs in the gas phase.



In the second step, a liquid-vapor transformation takes place at the film surface to maintain phase equilibrium between the liquid and vapor. This phase equilibrium is dependent on a diffusion motion, which is known as the evaporation phenomenon.

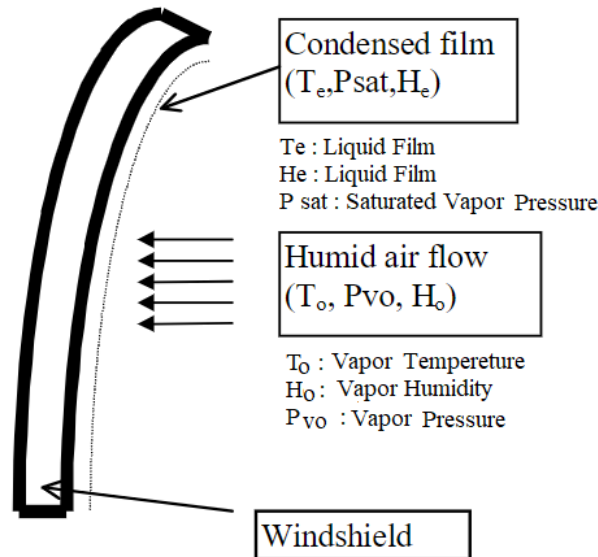


Figure 18. Condensation on Windshield Surface Source: (Hassan, et al. 1999)

Heat is transferred from water to air due to the difference in temperature, while the transfer of mass occurs from vapor to air due to the difference in pressure. The heat and mass transfers are interdependent and referred to as "latent heat transfer" (Hassan, et al. 1999).

The Eulerian Wall Film (EWF) model is a tool that can be employed to forecast the formation and movement of thin liquid films on wall surfaces. The k- $\omega$  SST turbulence model is used in the simulation.

The outcomes suggested that the SST k- $\omega$  turbulence model provided a more precise prediction of impinging jet heat transfer. This chapter provides a summary of the principles and equations that govern the techniques utilized in the EWF model. (ANSYS Inc. 2011) (Du, et al. 2016)

## 5.1. Governing Equation

The three major independent dynamical laws in continuum mechanics are the continuity equation, momentum equation, and energy equation. The computational fluid was incompressible.

### 5.1.1. Continuity, Momentum and Energy Equation

The continuity equation emphasizes the continuum assumptions. The continuum assumption is the density and velocity may be defined at every point in space. It is the foundation for all the basic laws of continuum mechanics. The continuity equation is based on conservation of mass (Panton 2013).

Reynolds (Ensemble) Averaging (RANS): Reynolds averaging involves breaking down the solution variables within the instantaneous (exact) Navier-Stokes equations into the mean (ensemble-averaged or time-averaged) and fluctuating components (ANSYS Inc. 2011).

Regarding the velocity components:

$$u_i = \bar{u}_i + u'_i \quad (1)$$

$\bar{u}_i$ : Mean Velocity,

$u'_i$ : Fluctuating Velocity

Velocity components  $i = 1, 2, 3$

Continuity Equation:

$$\frac{\partial \rho}{\partial t} + \frac{\partial}{\partial x_i} (\rho u_i) = 0 \quad (2)$$

Ensemble-averaged momentum equation:

$$\begin{aligned} & \frac{\partial}{\partial t} (\rho u_i) + \frac{\partial}{\partial x_j} (\rho u_i u_j) \\ & = -\frac{\partial p}{\partial x_i} + \frac{\partial}{\partial x_j} \left[ \mu \left( \frac{\partial u_i}{\partial x_j} + \frac{\partial u_j}{\partial x_i} - \frac{2}{3} \delta_{ij} \frac{\partial u_l}{\partial x_l} \right) \right] \\ & + \frac{\partial}{\partial x_j} (-\rho \overline{u'_i u'_j}) \end{aligned} \quad (3)$$

$-\rho \overline{u'_i u'_j}$ : Reynolds stresses

The Shear Stress Transport (SST) k- $\omega$  is a two-equation model that combines the k- $\omega$  and the k- $\epsilon$  turbulence models to provide more accurate predictions of the

boundary layer flow behavior.

The k-omega model is used to predict the turbulence behavior in the near-wall region, while the k-epsilon model is utilized for the outer flow region (ANSYS Inc. 2011).

Transport equations-Turbulence model (k-w SST):

$$\frac{\partial}{\partial t}(\rho k) + \frac{\partial}{\partial x_i}(\rho k u_i) = \frac{\partial}{\partial x_j} \left( \Gamma_k \frac{\partial k}{\partial x_j} \right) + \tilde{G}_k - Y_k + S_k \quad (4)$$

$$\frac{\partial}{\partial t}(\rho w) + \frac{\partial}{\partial x_i}(\rho w u_i) = \frac{\partial}{\partial x_j} \left( \Gamma_w \frac{\partial w}{\partial x_j} \right) + G_w - Y_w + D_w + S_w \quad (5)$$

The production of turbulence kinetic energy (k):

$$\tilde{G}_k = \min(G_k, 10 \rho \beta^* k w) \quad (6)$$

The production of the specific dissipation rate (w):

$$G_w = \alpha \frac{\omega}{k} \tilde{G}_k \quad (7)$$

Specific Dissipation Rate:

$$w = \frac{\epsilon}{\beta^* k} \quad (8)$$

Dissipation of k:

$$Y_k = \rho \beta^* k w \quad (9)$$

Coefficient  $\beta^*$ : 1

Dissipation of w:

$$Y_w = \rho \beta w^2 \quad (10)$$

k-w model closure coefficient of destruction term ( $\beta$ ): 0.075

Coefficient  $\alpha$ : 1

Effective Diffusivities:

$$\Gamma_k = \mu + \frac{\mu_t}{\sigma_k} \quad (11)$$

$$\Gamma_w = \mu + \frac{\mu_t}{\sigma_w} \quad (12)$$

Gradual change from the standard model in the inner region of the boundary layer to a high-Reynolds number version of the  $k$ - $\epsilon$  model in the outer part of the boundary layer (BSL, SST). Modified turbulent viscosity formulation to account for the transport effects of the principal turbulent shear stress (SST only).

$\sigma_k$  and  $\sigma_w$  are the turbulent Prandtl numbers for  $k$  and  $w$  respectively.  $\mu_t$  turbulent viscosity.  $D_w$  is the cross-diffusion term.  $S_k$  and  $S_w$  user-defined source terms. (ANSYS Inc. 2011)

Heat Transfer: Energy transfer into a region can occur through various means, and heat transfer is one of them. The heat flux vector  $q$ , with dimensions of energy/area  $\cdot$  time, represents the sum of all microscopic modes of energy transfer. Among these modes, conduction is the most encountered type of microscopic energy transfer. In addition to conduction, radiation, and the transport of energy by diffusion of different chemical species are other modes of energy transfer. The heat flux vector  $q$  provides information on the magnitude and direction of the flux for all these modes (Panton 2013).

Heat Transfer (Air Sub-domain): The air gains heat energy through the heater. When the flow coming out of the defroster vents hits the windshield, it transfers heat energy to the windshield. Equation 13 shows the heat transfer that occurs (Sadananda 2016).

$$\begin{aligned} & \frac{\partial}{\partial t}(\rho E) + \nabla \cdot (\vec{u} (\rho E + p)) \\ & = \nabla \cdot \left( k_{eff} \nabla T - \sum_j h_j \vec{j}_j + (\overline{\tau_{eff}} \cdot \vec{u}) + S_h \right) \end{aligned} \quad (13)$$

$$k_{eff} = k + k_t \quad (14)$$

$k_{eff}$  : The effective conductivity

$k_t$  : The turbulent thermal conductivity

$\vec{J}_j$  : The diffusion flux of species j

$k_{eff}\nabla T$  : Conductive heat transfer

$\sum_j h_j \vec{J}_j$  : Species diffusion

$\overline{\tau_{eff}} \cdot \vec{u}$  : Viscous dissipation

$S_h$  : Heat source supplied at the heater

$$E = h - \frac{p}{\rho} + \frac{u^2}{2} \quad (15)$$

$$h = \sum_j Y_j h_j \quad (16)$$

$Y_j$  : The mass fraction of species j

$h$  : Sensible enthalpy (for ideal gas);  $h_j$  : Enthalpy of species j

For incompressible flow:

$$h = \sum_j Y_j h_j + \frac{p}{\rho} \quad (17)$$

$$h = \int_{T_{ref}}^T c_{pj} dT \quad (18)$$

Heat Transfer (Solid Region): The windshield gains heat energy from the air. The gained heat is transferred to the mist on the windshield. Equation 19 shows the heat transfer that occurs. The first term is the heat carried to or from the glass, the second term is the heat conducted across the glass (Sadananda 2016).

$$\frac{\partial}{\partial t}(\rho h) = \frac{\partial}{\partial x_i} \left( k \frac{\partial T}{\partial x_i} \right) \quad (19)$$

I                      II

### 5.1.2. Eulerian Wall Film Model

Automotive and aeronautical companies consider fogging of automobile windshields a significant safety concern, particularly in cold ambient conditions. This occurs when water vapor condenses into small droplets or a thin film on the glass surface, leading to reduced visibility. Defogging is a critical process that involves blowing hot air to demist the windshield panes to ensure passenger safety. A key design consideration is the time required to defog the windshield using a hot temperature that does not cause cabin discomfort (ANSYS Inc. 2013). In this thesis, we utilize the Eulerian Wall Film (EWF) Model to model the defogging phenomenon on windshields.

The prediction of the formation and flow of thin liquid films on wall surfaces can be achieved using the EWF model. In the EWF model, the wall film is treated as a separate fluid phase, and the conservation equations for mass, momentum, and energy are solved separately for each fluid phase. The EWF model is an Eulerian method that requires fewer computational cells than the VOF model, making it computationally efficient for simulating wall films.

Although the volume of fluid method (VOF) can be used for simulations involving thin liquid layers, it requires a significant amount of computational power. EWF was used instead to speed up the simulation process. However, it should be noted that the model used in this study neglects the change in heat transfer resistance caused by the liquid wall film (Michal and Zachar 2019).

The conservation of mass for a two-dimensional film in a three-dimensional domain can be expressed as:

$$\frac{\partial h}{\partial t} + \nabla_s \cdot [h\vec{V}_l] = \frac{\dot{m}_s}{\rho_l} \quad (20)$$

$\rho_l$  : The liquid density

h: The film height

$\nabla_s$ : The surface gradient operator

$\vec{V}_l$  : The mean film velocity

$\dot{m}_s$ : The mass source per unit wall area due to droplet collection, film separation, film stripping, and phase change

$$\frac{\partial h \vec{V}_l}{\partial t} + \nabla_s \cdot (h \vec{V}_l \vec{V}_l) = - \frac{h \nabla_s P_L}{\rho_l} + (\vec{g}_t) h + \frac{3}{2 \rho_l} \vec{\tau}_{fs} - \frac{3 \nu_l}{h} \vec{V}_l + \frac{\dot{q}}{\rho_l} \quad (21)$$

I
II
III
IV
V
VI

Where

$$P_L = P_{gas} + P_h \quad (22)$$

$$P_h = -\rho h (\vec{n} \cdot \vec{g}) \quad (23)$$

Equation 21 is divided into left-hand side terms representing transient and convection effects, and right-hand side terms encompassing five factors.

II is the impact of gas-flow pressure and the component of gravity perpendicular to the wall, referred to as spreading. III accounts for the influence of gravity on the film in the parallel direction. IV relates to the viscous shear force at the interface between the gas and film. V signifies the viscous force within the film itself. Finally, VI is related to droplet separation or collection.

It is important to note that while calculating the shear and viscous terms on the right-hand side, we have the assumption of a parabolic film velocity profile (ANSYS Inc. 2011).

Conservation of film energy:

$$\frac{\partial h T_f}{\partial t} + s \cdot (\vec{V}_f h T_f) = \frac{1}{\rho C_p} \cdot \left\{ 2k_f \left[ \frac{T_s + T_w}{h} - \frac{2 T_f}{h} \right] + \dot{q}_{imp} + \dot{m}_{vap} L(T_s) \right\} \quad (24)$$

$T_s$  : The temperature at the film–gas interface

$T_w$ : The wall temperature

$T_f$ : The average film temperature (Dependent variable)

$\dot{q}_{imp}$ : The source term

$\dot{m}_{vap}$ : The mass vaporization or the condensation rate

$L(T_s)$ : The latent heat associated with the phase change

Note: The film temperature varies;

In the lower half of film  $\rightarrow$  from  $T_w$  to  $T_f$ ; In the higher half of film  $\rightarrow$  from  $T_f$  to  $T_s$

Equation 20 and Equation 21 establish the basis of modeling evaporative heat and mass transfer in thin films. We can optionally use Equation 24, when we require thermal modelling. We apply these equations to the surface of a wall boundary. Given that the film is thin, the lubrication approximation that assumes parallel flow is valid. As a result, we use these equations using local coordinates that run parallel to the surface (ANSYS Inc. 2011).

## 5.2. Design of Experiment

Experiments Design of Experiments (DoE) allows the evaluation of many reaction parameters in a small number of experiments. It is a statistical analysis and modeling technique used to optimize (improve) products and/or processes during the design and production stages.

Design Expert Software is a utility for setting up an ideal experiment. The meanings of the terms specified in the Design Expert Software are as follows.

Table 9 shows that the evaluations of significant level. The significance level helps researchers make decisions about whether to reject or fail to reject the null hypothesis based on the results of a statistical test. When p-value (probability value) is less than 0.05, the researcher would reject the null hypothesis.

- Source: A meaningful name
- Sum of Squares:

$$\sum (x_i - \bar{x})^2 \quad (25)$$

- Degrees of Freedom (df):

$$n - 1 \quad (26)$$

- Mean Square (sample variance):

$$s^2 = \sum (x_i - \bar{x})^2 / n - 1 \quad (27)$$



- F Value: Test for comparing the source's mean square to the residual mean square.
- Probability > F: The probability equals the integral under the curve of the F-distribution that lies beyond the observed F-value.

Table 9. Significant Level Source: (Schmidt and Osebold 2017)

Significance level		Specification
$P > 0.05$	(5%)	Not significant
$P \leq 0.05$	(5%)	Significant
$P \leq 0.01$	(1%)	Very significant
$P \leq 0.001$	(0.1%)	Highly significant

### 5.2.1. Full Factorial Design

A full factorial design is a type of experimental design used in statistics and experimental research to study the effects of multiple factors on a response variable. It involves systematically studying all possible combinations of the levels of the factors in a study. This type of design is particularly useful when investigating the interactions between different factors. Factors are the independent variables in an experiment. Each factor can have multiple levels or variations. Levels represent the different variations or settings of each factor. We use the two-level factorials with three factors ( $2^3$ ). Two-level design on third factors produces 8 runs. Figure 19 shows the view of the Design Expert Software- Type of Full Factorial Design.

<b>Runs</b>	2	3	4	5
4	$2^2$	$2^{3-1}$ III		
8		$2^3$	$2^{4-1}$ IV	$2^{5-2}$ III
16			$2^4$	$2^{5-1}$ V
32				$2^5$

Figure 19. Design Expert Software- Type of Full Factorial Design

### 5.3. Boundary Condition

Two types of conditions exist: one involves fixed mass and momentum fluxes, while the other entails the specification of the initial film height and velocity. (ANSYS Inc. 2011). The inlet setting was determined with the test equipment placed on the defroster outlet, as specified in Test Requirements (Chapter 3.2.). The Truck cabin is conditioned in the test room at a temperature of 270 K. Subsequently, a steam generator is used, and fog formation is induced on the windshield.

Figure 20, figure 21 and figure 22 show the truck cabin models and the defroster duct model respectively. The 2D model is obtained from the xz plane of the 3D model. In the optimization study, 3D, 2D cabin models and defroster duct model were used to observe the effects of vent position parameters and defroster duct shape. Details are stated in chapter 7. The boundary conditions settings specified in Table 10 are used in the analyses conducted in this study.

Table 10. Boundary Conditions

<b>Boundary Conditions</b>	<b>Setting</b>	<b>Value</b>
Inlet	Air Mass Flow	0.114643 kg/s
	Mass Fraction	$Y_{H_2O} = 0.004$
	Temperature	288 K
Outlet	Pressure outlet	101325 Pa
Windshield	Stationary Wall-No Slip- Zero Diffusion Flux	-
	Initial Condensed Film	$1.3 \times 10^{-5} \text{m}$
Wall Thermal	Adiabatic (The walls are assumed thermally insulated)	-
Computational Domain	Initial Temperature	270 K
	Initial Mass Fraction	$Y_{H_2O} = 0.0015$

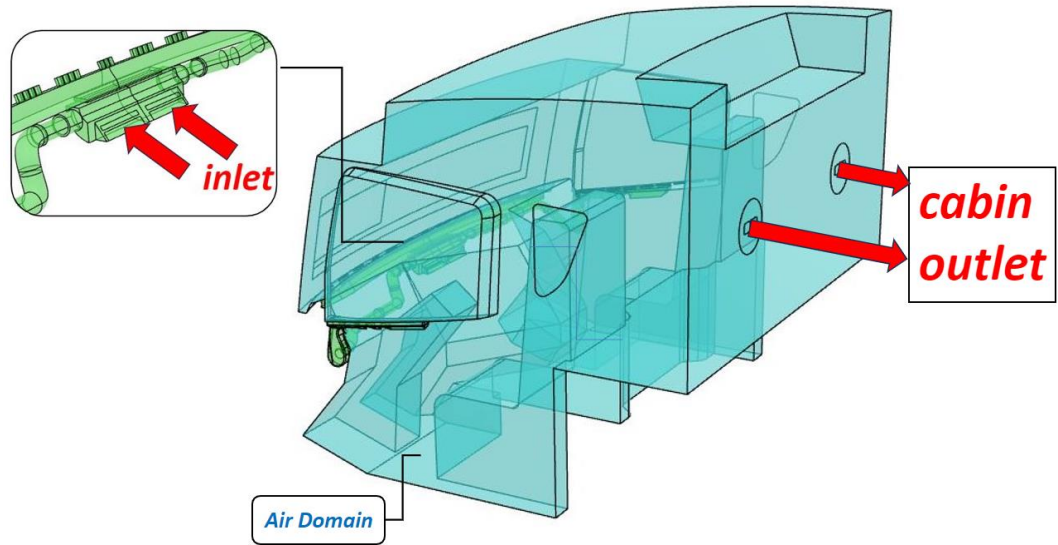


Figure 20. Truck Cabin (3D Model)

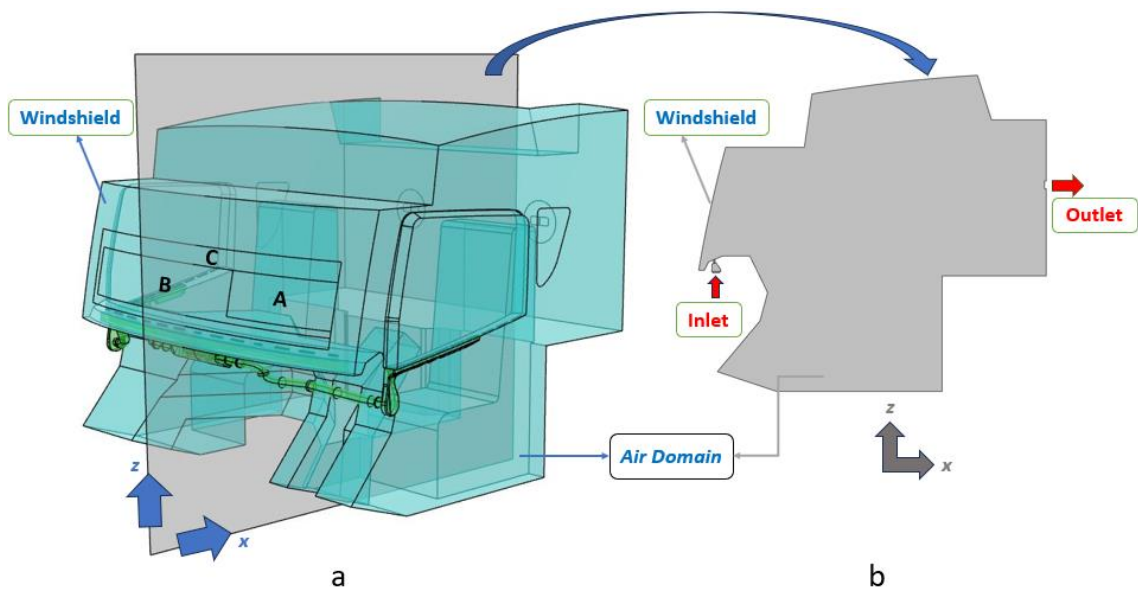


Figure 21. Truck Cabin (a. 3D Model and b. 2D Model)

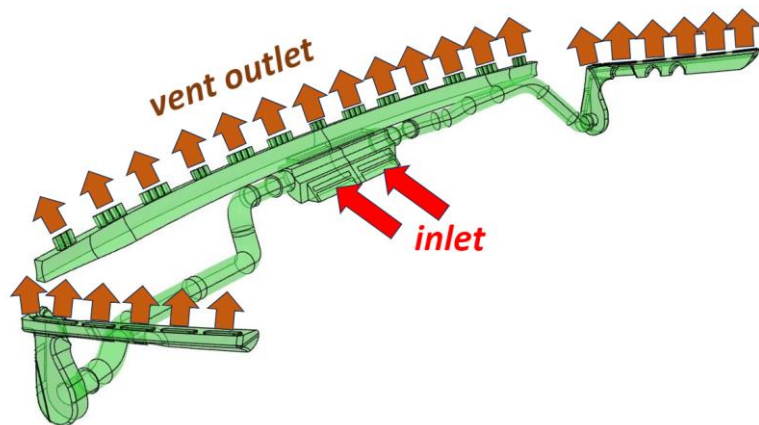


Figure 22. Defroster Duct Model

## CHAPTER 6

### MODEL AND NUMERICAL ANALYSIS

The objective of this study is to solve a simulated problem by utilizing the 3D geometries of a cabin and HVAC duct, while excluding thermal radiation. The model designs are created using Catia V6 software, and the simulation generated the corresponding model outputs. The ANSYS FLUENT program is employed to conduct the simulation, and the model outputs from Catia V6 are transferred to ANSYS FLUENT.

The study included the setup and modeling of the defogging analysis for the front windshield of the cabin. The defogging model assume that fogging occur solely on the inner surface of the windshield. Relevant literature studies and test documents are consulted to determine the boundary conditions and test parameters.

The first step involve investigating the reliability of the model, which is accomplished by validating the numerical analysis through experimental tests. Following that, simplified models are utilized to examine the parameters that influence the defogging time.

#### 6.1. Cabin Geometry

The truck model has a complex structure with interior equipment such as bed, front and rear cabinets, steering wheel, and seats. The complexity of this intricate model hinders the analysis feasibility. Therefore, it is necessary to restructure the model. The areas occupied by the equipment within the interior were removed to simplify the model, and the gaps between components were filled.

Figure 23 shows visual representations of the truck model, including the cabin and defroster duct. The designated areas on the windshield adhere to the test procedure requirements.

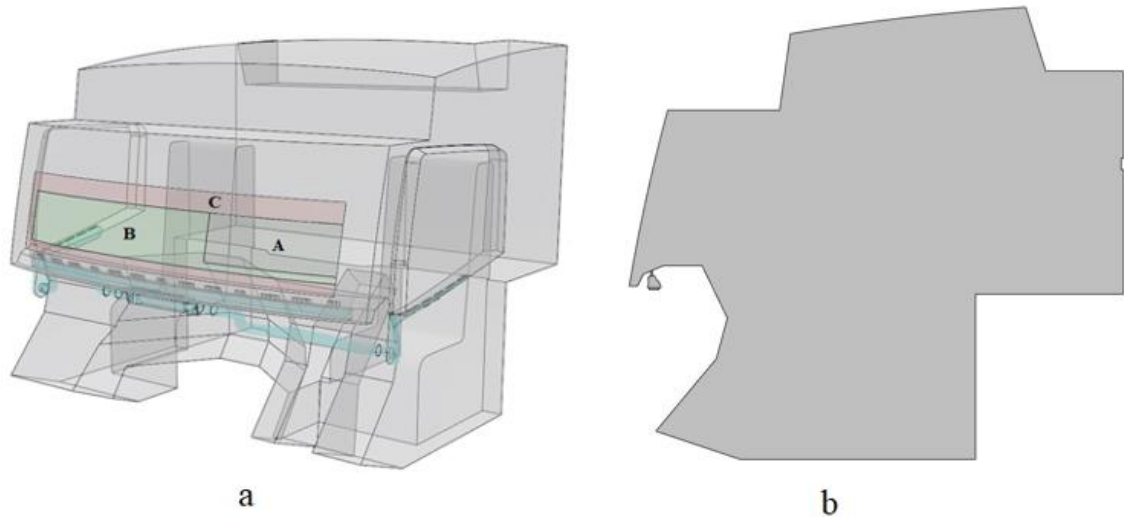


Figure 23. Truck Cabin Model (a. 3D Model and b. 2D Model)

## 6.2. Defrost Duct Geometry

The defrost duct model consists of various assembled components. The gaps present in the complex model were filled to simplify the model. Figure 24 shows the isometric view of the defrost duct model.

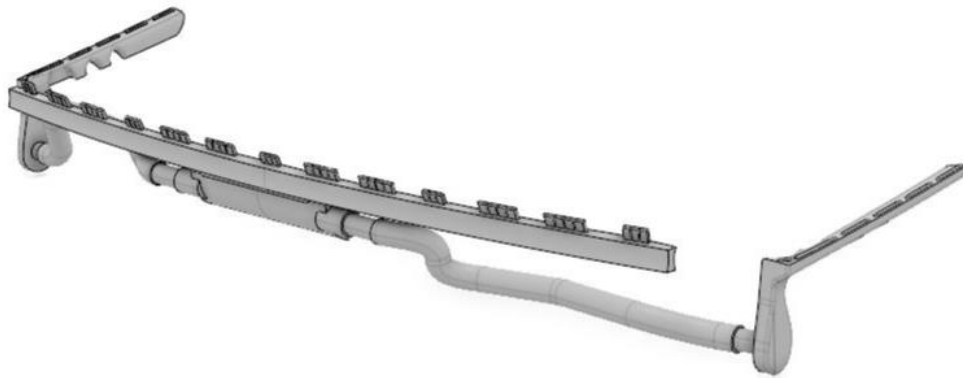


Figure 24. Defroster Duct Model (Isometric View)

Figure 25 shows the top view of defroster duct model. The air outlets are numbered according to the model image. Vents numbered 1 to 13 represent the windshield area, and other numbered vents represent the door window area.

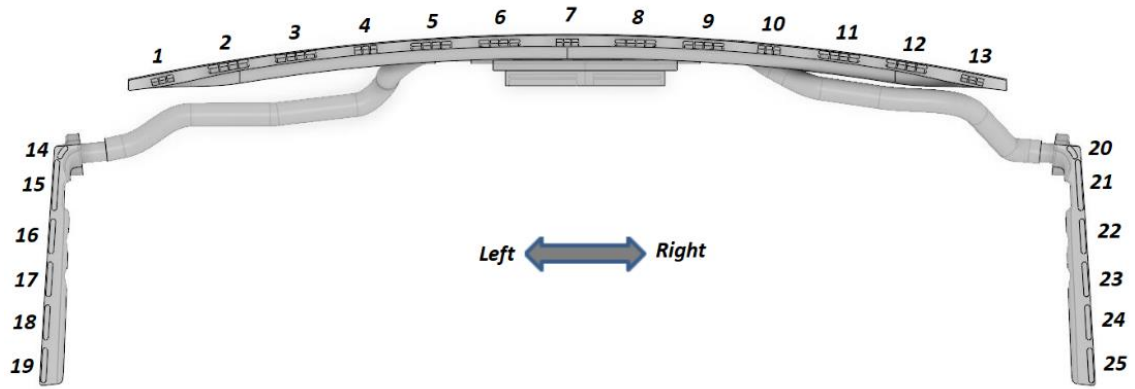


Figure 25. Defroster Duct Model (Top View)

### 6.3. CFD Analysis

In this section, the general structure of the analysis steps is described. The analysis consists of three stages: pre-processing, solver, and post-processing, in that order. The details of these stages are elaborated in the following sections. Figure 26 illustrates a schematic representation of the ANSYS analysis steps.

In the initial stage, Fluent Workbench is launched. Cabin models designed in CATIA V6 are imported. Mesh is created, and the CFD Setup application is opened to input boundary conditions, materials, and cell zone condition values. Solvers are specified, and the simulation run is initiated.

Table 11 shows the analysis details used in this thesis. Mesh type, turbulence material and solver information are obtained by using ANSYS Tutorial and literature research.

Table 11. Analysis Steps

Method	Computational Fluid Dynamic
Geometry Modelling	Truck Cabin (2D and 3D Model)
Meshing	Surface Meshing-Triangular (for 2D Model) and Volume Meshing-Polyhedral (for 3D Model)
Analysis	Transient-Turbulent Flow ( $k-\omega$ SST)
Assumption	Radiation Effect (No have any influence on simulation)
Solver	PISO Scheme (First Order Upwind)

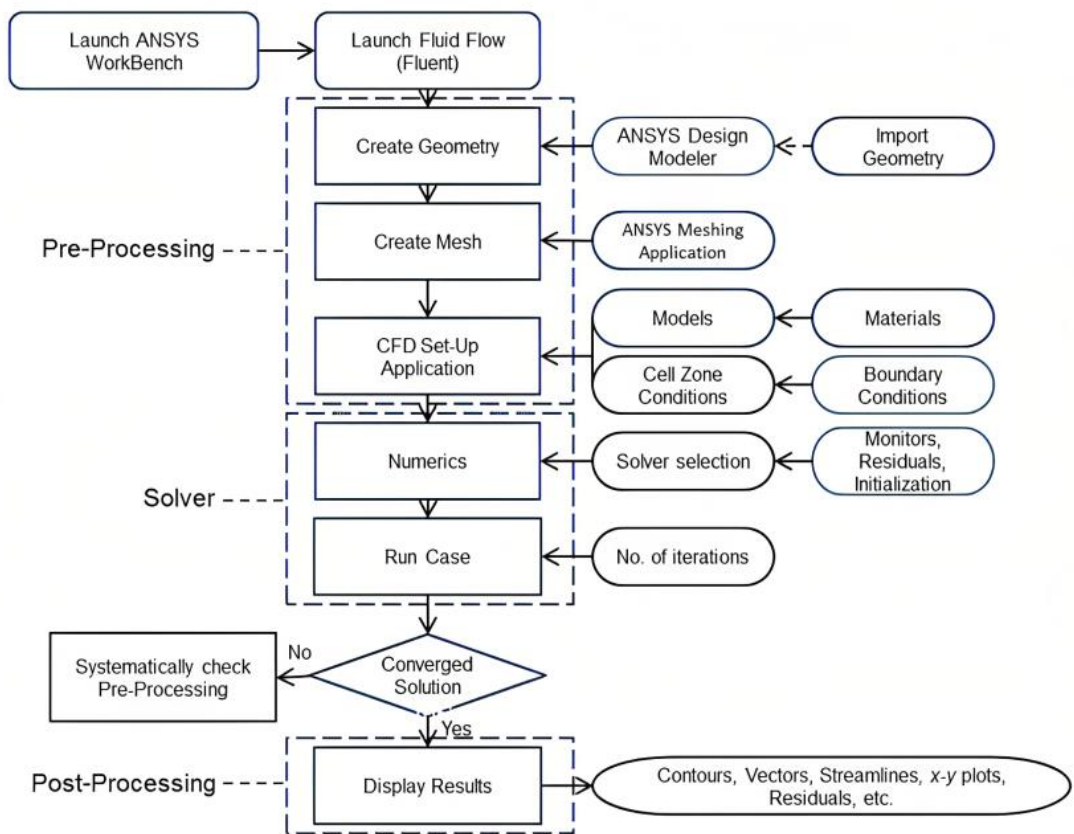


Figure 26. ANSYS Analysis Steps Source: (ANSYS Inc. 2011)



### 6.3.1. Pre-Processing

The pre-processing phase in ANSYS Fluent involves several steps to prepare the computational domain, define boundary conditions, and specify material properties. Here is a general overview of the preprocessing steps in ANSYS Fluent. The first step is to create or import the geometry of the problem domain. We use CATIA V6 software to create geometry. After importing the geometry, we perform some cleanup operations to remove any imperfections, such as gaps, overlaps, or holes. This step ensures a watertight geometry for accurate simulation. The third step is to generate a mesh to discretize the domain into smaller elements or cells. We use the polyhedral meshing in ANSYS Fluent Meshing. All domains have 1849450 nodes and 372644 elements. The cabin domain has 1161743 nodes, 221943 elements and defroster duct domain has 687707 nodes and 150701 elements.

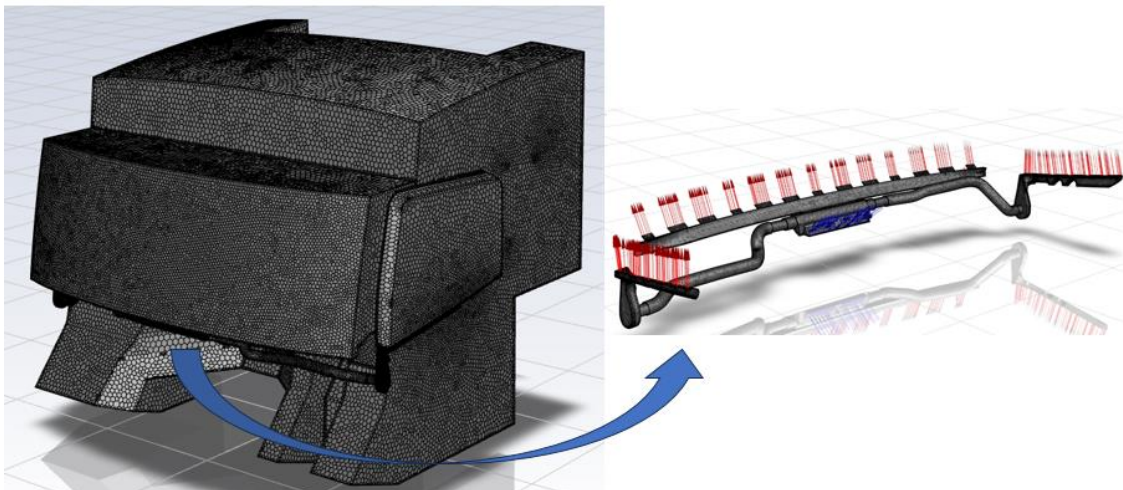


Figure 27. Mesh Domain (3D Model)

After meshing, we have defined the boundary conditions that specify how the fluid interacts with the boundaries of the domain. This includes setting the velocity, pressure, temperature, and other relevant properties at the boundaries. Details are shown in Boundary Conditions (Chapter 5.3.).

The next step involves defining the material properties of the fluid or fluids being simulated. This includes specifying properties such as density, viscosity, thermal conductivity, and specific heat. Table 12 shows the material properties of air and glass.

Table 12. Material Properties

Quantity	Air	Glass
Density (kg/m <sup>3</sup> )	1.21035	2707
Specific Heat (J/ kg.K)	1006	800
Thermal Cond. (W/m.K)	0.02637	0.76
Dynamic viscosity (kg/ m. s)	$1.81 \times 10^{-6}$	-

### 6.3.2. Solver

We need to specify the solver settings and solution controls before running the simulation. This includes selecting the appropriate solver algorithm, convergence criteria (for continuity 0.0001) and time step size (0.05 s). The ANSYS EWF document is followed for solver information. The PISO Pressure-Velocity Coupling Scheme is selected. In addition, we selected PRESTO! for Pressure and first order upwind for momentum under the Spatial Discretization. Finally, we apply an initial condition to start the simulation and we run it. The simulation took approximately 72 hours. The features of the computer used in analyzes are stated below:

- Processor: intel(r) Xeon(r) CPU E5-2620 v4 @ 2.20GHz (2 processor)
- Installed memory (RAM): 128 GB
- System Type: 64-bit Operating System

### 6.3.3. Post-Processing

Post-processing refers to the process of analyzing and visualizing simulation results obtained from computational fluid dynamics (CFD) simulations. Figure 28 and Figure 30 show that contours of film thickness and temperature of current cabin model at 300 second intervals. The film has a thickness of  $1.3 \times 10^{-5}$  in the initial condition. Initial conditions were determined by examining the effect of international test standards and data obtained from literature research on the test results. The data obtained in the test and analysis and the standard requirements are stated in the Table 13. The windshield is considered transparent if the thickness of the film is less than  $5 \times 10^{-6}$  m (Hassan, et al. 1999). Therefore, it was accepted that the windshield started to defog at values below

$5 \times 10^{-6} \text{m}$ . The analysis results were evaluated in two parts. The first part of results shows the percentage of defogging areas below  $5 \times 10^{-6} \text{m}$  (Transparent + Net area). The second part shows the percentage of defogging areas the fog is completely dissolved (Net area).

Figure 29 shows the film thickness of area A+B. The red contour of film thickness blocks the vision of the driver. The contours between the blue and red colors show the transparent area. The visibility has started in this region, but it is not clear. The blue contour of film thickness (net area) is completely resolved. The visibility is clear in this region.

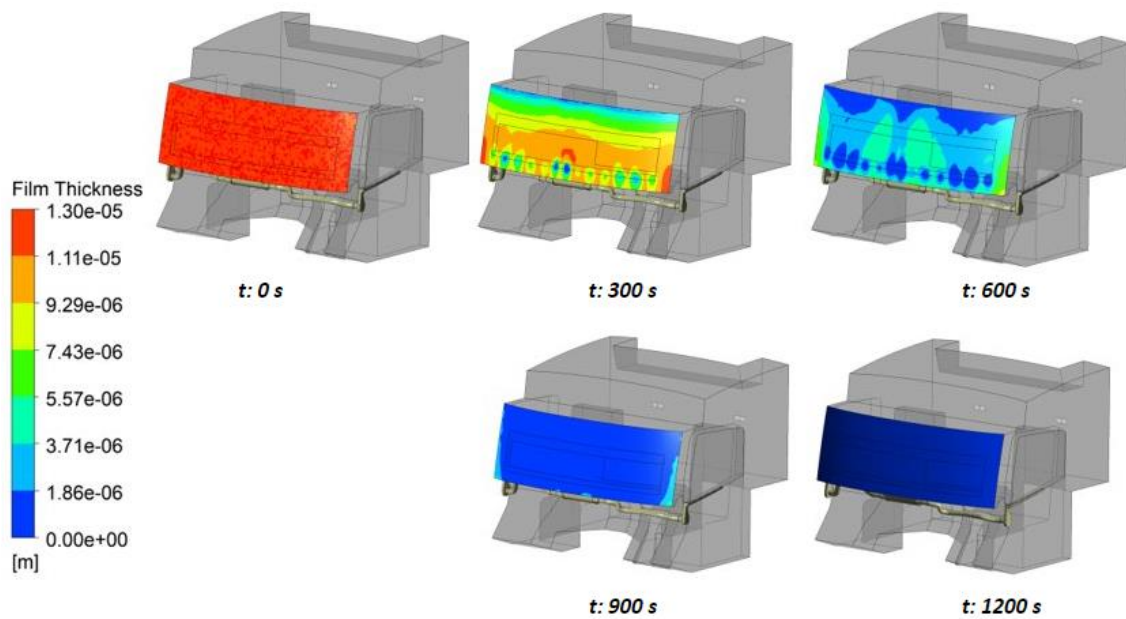


Figure 28. Film Thickness on the Windshield (Current Model)

Table 13. The Percentages of Defogged Area

Time	Acceptance Criteria	Analysis Results (Transparent + Net area)	Analysis Results (Net area)
600 s	Area A 90%	Area A 91.7%	Area A 3%
	Area B 80%	Area B 79 %	Area B 8%
1200 s	Area A+B 100 %	Area A 100%	Area A 100%
		Area B 100%	Area B 100%

As a result, it is seen that it exhibits similar behavior to the results of film thickness when the film temperature on glass is examined. Film thickness decreases to minimum levels in regions with high glass film temperature increases. In line with these data, glass

temperature increase can be examined in preliminary studies. However, film thickness should be examined in final analysis to obtain definitive results.

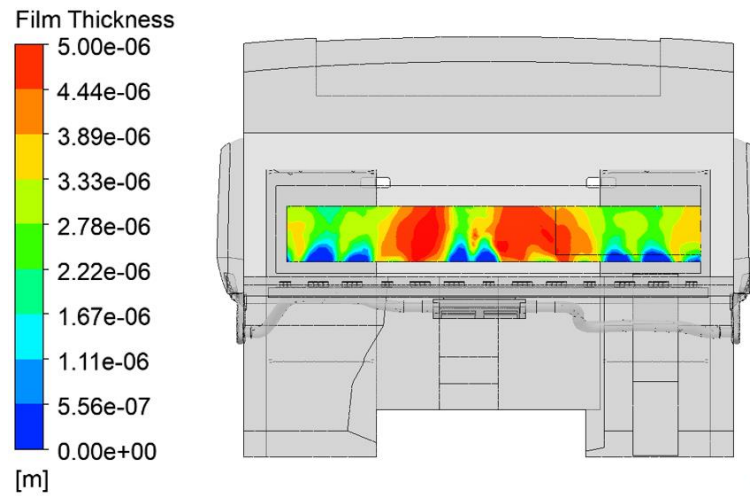


Figure 29. Film Thickness of Area A and B (Current Model) (t: 600 s)

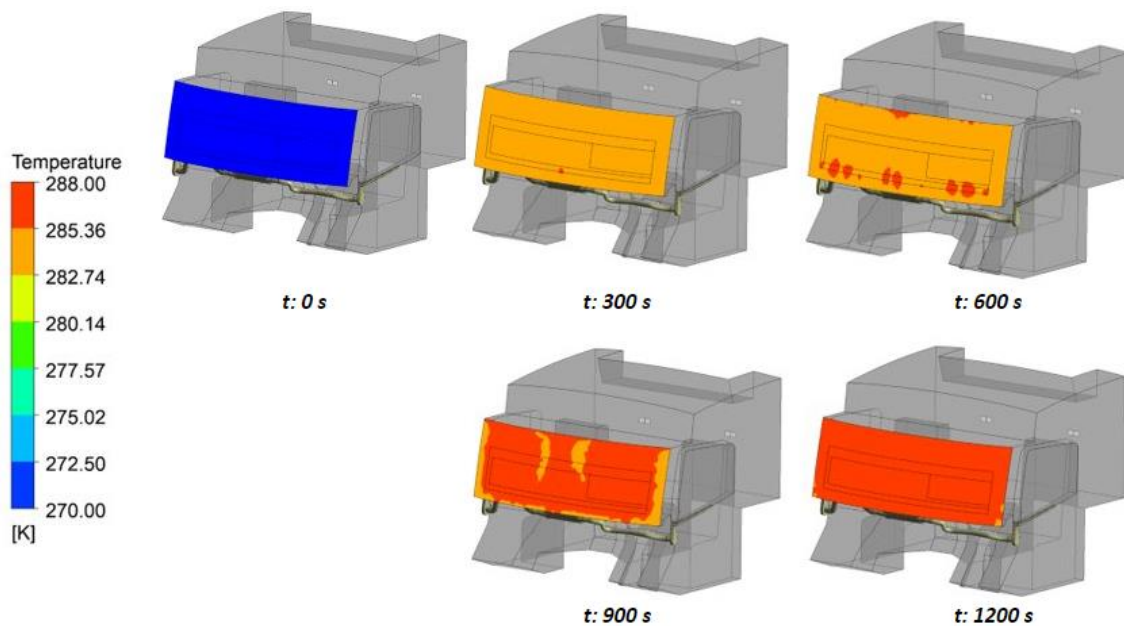


Figure 30. Film Temperature on the Windshield (Current Model)

### 6.3.4. Model Validation

Model validation refers to the process of ensuring that the simulation model accurately represents the physical system it is intended to simulate. This involves comparing the simulation results with experimental data or known theoretical values to assess the accuracy and reliability of the simulation. The subjoined images provide a

comparative analysis of the test data and analysis results at 300-second intervals.

Figure 31 serves as the initial reference point, encapsulating the onset of the examination in both the analytical and empirical testing phases. At the initiation, precisely at  $t: 0$  seconds, the windshield is notably enveloped in a misty layer.

Moving to Figure 32, a juxtaposition between the analysis and test results at the 300-second is presented. It is noteworthy that regions manifesting defogging effects are concentrated proximate to the instrument panel, aligning with the defroster duct's designated location.

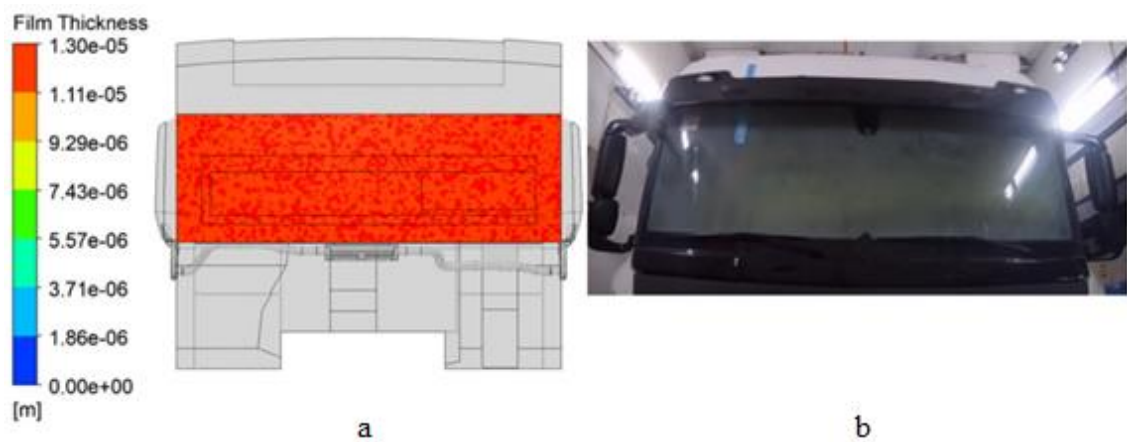


Figure 31. Comparison of Results (a. Current Model; b. Test Cabin) ( $t: 0$  s)

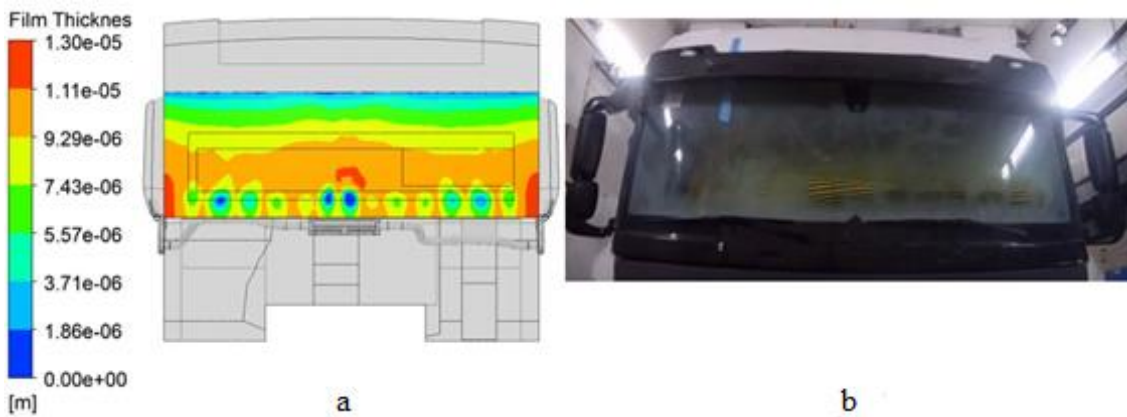


Figure 32. Comparison of Results (a. Current Model; b. Test Cabin) ( $t: 300$  s)

In continuing to Figure 33, a comparison unfolds between the analysis result and the test outcome at 600 seconds. Notably, the dissipated areas migrate towards regions A and B of the glass. The crux of the evaluation lies in the acceptance criterion, where observable regions in the test expand over a broader expanse compared to the analytically



clearly defogged areas. Considering the metric of visibility enhancement at values below  $5 \times 10^{-6}$  m film thickness, the congruence between the test and simulation results becomes apparent. This concordance underscores the alignment of the empirical and analytical perspectives.

In Figure 34, the status of both the analysis and test at the 900-second mark is depicted. Notably, a significant portion of the windshield exhibits successful defogging. However, condensation becomes discernible in the corner regions of the windshield, proximate to the side mirror.

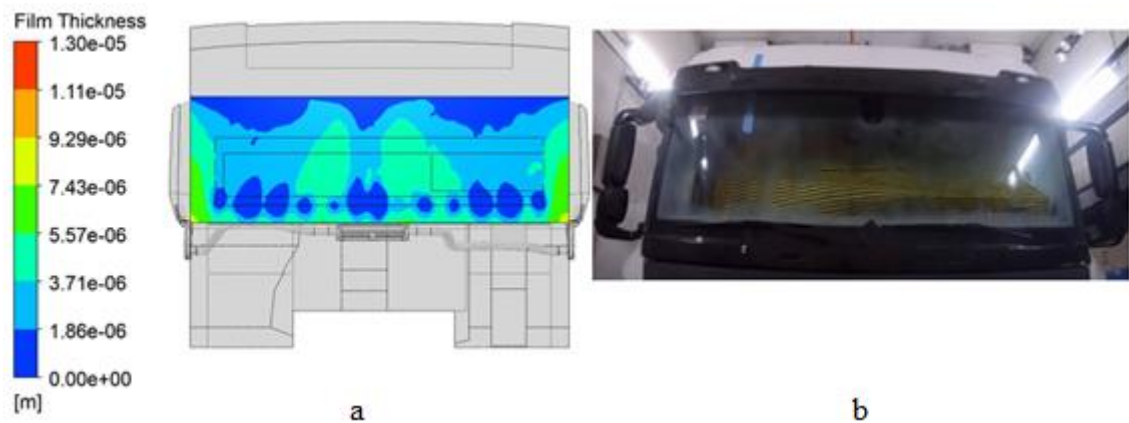


Figure 33. Comparison of Results (a. Current Model; b. Test Cabin) (t: 600 s)



Figure 34. Comparison of Results (a. Current Model; b. Test Cabin) (t: 900 s)

Figure 35 illustrates the status of both the analysis and test at the 1200-second mark, representing the critical evaluation point guided by the acceptance criterion. Notably, the fog that initially obscured the windshield has entirely dissipated. This pivotal juncture underscores the efficacy of the defogging process, culminating in the successful removal of condensation and the restoration of optimal visibility.

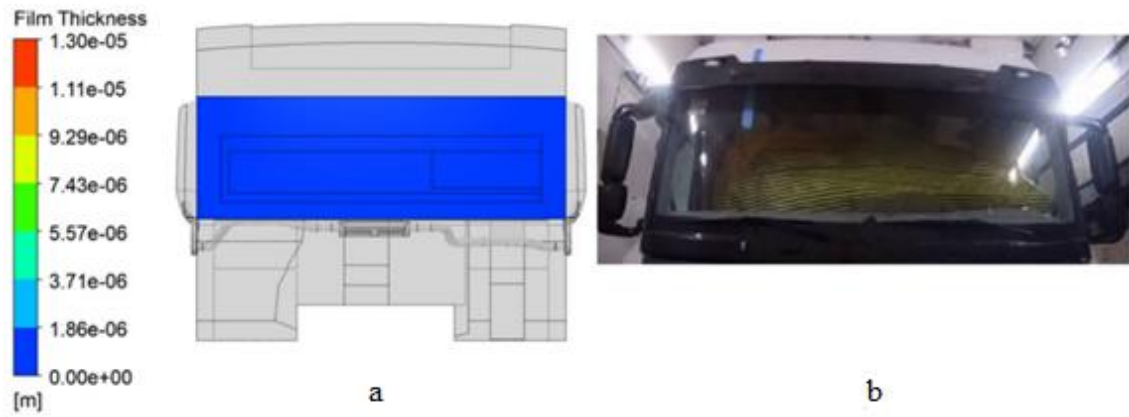


Figure 35. Comparison of Results (a. Current Model; b. Test Cabin) (t: 1200 s)

Table 14 shows percentages of defogged areas on the windshield at the acceptance criteria stage. The first part of results expresses the analysis results, the second part expresses the test results. Net area refers to the surfaces where the fog is completely dissolved.

Table 14. The percentages of defogged areas on the windshield

Time	Acceptance Criteria	Analysis Results (Net area)	Test Results (Net area)
600 s	Area A 90%	Area A 3%	Area A 5%
	Area B 80%	Area B 8%	Area B 12%
1200 s	Area A+B 100 %	Area A 100% Area B 100%	Area A 100% Area B 100%

## CHAPTER 7

### MODEL OPTIMIZATION

Optimizing model systems using ANSYS simulations allows for the design of energy-efficient and effective heating and cooling distribution systems. This process involves a combination of numerical simulations, optimization algorithms, and validation to ensure that the optimized duct system meets the specific performance criteria for HVAC applications.

In this section, we first investigate the effect of defroster duct size and location on defrosting. We use the  $2^3$  full factorial experimental design methodology to investigate the effects of factors on defogging time. The experimental design is conducted using Design Expert Version 11.1.0.1 software and analysis Experimental design consists of two levels and three factors. The experiment is reviewed with Designer Software. In the end, the result of the analysis of variance is evaluated and suggestions are given to develop the experiment and to observe the effect of factors. The simulation design consists of two parts. In the first part, the section taken from the cabin is examined. Analyzes were performed in 2D. The effect of defroster duct size and location on glass temperature increase was investigated. In the second part, analyzes were carried out in 3D. The film thickness was examined in 600 seconds. The effect of defroster duct size and location on film thickness was examined. Secondly, we examined the defroster duct system. Pressure drop and mass flow were examined in the defroster duct system.

Finally, final analysis was made with the defroster duct system that gave the best results in line with the data obtained. The results were compared with the first validation analysis model. The amount of improvement was observed.

#### 7.1. The Effect of Vent Position Parameters

In our experimentation, we have adopted a two-level factorial design with three factors, denoted as  $2^3$ , resulting in a total of 8 runs. Among these factors, parameter A signifies the distance between the vent and the defroster duct, parameter B represents the width of the vent, and parameter C characterizes the angle of the vent. Notably,



parameters A and C are specifically associated with the vent's location. This factorial design allows us to systematically explore and evaluate the impact of varying distances, widths, and angles of the vent on the performance of the defroster system. The resulting 8 runs provide a comprehensive dataset that enables a thorough analysis of the interactions and influences of these factors, facilitating insights into the optimal configuration for efficient defogging.

### **7.1.1. Cabin Model Geometry and Analysis of Variance**

Our investigation delves into the impact of the HVAC vent position on both 3D and 2D models of a truck. The alteration of the HVAC vent position induces variations in the pressure drop within the system. Specifically, in the 2D model, distinct values of temperature gradient on the glass surface are observed because of the HVAC vent repositioning. Moreover, the change in the HVAC vent position prompts adjustments in the total pressure drop spanning from the vent inlet to the outlet in the 3D model. Concurrently, a discernible shift in the demisting time on the windshield is noted.

These findings underscore the intricate relationship between HVAC vent position alterations and the consequential effects on pressure dynamics and demisting performance, offering valuable insights into the optimization of vehicle climate control systems. Figure 37 and Figure 39 shows the parameters of experiment design 2D and 3D truck cabin models. A parameter is the distance measure of the vent, B parameter is the vent width measurement and C parameter is the angle of vent for experimental design. Note: Boundary conditions are detailed in chapter 5.3., and analysis stages are detailed in chapter 6.3.

#### **7.1.1.1. Hypothesis for Models**

The hypothesis refers to a scientifically testable statement about the relationship between two or more variables. Table 15 shows the factors and their min-max values. These factors refer to the independent variables that are manipulated in an experiment to study their effects on the dependent variable. Table 16 and 17 show the responses of experiments. The tables contain the minimum and maximum values of the responses. (Observation: 8; Analysis: Factorial)

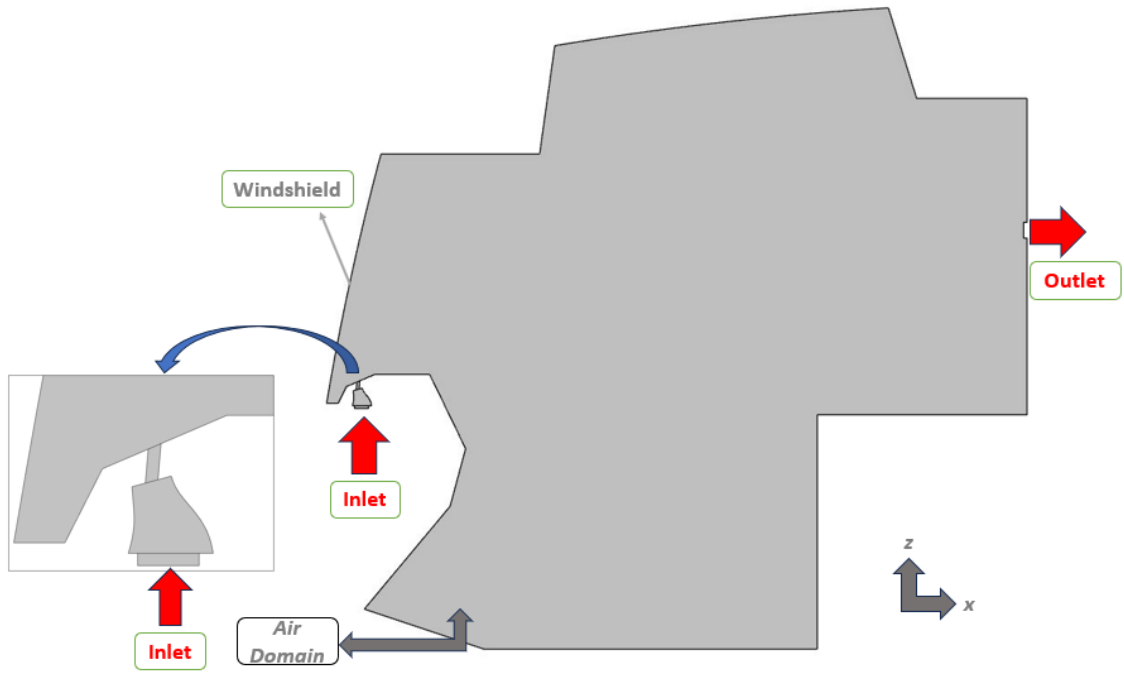


Figure 36. Truck Cabin (2D Model)

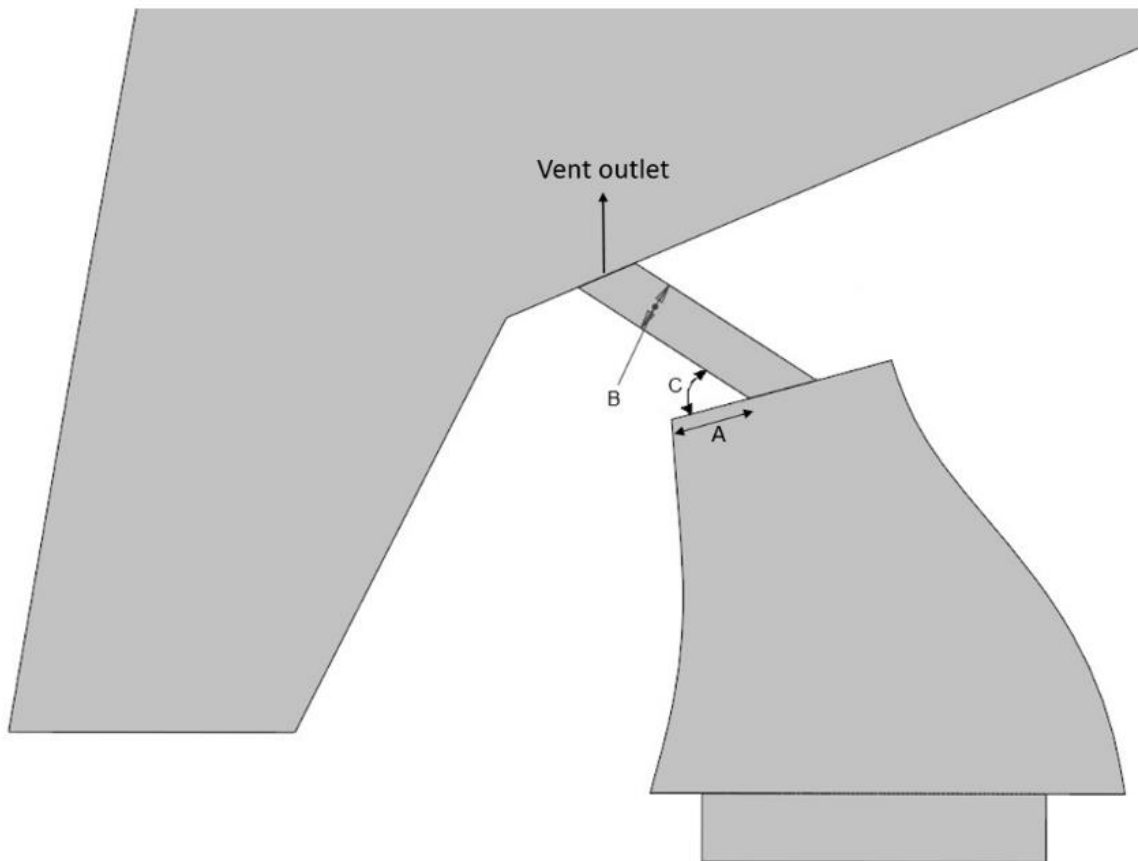


Figure 37. Parameters for 2D Model

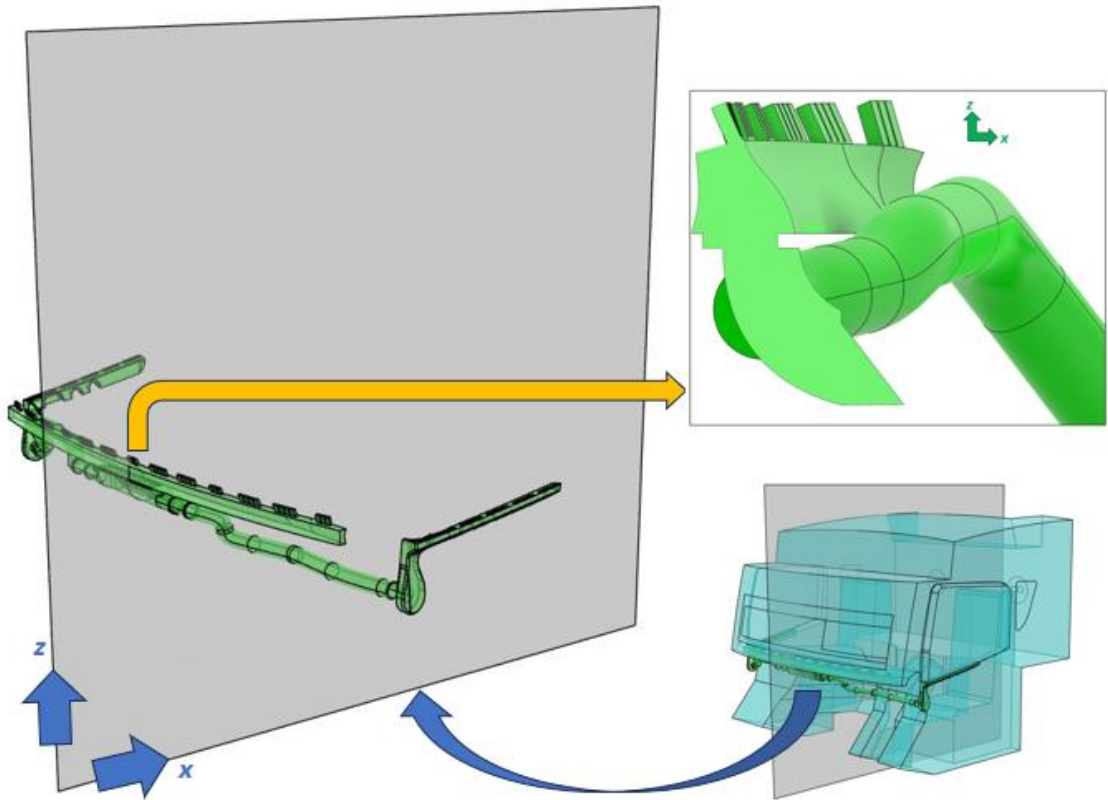


Figure 38. Truck Cabin (3D Model)

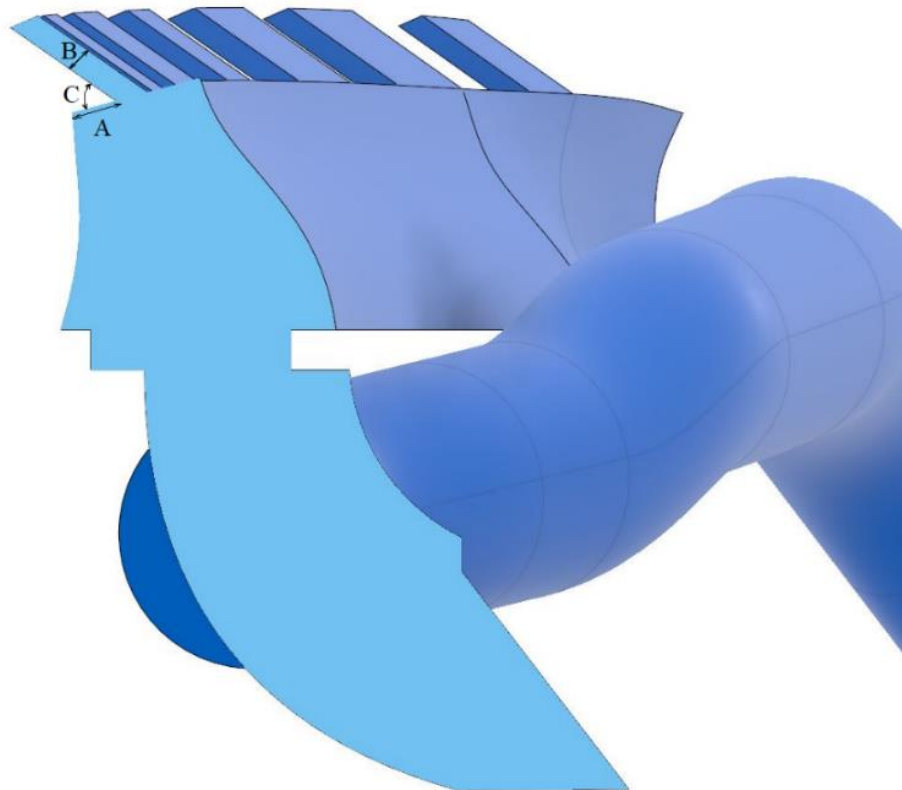


Figure 39. Parameters for 3D Model (xz Section View)

Response Variable (Dependent Variable): This is the main outcome or variable of interest that researchers measure to assess the effects of the independent variables. The response variable is what researchers want to understand, explain, or predict.

Independent Variable (Factor): These are the variables that the researcher manipulates or controls in the experiment to observe their effects on the response variable. Independent variables are the potential causes or predictors of changes in the response.

Levels: Each independent variable may have different levels or values. The combination of levels across all independent variables defines the experimental conditions or treatments.

Observation: There are eight sets of data or measurements collected in your experiment. Each observation represents a unique combination of variables or conditions that are being studied.

Table 15. Factors for Models

Factor	Name	Units	Min	Max	Mean	Std. Dev.
A	Distance A	mm	5	9	7	2.14
B	Distance B	mm	5	8	6.50	1.60
C	Angle C	Degree	50	110	80	32.07

Table 16. Responses for 2D Model

Response	Name	Units	Min	Max
R1	Temperature Gradient of Windshield	K/m	4.993	6.456
R2	Pressure Drop	Pa	50.15	169.02

Table 17. Responses of 3D Model

Response	Name	Units	Min	Max
R1	Average Film Thickness on A Windshield (t: 600 s)	m	$4.209 \times 10^{-7}$	$2.299 \times 10^{-6}$
R2	Average Film Thickness on B Windshield (t: 600 s)	m	$1.014 \times 10^{-7}$	$1.503 \times 10^{-6}$
R3	Average Film Thickness on C Windshield (t: 600 s)	m	$4.094 \times 10^{-7}$	$1.588 \times 10^{-6}$

### 7.1.1.2. Design Layout for Models

Design Expert Software is a utility for setting up an ideal experiment. The meanings of the terms specified in the Design Expert Software are as follows.

Table 18 and 19 show that design layout of experiments. The sequence in which experimental runs are conducted can influence the results, particularly if there's a risk of carryover effects. Randomization of the order of runs can help mitigate this.

Table 18. Design Layout for 2D Model

Std	Run	Factor 1 A: Distance A (mm)	Factor 2 B: Distance B (mm)	Factor 3 C: Angle C (Degree)
8	1	9	8	110
5	2	5	5	110
3	3	5	8	50
6	4	9	5	110
2	5	9	5	50
4	6	9	8	50
1	7	5	5	50
7	8	5	8	110

Table 19. Design Layout for 3D Model

Std	Run	Factor 1 A: Distance A (mm)	Factor 2 B: Distance B (mm)	Factor 3 C: Angle C (Degree)
8	1	9	8	110
4	2	9	8	50
3	3	5	8	50
6	4	9	5	110
2	5	9	5	50
5	6	5	5	110
7	7	5	8	110
1	8	5	5	50

### 7.1.1.3. Half Normal Plot for Models

Half Normal Plot is a graphical tool. It helps to predict and order which factors effects are important and which are not. The absolute value of each effect (plotted as squares) on a half-normal probability plot is shown by the Design Expert application (Stat-Ease 2023).

Figure 40 and Table 20 shows the half normal plot and model effects of temperature gradient of windshield. Figure 41 and Table 21 shows the half normal plot and model effects of pressure drop between inlet and vent outlet (cabin inlet). A refers to distance A, B refers to distance B, and C refers to Angle C. Blue squares have negative effects, orange squares are the positive effects. We select significant terms of models. The temperature gradient models for Analysis of Variance (ANOVA) are A, B, C, AB, BC, and AC and pressure drop models for Analysis of Variance (ANOVA) are A, B, C, BC, and AC respectively.

Table 20. Model Effects of Temperature Gradient

Models	Positive Effects	Negative Effects
A	x	
B	x	
C		x
AB		x
AC	x	
BC		x

Table 21. Model Effects of Pressure Drop

Models	Positive Effects	Negative Effects
A		x
B		x
C		x
AC		x
BC		x

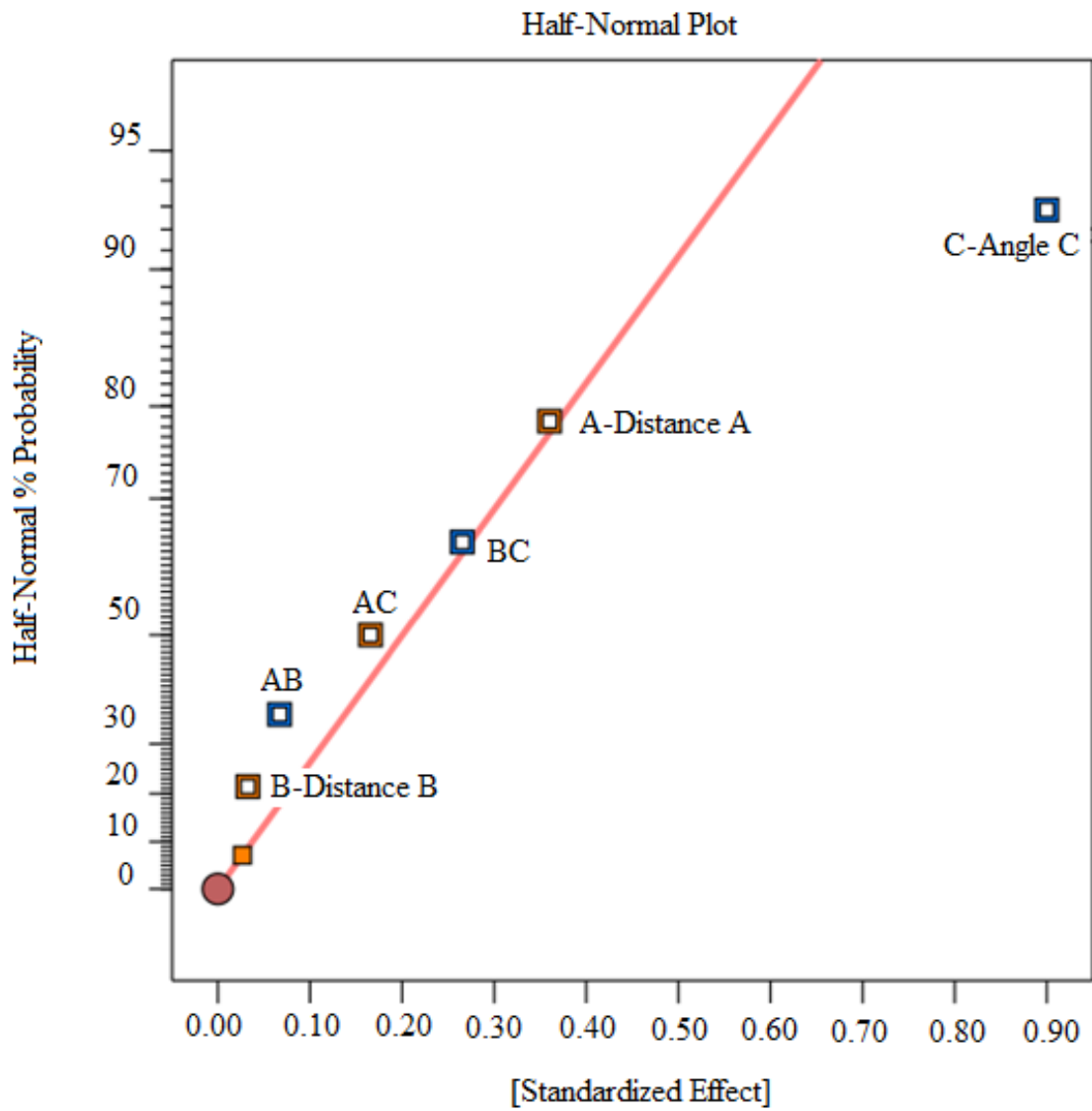


Figure 40. Temperature Gradient - Half Normal Plot

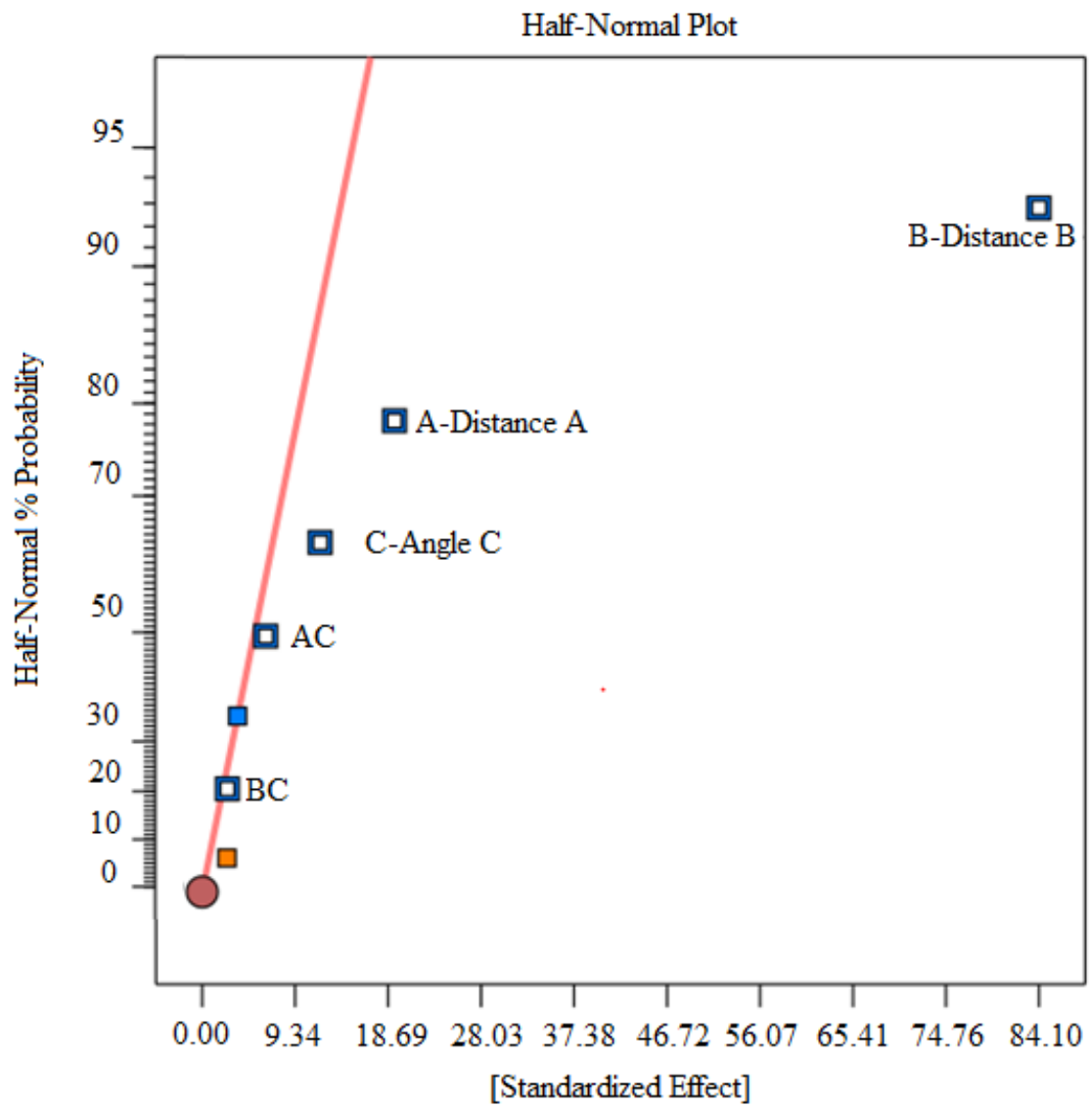


Figure 41. Pressure Drop- Half Normal Plot



Figures 42, 43, and 44, accompanied by Tables 22, 23, and 24, present comprehensive half normal plots and model effects for A, B, and C windshields, respectively. Notably, A corresponds to distance A, B to distance B, and C to Angle C. Blue squares denote negative effects, while orange squares signify positive effects. Further, we conducted Analysis of Variance (ANOVA) to identify significant terms for each windshield type. The significant terms are A, B, C, AC, and BC for A Windshield; A, B, C, AB, and BC for B Windshield; and A, B, C, AB, and BC for C Windshield.

Table 22. Model Effects of Average Film Thickness on A Windshield

Models	Positive Effects	Negative Effects
A		x
B		x
C	x	
AC		x
BC		x

Table 23. Model Effects of Average Film Thickness on B Windshield

Models	Positive Effects	Negative Effects
A	x	
B		x
C	x	
AB		x
BC		x

Table 24. Model Effects of Average Film Thickness on C Windshield

Models	Positive Effects	Negative Effects
A		x
B		x
C	x	
AB		x
BC		x

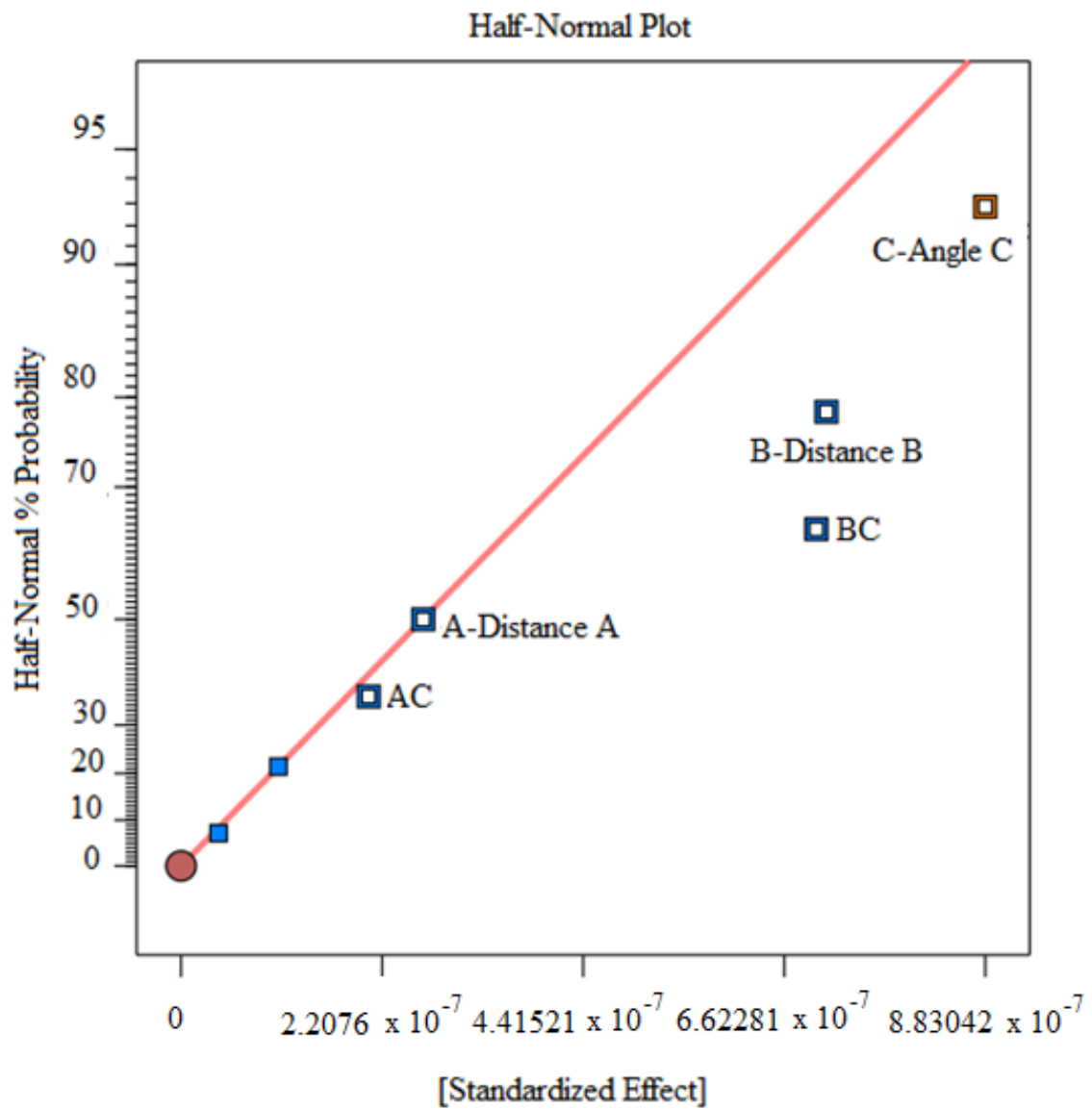


Figure 42. Average Film Thickness on A Windshield (t: 600 s)

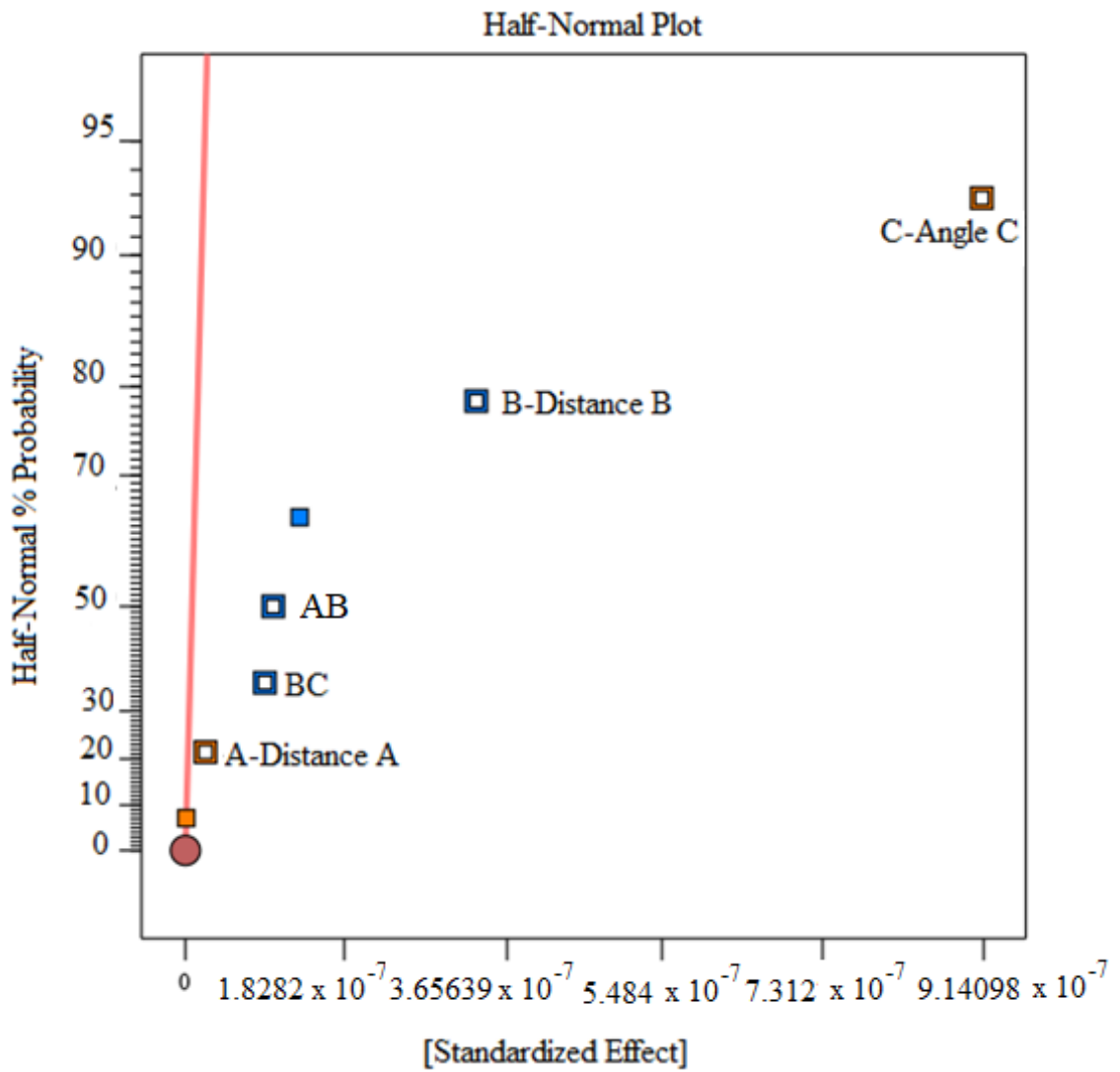


Figure 43. Average Film Thickness on B Windshield (t: 600 s)

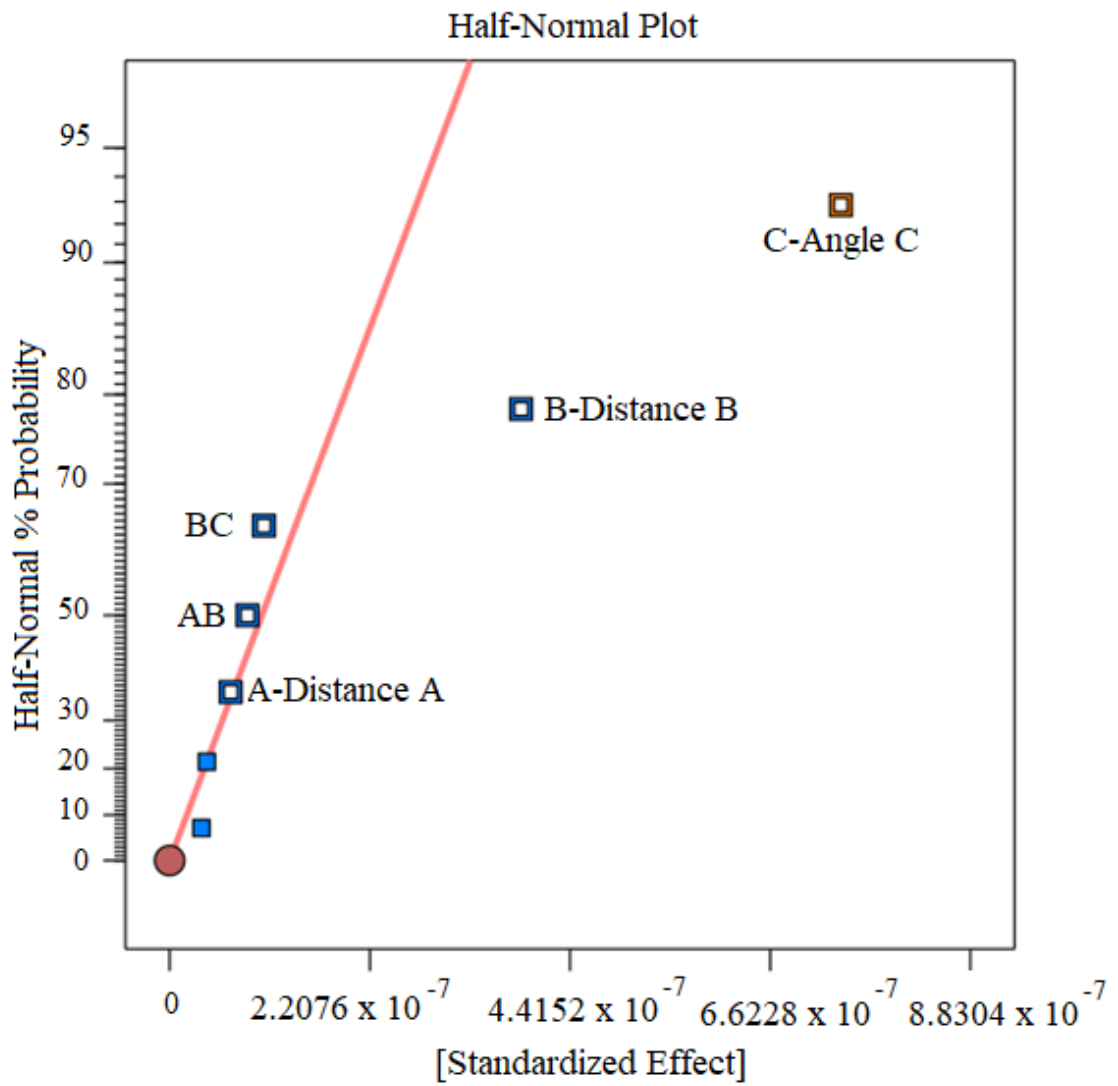


Figure 44. Average Film Thickness on C Windshield (t: 600 s)

#### 7.1.1.4. Analysis of Variance (ANOVA)

Factorial models refer to experimental designs that involve multiple factors or independent variables. These factorial models aim to examine the effects of different combinations of factors on the dependent variable. Table 25 and 26 are for 2D model and Table 27, 28, and 29 are for 3D model. The utilization of Analysis of Variance (ANOVA) allows for a rigorous examination of variance and facilitates informed comparisons between different vent positions in both 2D and 3D models.

Table 25 shows ANOVA for selected factorial model (temperature gradient). The significance of the model can be determined by the Model F-value, which in this case is 244.47. With a significance level of 4.89 %, there is a low probability that such a large F-value could occur due to random variation. Model terms with p-values less than 0.0500 are considered significant, indicating that variables A, and C are significant in this case. On the other hand, model terms with p-values greater than 0.1000 are considered not significant. They are B, AB, AC, and BC respectively. Therefore, the model is significant. I have enough evidence to reject the null hypothesis.

Table 25. Temperature Gradient -ANOVA

Source	Sum of	df	Mean	F-value	p-value	
Model	2.09916	6	0.34986	244.466	0.04892	Significant
A-Distance A	0.261	1	0.261	182.376	0.04705	
B-Distance B	0.00215	1	0.00215	1.49891	0.43602	
C-Angle C	1.62992	1	1.62992	1138.9	0.01886	
AB	0.00905	1	0.00905	6.32029	0.24101	
AC	0.05528	1	0.05528	38.6256	0.10156	
BC	0.14178	1	0.14178	99.0676	0.06375	
Residual	0.00143	1	0.00143			
Cor Total	2.1006	7				

Table 26 shows ANOVA for selected factorial model (pressure drop). The significance of the model can be determined by the Model F-value, which in this case is 160.89. With a significant level of 0.619 %, there is a low probability that such a large F-value could occur due to random variation.

Model terms with p-values less than 0.0500 are considered significant, indicating that variables A, and B are significant in this case. On the other hand, model terms with p-values greater than 0.1000 are considered not significant. They are C, AB, AC, and BC respectively. Therefore, the model is significant. I have enough evidence to reject the null hypothesis.

Table 26. Pressure Drop -ANOVA

Source	Sum of	df	Mean	F-value	p-value	
Model	15269.1	5	3053.83	160.891	0.00619	Significant
A-Distance A	747.684	1	747.684	39.3918	0.02446	
B-Distance B	14145.6	1	14145.6	745.262	0.00134	
C-Angle C	281.319	1	281.319	14.8213	0.06133	
AC	81.6642	1	81.6642	4.30248	0.17376	
BC	12.8525	1	12.8525	0.67713	0.49708	
Residual	37.9615	2	18.9807			
Cor Total	15307.1	7				

Table 27 shows ANOVA for selected factorial model (Average Film Thickness on A Windshield). The significance of the model can be determined by the Model F-value, which in this case is 57.34. With a significance level of 1.72 %, there is a low probability that such a large F-value could occur due to random variation.

Table 27. Average Film Thickness on A Windshield -ANOVA

Source	Sum of	df	Mean	F-value	p-value	
Model	$3.763 \times 10^{-12}$	5	$7.527 \times 10^{-13}$	57.3393	0.01723	Significant
A-Distance A	$1.415 \times 10^{-13}$	1	$1.415 \times 10^{-13}$	10.7795	0.08158	
B-Distance B	$1.004 \times 10^{-12}$	1	$1.004 \times 10^{-12}$	76.5125	0.01282	
C-Angle C	$1.55 \times 10^{-12}$	1	$1.559 \times 10^{-12}$	118.796	0.00831	
AC	$8.489 \times 10^{-14}$	1	$8.489 \times 10^{-14}$	6.46654	0.12606	
BC	$9.733 \times 10^{-13}$	1	$9.733 \times 10^{-13}$	74.1417	0.01322	
Residual	$2.625 \times 10^{-14}$	2	$1.312 \times 10^{-14}$			
Cor Total	$3.789 \times 10^{-12}$	7				

In the Table 27, model terms with p-values less than 0.0500 are considered significant, indicating that variables B, C and BC are significant in this case. On the other hand, model terms with p-values greater than 0.1000 are considered not significant. They are A and AC respectively. Therefore, the model is significant. I have enough evidence to reject the null hypothesis.

Table 28 shows ANOVA for selected factorial model (Average Film Thickness on B Windshield). The significance of the model can be determined by the Model F-value, which in this case is 22.44. With a significance level of 4.32 %, there is a low probability that such a large F-value could occur due to random variation. Model terms with p-values less than 0.0500 are considered significant, indicating that variables C is significant in this case. On the other hand, model terms with p-values greater than 0.1000 are considered not significant. They are A, B, AB, and BC respectively. Therefore, the model is significant. I have enough evidence to reject the null hypothesis.

Table 28. Average Film Thickness on B Windshield -ANOVA

Source	Sum of	df	Mean	F-value	p-value	
Model	$1.932 \times 10^{-12}$	5	$3.864 \times 10^{-13}$	22.43784	0.043213	significant
A-Distance A	$1.067 \times 10^{-15}$	1	$1.067 \times 10^{-15}$	0.06199	0.826612	
B-Distance B	$2.230 \times 10^{-13}$	1	$2.230 \times 10^{-13}$	12.951	0.069285	
C-Angle C	$1.671 \times 10^{-12}$	1	$1.671 \times 10^{-12}$	97.02821	0.01015	
AB	$2.030 \times 10^{-14}$	1	$2.030 \times 10^{-14}$	1.178816	0.391038	
BC	$1.669 \times 10^{-14}$	1	$1.669 \times 10^{-14}$	0.969173	0.428675	
Residual	$3.444 \times 10^{-14}$	2	$1.722 \times 10^{-14}$			
Cor Total	$1.966 \times 10^{-12}$	7				

Table 29 shows ANOVA for selected factorial model (Average Film Thickness on C Windshield). The significance of the model can be determined by the Model F-value, which in this case is 98.92. With a significance level of 1.0 %, there is a low probability that such a large F-value could occur due to random variation. Model terms with p-values less than 0.0500 are considered significant, indicating that variables B and C are significant in this case. On the other hand, model terms with p-values greater than 0.1000 are considered not significant. They are A, AB, and BC respectively. Therefore, the model is significant. I have enough evidence to reject the null hypothesis.

Table 29. Average Film Thickness on C Windshield -ANOVA

Source	Sum of	df	Mean	F-value	p-value	
Model	$1.442 \times 10^{-12}$	5	$2.884 \times 10^{-13}$	98.92437	0.010038	Significant
A-Distance A	$9.078 \times 10^{-15}$	1	$9.078 \times 10^{-15}$	3.113688	0.219684	
B-Distance B	$3.005 \times 10^{-13}$	1	$3.005 \times 10^{-13}$	103.0744	0.009563	
C-Angle C	$1.096 \times 10^{-12}$	1	$1.096 \times 10^{-12}$	375.9438	0.002649	
AB	$1.477 \times 10^{-14}$	1	$1.477 \times 10^{-14}$	5.068662	0.153205	
BC	$2.163 \times 10^{-14}$	1	$2.163 \times 10^{-14}$	7.421269	0.112467	
Residual	$5.831 \times 10^{-15}$	2	$2.915 \times 10^{-15}$			
Cor Total	$1.447 \times 10^{-12}$	7				

### 7.1.1.5. Optimization Results

We have 54 solutions for 2D model optimization and 70 solutions for 3D model optimization. Our goals are to maximize the temperature gradient of the windshield, and to minimize the pressure drop between the inlet and the vent outlet for 2D model and to minimize the Average Film Thickness (AFT) on the windshield for 3D model. Table 30 show that constraints for models and Table 31 and 32 show that selected tables for models.

Table 30. Constraints for Models

Name	Goal	Units	Lower Limit	Upper Limit
A: Distance A	is in range	mm	5	9
B: Distance B	is in range	mm	5	8
C: Angle C	is in range	Degree	50	110
Temperature Gradient	max	K/m	4.993	6.456
Pressure Drop	min	Pa	50.15	169.02
AFT on A Windshield (t: 600 s)	min	m	$4.209 \times 10^{-7}$	$2.299 \times 10^{-6}$
AFT on B Windshield (t: 600 s)	min	m	$1.014 \times 10^{-7}$	$1.503 \times 10^{-6}$
AFT on C Windshield (t: 600 s)	min	m	$4.094 \times 10^{-7}$	$1.588 \times 10^{-6}$



Table 31. Selected Solution Table for 2D Model

Number	Distance A	Distance B	Angle C	Desirability	
1	9.00	8.00	50.80	0.907	Selected

Table 32. Selected Solution Table for 3D Model

Number	Distance A	Distance B	Angle C	Desirability	
1	8.99	7.99	50.90	0.98	Selected

### 7.1.1.6. Model Cube Graph and Desirability

We examine Figure 45 and Figure 46 and to see the predicted response as a function of three factors that create significant effects. This chart shows how three factors come together to influence the response. All values shown are estimated values, allowing plots to be made even if actual data is missing (Stat-Ease 2023). The desirability graphs show the optimal design values.

We have strong data to reject the null hypothesis based on the results of the statistical analysis. The null hypothesis is rejected when there is a substantial effect or relationship in the data that cannot be explained by chance alone.

The alternative hypothesis is strongly supported by rejecting the null hypothesis, but this does not mean that the alternative hypothesis is necessarily true. The established threshold for assuming the probability of Type I error is represented by the significance level, which is commonly set at 0.05. We have increased the rigor of the evaluation and decreased the possibility of incorrectly rejecting the null hypothesis by choosing a lower significance level.

Ultimately, the results of the statistical analysis improve our understanding of the current research question by providing strong evidence supporting the existence of a significant effect or relationship in the data.

In light of these meticulous statistical analyses, our study not only advances the current understanding of the investigated phenomena but also underscores the reliability and validity of the observed effects, thus fostering confidence in the broader implications of our research within the academic community.

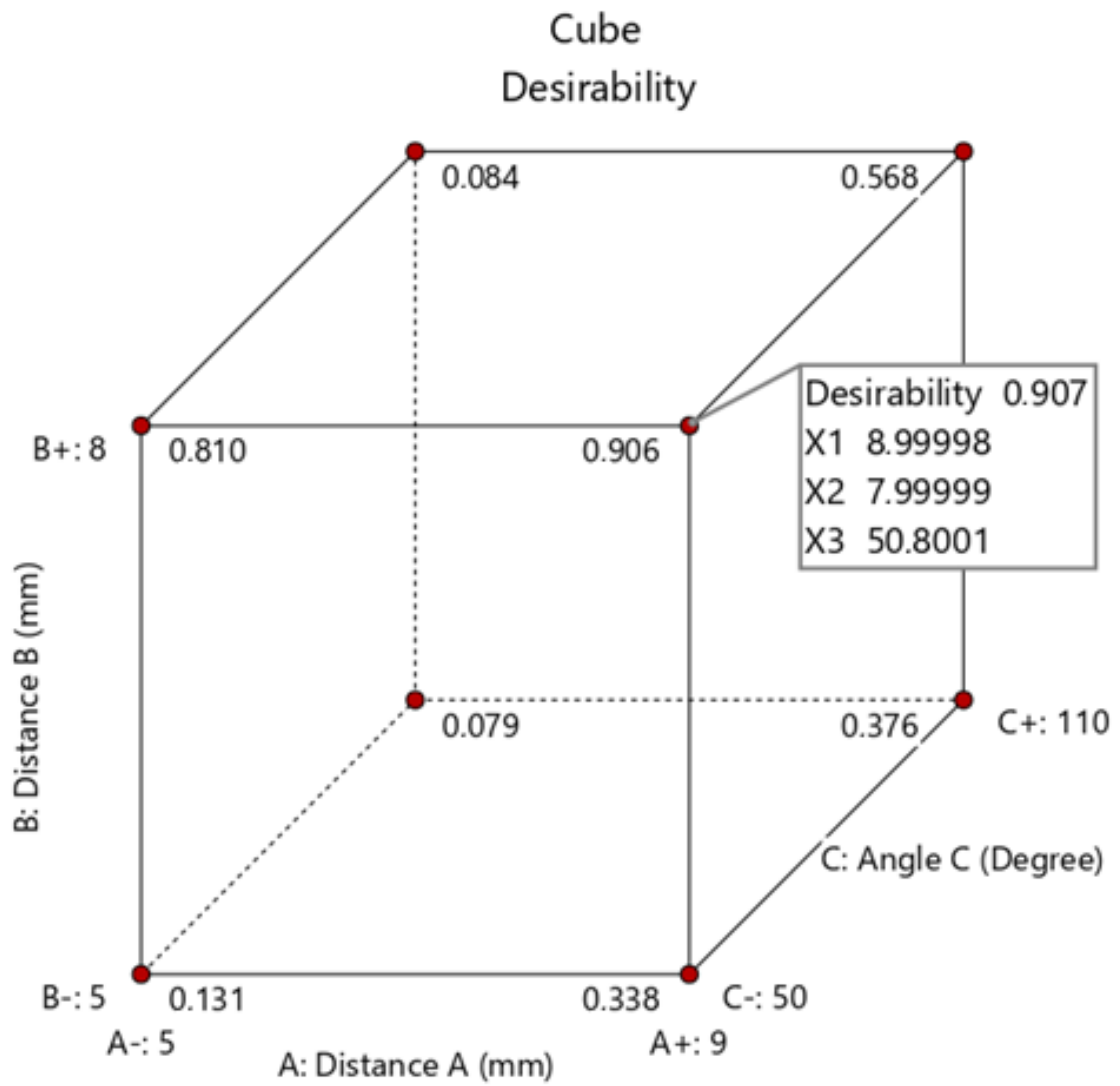


Figure 45. Cube Desirability for 2D Model

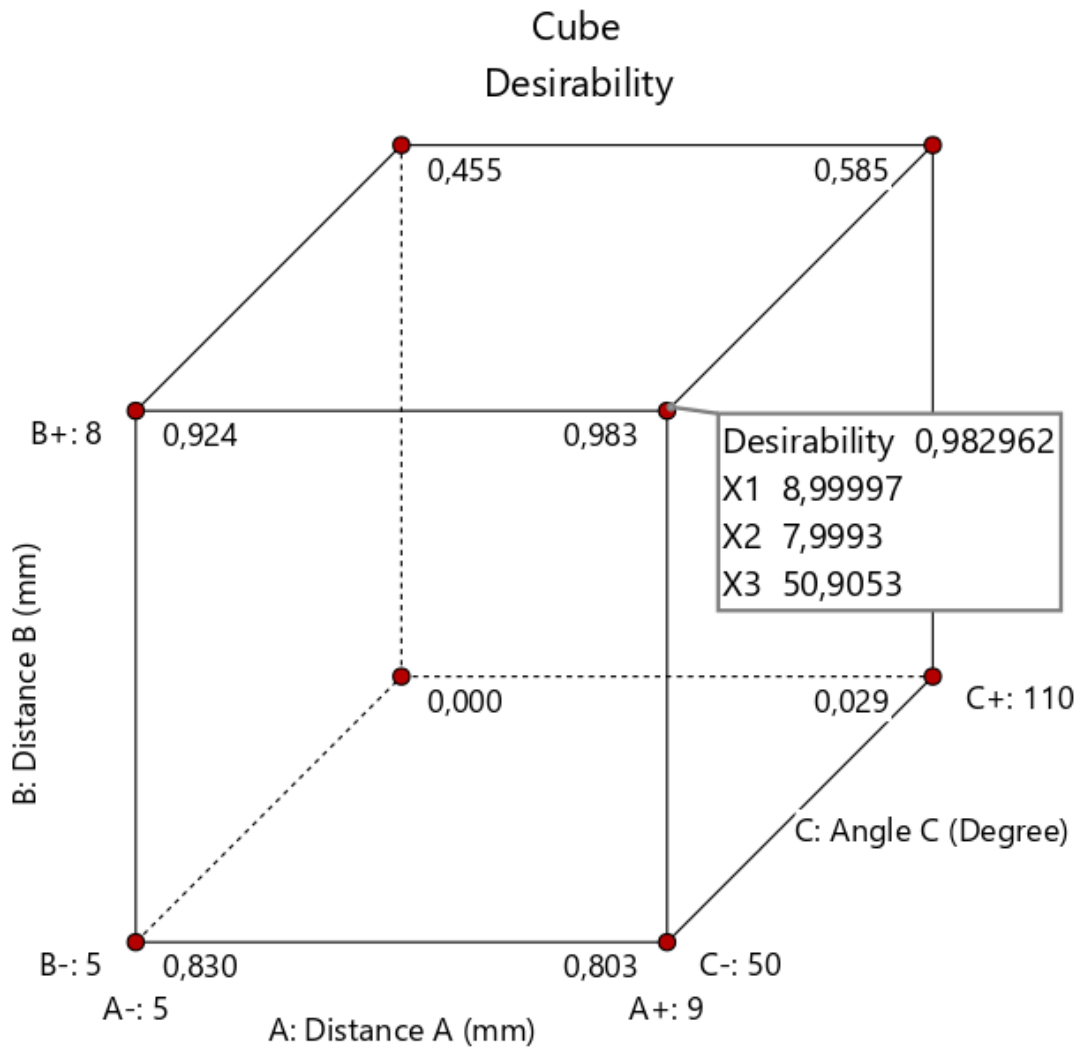


Figure 46. Cube Desirability for 3D Model

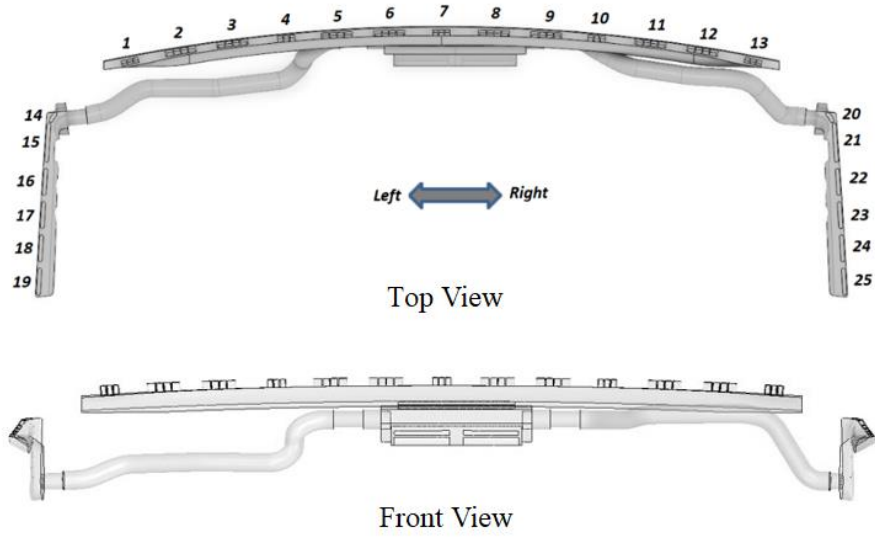
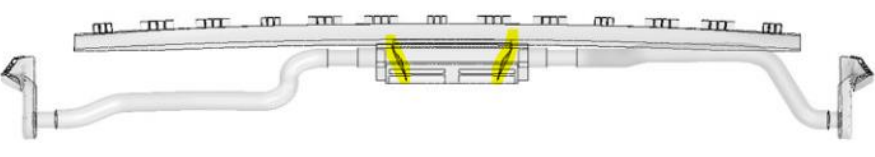
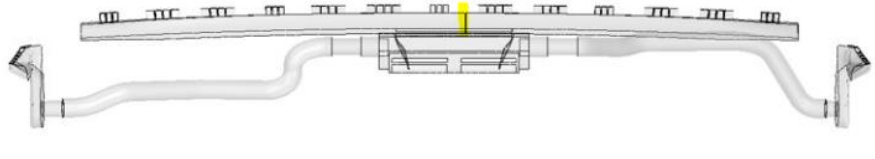
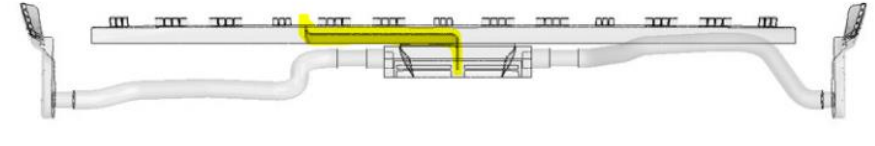
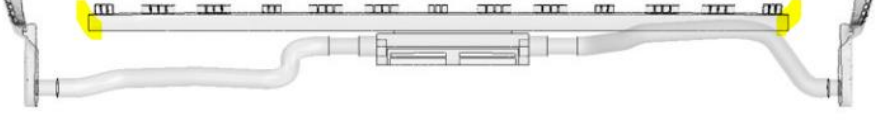
## 7.2. The Effect of Defroster Duct Shape

Within the defrosting duct, optimal alignment of deflectors with the airflow holds paramount importance, ensuring a seamless transition and preventing undue contraction in the section. Excessive shrinkage rates may impede airflow, detrimentally affecting the vehicle's defogging performance. The correlation between the average air velocity in distinct windshield zones and the corresponding average Nusselt number reveals a robust and linear relationship. The augmentation of the coverage area with heightened air velocity promotes enhanced convection and heat transfer capabilities on the windshield. Consequently, the expansive coverage area of elevated air velocity on the windshield emerges as a valuable benchmark for assessing the vehicle's defogging efficacy (Davis, Dage and Hoeschele 2001).

In this section, a discrete examination of the defroster duct model was conducted. Our objective was to augment airflow directed towards the driver's side while concurrently mitigating pressure drop by implementing varied separator designs within the duct pipe. A comparative analysis was undertaken, contrasting the proposed defroster duct models with the existing model in use within the cabin. The corresponding models are visually represented in the appended images, with the revisions highlighted in yellow. (Note: Defroster Duct Model-1 (DF-1) denotes the current model implemented in the cabin.) This deliberate investigation seeks to discern improvements in air distribution and pressure dynamics, thereby contributing to the refinement of the defroster system for enhanced vehicular performance.

As a result, we evaluate the models based on the total air flow rates coming out of the outlets in the driver's area and the pressure drop in the system. We define air intake with constant air flow rate and temperature in all models. In the results section, we visualized the air speeds and streamlines coming out of the outlets. We have indicated the system pressure drop and the flow rate from the outlets in the tables. In the DF-3 model, the flow rate in the driver's area increased at the best rate compared to other models. However, we observe that the total pressure drop in the system increases. The increase in system total pressure drop negatively affects the fan characteristics and causes a decrease in system volumetric flow rate. In the DF-5 model, the system total pressure drop decreased and the total flow rate to the driver's side increased.

Table 33. Defroster Duct Models

<p>DF-1</p>	 <p>Top View</p> <p>Front View</p>
<p>DF-2</p>	
<p>DF-3</p>	
<p>DF-4</p>	
<p>DF-5</p>	

## 7.2.1. Optimization Results

This section pertains to the procedure of examining and illustrating the outcomes of simulation obtained from computational fluid dynamics (CFD) simulations.

Figures 47 and 48 show the streamline lines of the current HVAC duct model used in the vehicle. The air entering from the inlet is divided into 4 parts. It seems that the air speeds coming out of the outlets located in the central area are high.

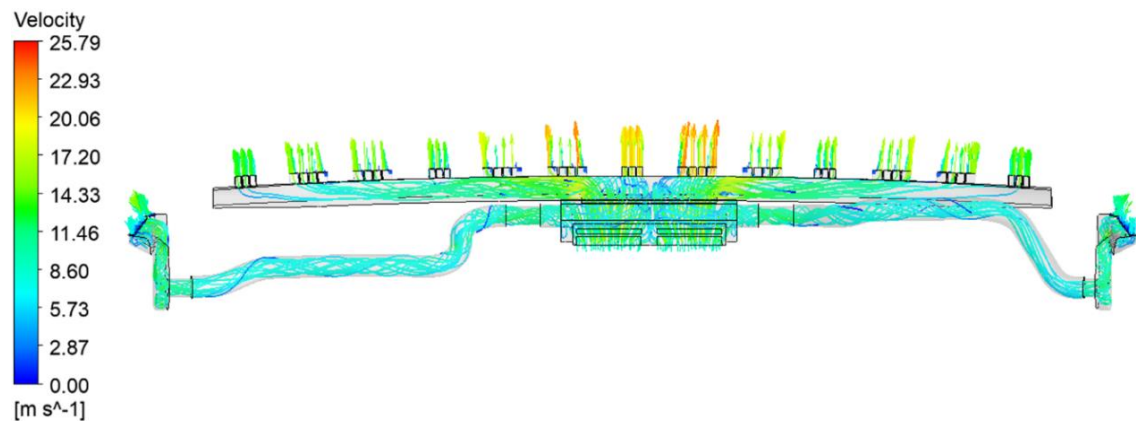


Figure 47. Defroster Duct Model-1 (DF-1)

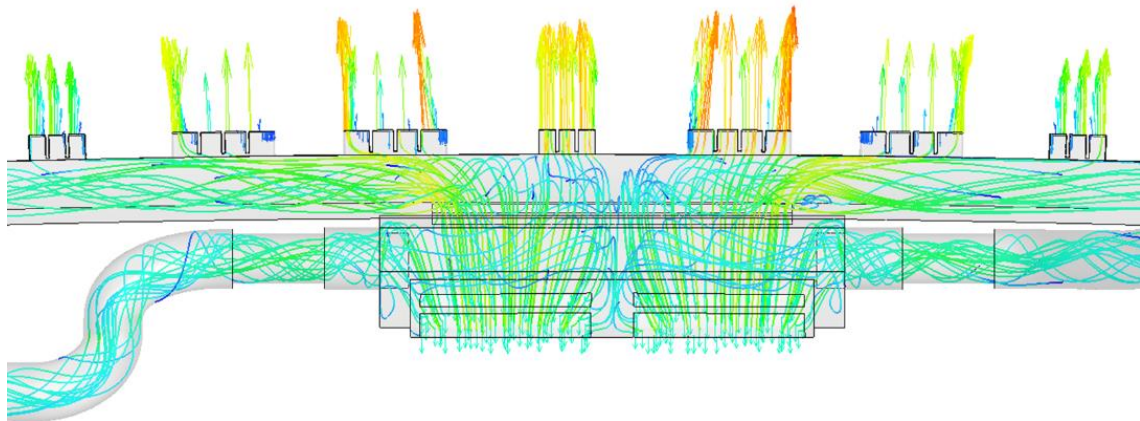


Figure 48. Defroster Duct Model-1

We add separators to distribute the air flow properly in the Defroster Duct Model-1. Additionally, we aim to increase the flow rate at the exits in the driver's area with separators. Figures 49 and 50 show the streamliner of the Defroster Duct Model-2.

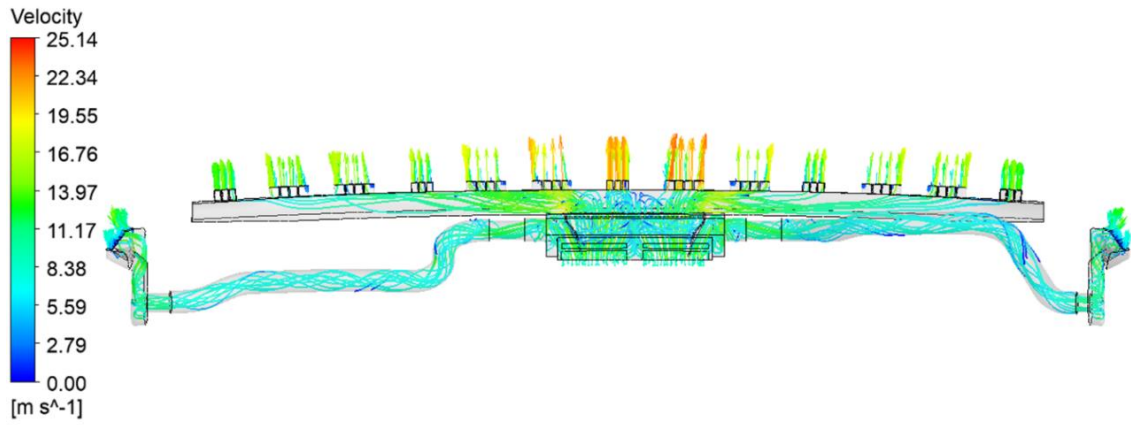


Figure 49. Defroster Duct Model-2 (DF-2)

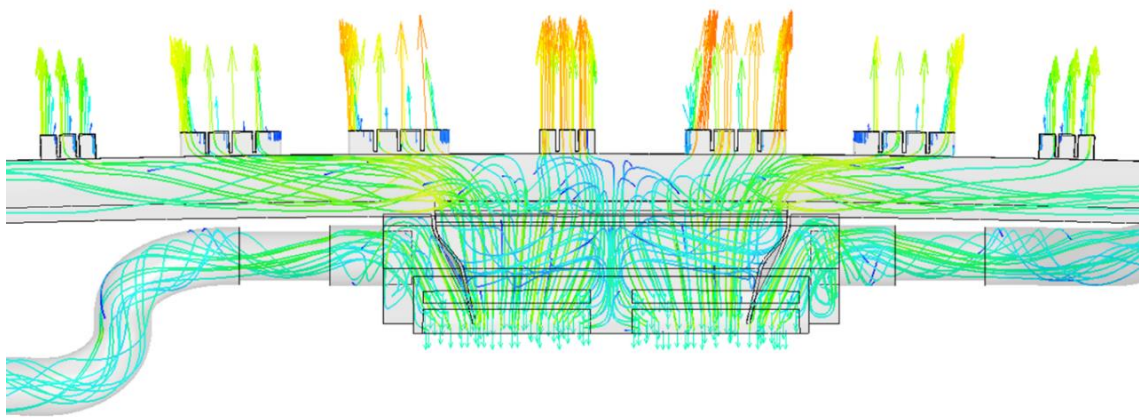


Figure 50. Defroster Duct Model-2

We add a separator to the upper pipe in addition to the separators in DF-2. Figures 51 and 52 show the streamline of the Defroster Duct Model-3.

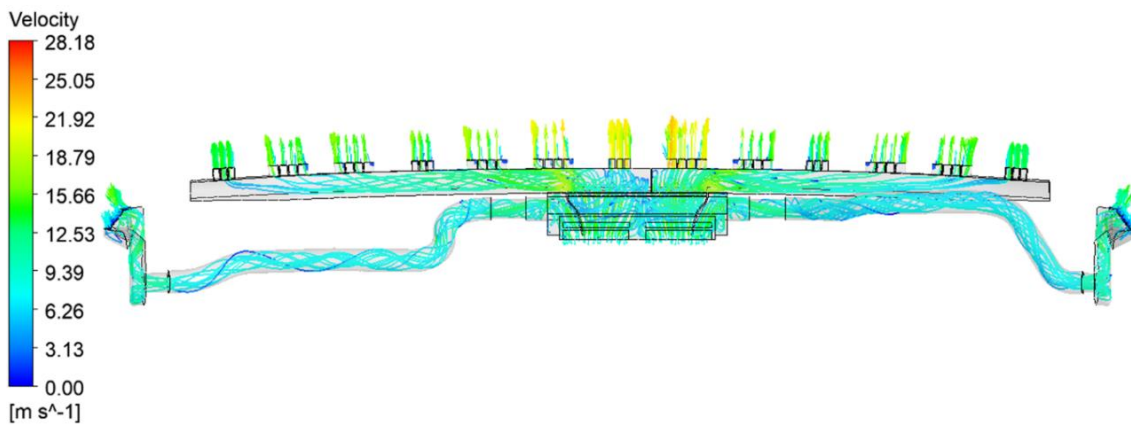


Figure 51. Defroster Duct Model-3 (DF-3)



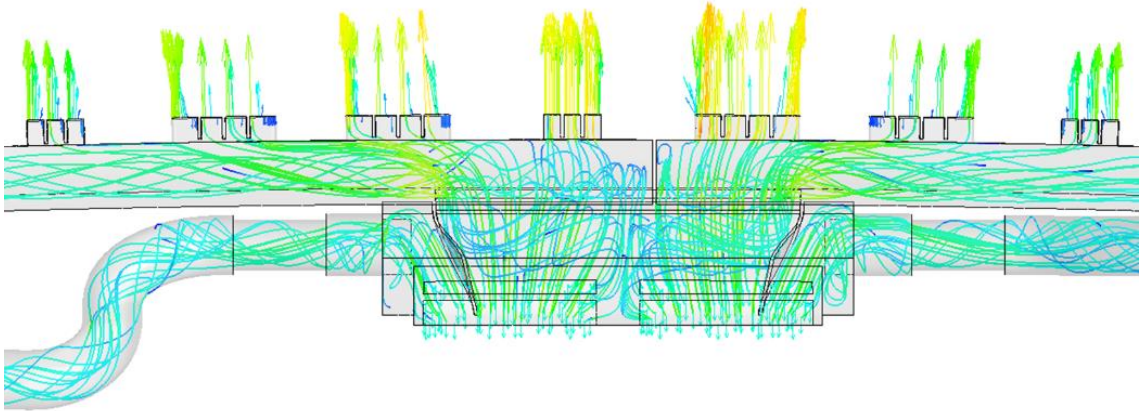


Figure 52. Defroster Duct Model-3

We added a separator starting from the inlet area and extending to the driver area in addition to the separators in DF-2. Figures 53 and 54 show the streamline of the Defroster Duct Model-4.

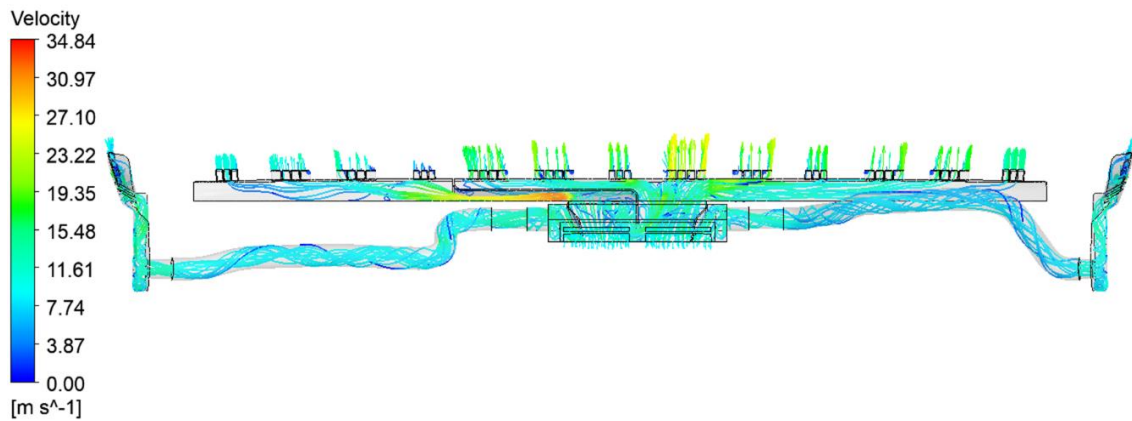


Figure 53. Defroster Duct Model-4 (DF-4)

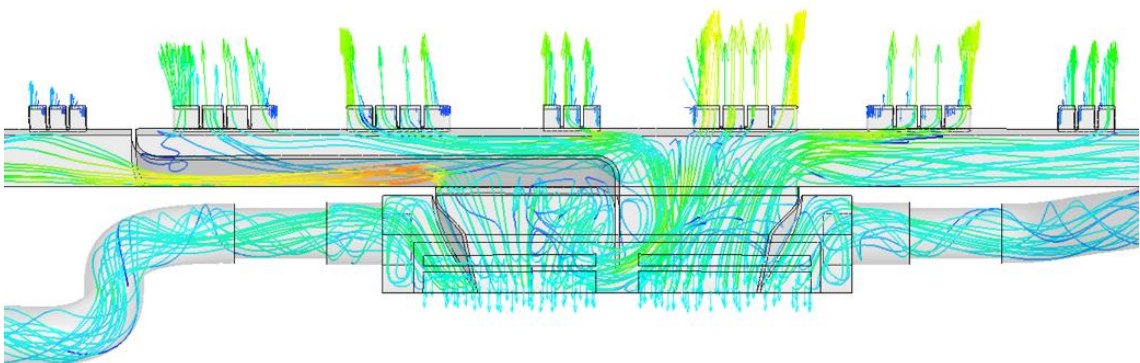


Figure 54. Defroster Duct Model-4



We detect inefficient areas in the end regions of the upper pipe in the DF-1 model. We shorten it to areas close to outlet 1 and 13.

Figures 55 and 56 show the streamliner of the Defroster Duct Model-5.

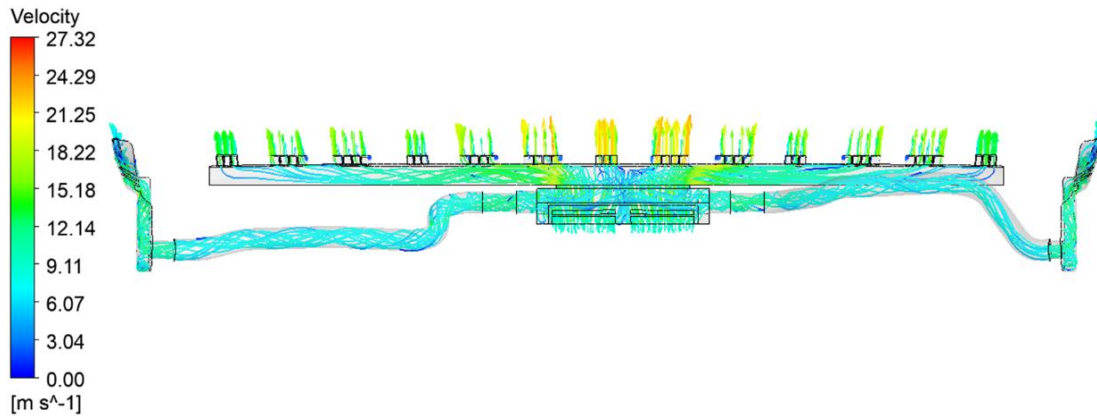


Figure 55. Defroster Duct Model-5 (DF-5)

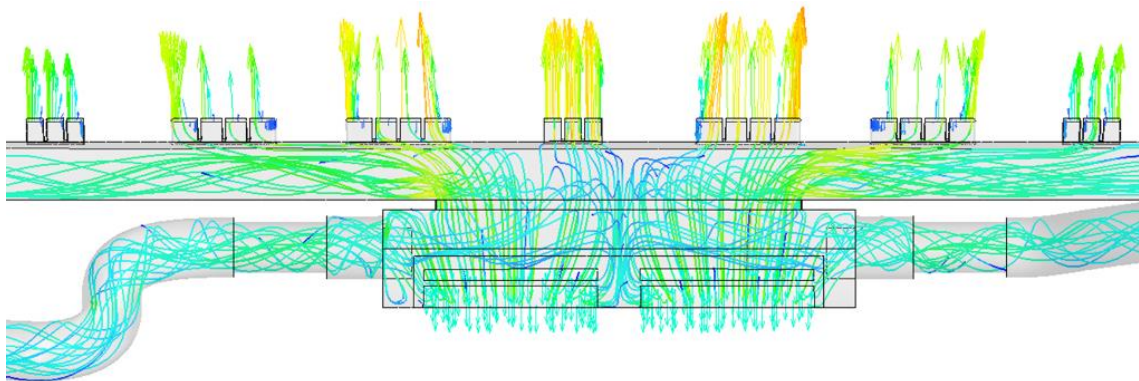


Figure 56. Defroster Duct Model-5

We examine the Percentage of Total Mass Flow Rate of Vents and Total Pressure Drops ( $\Delta P$ ) to evaluate models against each other. Table 34 shows the Percentage of Total Mass Flow Rate of Vents (%) and Table 35 shows the Total Pressure Drop (Pa) between inlet and outlet in the models.

We see an increase in the amount of total air flow rate and pressure drop coming to the driver's area in DF-2 and DF-3. We think that the separator would have a positive effect on DF-4. However, the flow rate in the driver's area decreased. The added separator causes a high Total Pressure Drop ( $\Delta P$ ). The improvement made in the DF-5 increased the flow rate in the driver's area and reduced the total pressure drop in the system.

Table 34. Percentage of Total Mass Flow Rate of Vents (%)

		Percentage of Total Mass Flow Rate of Vents (%)				
		1-2-3-4-5	6-7-8	9-10-11-12-13	14-15-16-17-18-19	20-21-22-23-24-25
Duct Models	DF-1	-23.37	-23.43	-23.41	-14.96	-14.82
	DF-2	-23.91	-22.67	-23.80	-14.91	-14.67
	DF-3	-24.09	-23.40	-22.77	-15.02	-14.70
	DF-4	-21.12	-21.18	-24.84	-17.59	-15.27
	DF-5	-23.42	-23.58	-23.12	-14.91	-14.97

Table 35. The Total Pressure Drop of Duct Models

		Total Pressure Drop (Pa)
Duct Models	DF-1	325.574
	DF-2	331.934
	DF-3	338.098
	DF-4	455.433
	DF-5	325.211

In this section, we undertake an examination of defroster duct models characterized by distinct structural configurations. The assessment of these models is predicated upon the comprehensive analysis of both the aggregate air flow rates emanating from the outlets within the driver's domain and the associated pressure drop in the system. To maintain methodological consistency, we establish uniformity in air intake, ensuring a constant air flow rate and temperature across all models.

The results section features visual representations of air velocities and streamlines emerging from the outlets. Systemic parameters, namely system pressure drop and outlet flow rates, are delineated in tabular form. Within the context of the DF-3 model, noteworthy is the observation that the flow rate within the driver's area exhibits optimal augmentation compared to alternative models. However, concomitant with this enhancement, there is an observable escalation in the overall pressure drop across the system. This rise in total system pressure drop detrimentally impacts fan characteristics, contributing to a concomitant reduction in system volumetric flow rate. Conversely, the

DF-5 model manifests a decline in system total pressure drop, concomitant with an elevation in the aggregate flow rate directed towards the driver's side. Given these salient outcomes, the decision is made to implement the modifications realized in the DF-5 model onto the extant model, a determination substantiated by the data pertaining to system pressure drop and outlet flow rates as encapsulated within the presented tables.

## CHAPTER 8

### RESULTS AND DISCUSSIONS

The misting and defrosting systems used in the vehicle increase energy consumption. Nowadays, this issue becomes more prominent with the increase in electric vehicles. Therefore, we need system improvement efforts. In this study, we aim to reduce energy consumption by making changes to the defroster duct model used in the vehicle.

We conducted an investigation into the impact of changes on the defroster system in a vehicle. This involved altering the angle, width, and position of the vents in addition to introducing various separators into the defroster duct pipe. The study aimed to understand how these modifications influenced the performance of the glass. The results include a comparison between the original vehicle model and the improved model, providing insights into the effectiveness of the adjustments made.

Figure 57 illustrates the condition of both the extant model and the optimized model at time  $t: 0$  s. Initially, the film thickness on the truck's windshield is defined at  $1.3 \times 10^{-5}$  m.

Moving forward, Figure 58 delineates the status of the current model and the optimization model at time  $t: 300$  s. In particular, a heightened degree of defogging is discernible, particularly in regions equipped with vents located at the bottom of the windshield.

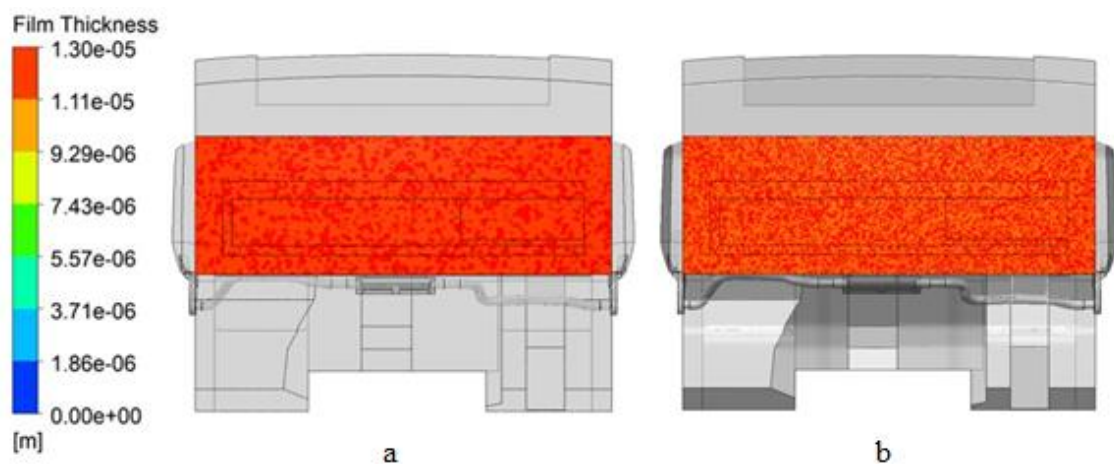


Figure 57. Comparison of Results (a. Current Model; b. Optimized Model) (t: 0 s)

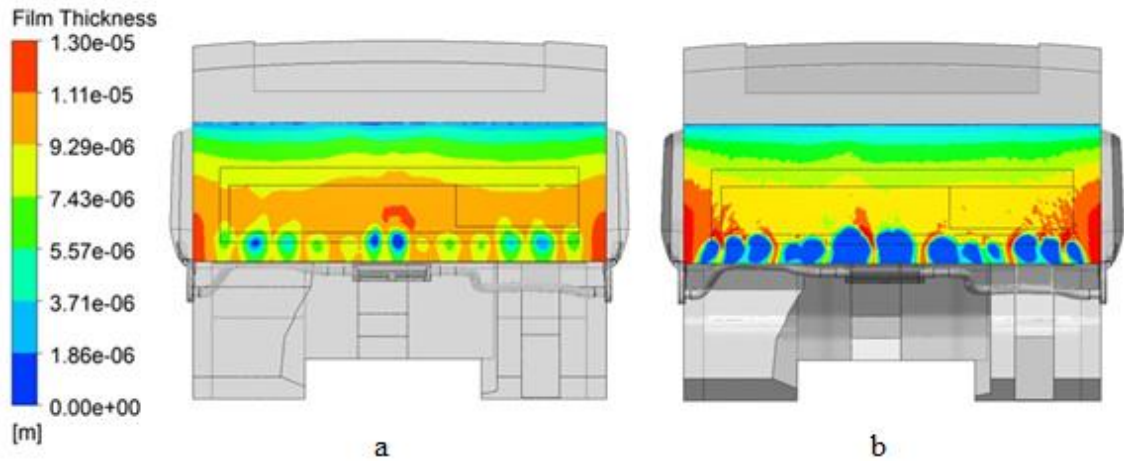


Figure 58. Comparison of Results (a. Current Model; b. Optimized Model) (t: 300 s)

Continuing the temporal analysis, Figure 59 portrays the conditions at time t: 600 s for both the current model and the optimized model. A similar trend is observed between the two models, wherein an increased degree of defogging is evident in areas housing vents at the lower extremities of the windshield.

Subsequently, Figure 60 encapsulates the status of the models at time t: 900 s. Within the optimization model, conspicuous defogging is noted in the right and left corners of the windshield.

Figure 61, representing the temporal milestone at time t: 1200 s, showcases that all segments of the windshield have achieved complete defogging in both the current model and the optimized model.

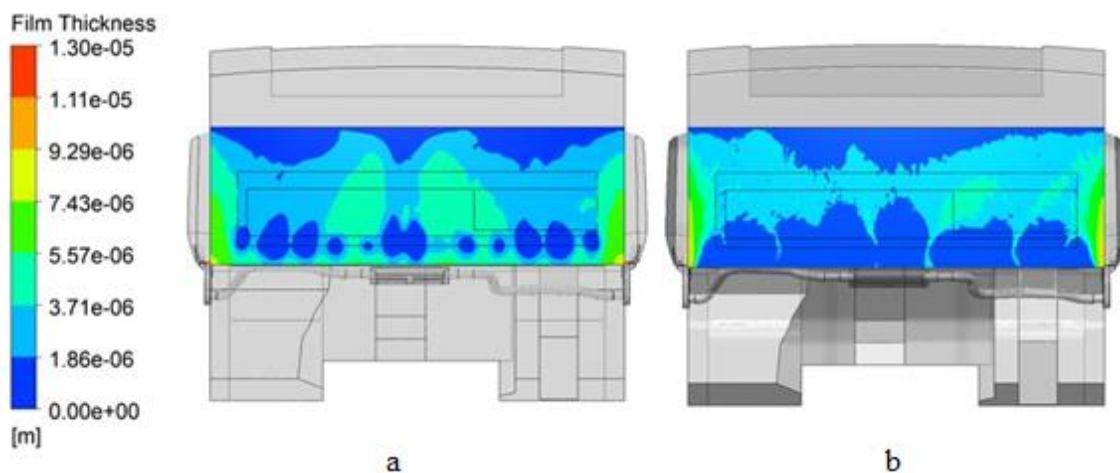


Figure 59. Comparison of Results (a. Current Model; b. Optimized Model) (t: 600 s)



Figure 60. Comparison of Results (a. Current Model; b. Optimized Model) (t: 900 s)



Figure 61. Comparison of Results (a. Current Model; b. Optimized Model) (t: 1200 s)

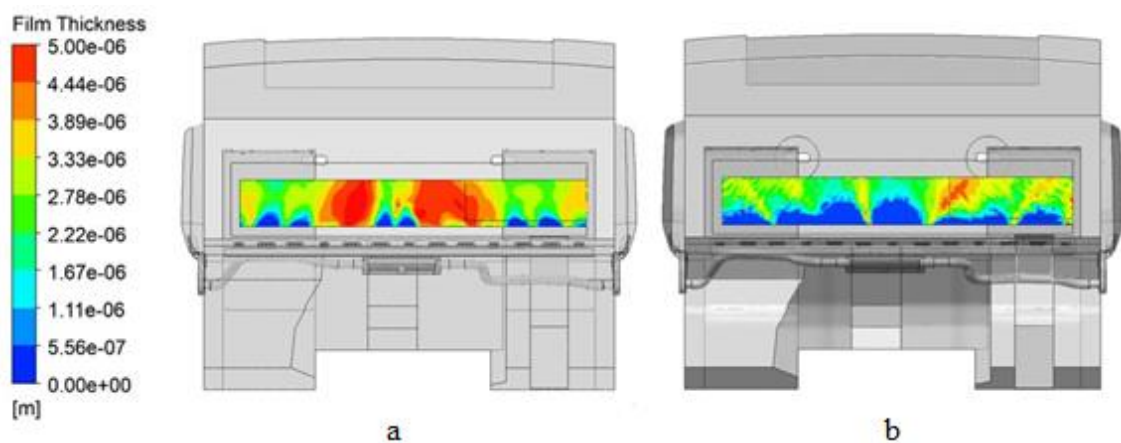


Figure 62. Comparison of Results (a. Current Model; b. Optimized Model) (t: 600 s)

Figure 62 illustrates the film thickness in the combined region A and B. The red film thickness contour obstructs the driver's view, while the areas between the blue and red contours are partially transparent, indicating that visibility begins in this zone,

although it remains somewhat unclear. In contrast, the blue film thickness contour, representing the net area, is entirely clear, ensuring clear visibility in this specific area.

Table 36. The Percentages of Defogged Area

Time	Current Model Analysis Results (Transparent + Net area)	Current Model Analysis Results (Net area)	Optimized Model Analysis Results (Transparent + Net area)	Optimized Model Analysis Results (Net area)
600 s	Area A 91.7% Area B 79 %	Area A 3% Area B 8%	Area A 98 % Area B 99 %	Area A 10 % Area B 30 %
1200 s	Area A 100% Area B 100%	Area A 100% Area B 100%	Area A 100% Area B 100%	Area A 100% Area B 100%

We compare the percentage of defogged area and the average film thickness of current model and optimized model at times 600 s and 1200 s in Table 36 and Table 37. We see that the average film thickness decreases by 8.2% in region Area A of the optimized model, and we see that the average film thickness decreases by 48.1% in region B of the optimized model.

Table 37. Average Film Thickness of Windshield

Time	Average Film Thickness of Windshield			
	Current Model		Optimized Model	
	Area A (m)	Area B (m)	Area A (m)	Area B (m)
600 s	$3.15942 \times 10^{-6}$	$3.35747 \times 10^{-6}$	$2.89749 \times 10^{-6}$	$1.74208 \times 10^{-6}$
1200 s	0	0	0	0



## CHAPTER 9

### CONCLUSIONS

The problems of fogging and icing on windshields pose significant challenges to both driving safety and energy consumption. It is imperative to swiftly mitigate these issues to ensure safe driving, while acknowledging that traditional defogging systems can incur higher energy consumption. This study was undertaken with the overarching goal of enhancing the truck windshield defogging system's efficiency and simultaneously reducing energy consumption.

In pursuit of this objective, we employed a comprehensive approach that involved 3D modeling of the vehicle and rigorous validation through empirical testing. Our investigation was multi-faceted, commencing with a detailed exploration of the influence of vent position and width in relation to the glass. To expedite the assessment of vent adjustments, we initiated our analysis in a 2D setting on the truck's xz plane, and subsequently extended our study to a 3D duct model with modified parameters.

Notably, the results from both phases unequivocally revealed that independent variables wielded a statistically significant impact on the dependent variables. Through the application of the Analysis of Variance method, we identified the parameters with the highest desirability values, enabling us to make informed adjustments.

Moreover, our study encompassed the integration of various separators into the duct model, thereby facilitating an exploration of the total mass flow rate directed towards the driver's side and the associated total pressure drop. These intricate investigations were crucial in shedding light on the holistic performance of the defogging system.

In addressing the modeling of the defogging phenomenon on windshields, we adopted the Eulerian Wall Film (EWF) Model. This approach treated the wall film as a distinct fluid phase, allowing us to independently solve the conservation equations for mass, momentum, and energy for each fluid phase. Such an approach provided a comprehensive perspective on the intricate processes at play during defogging.

As a result of our rigorous research and analysis, we were able to apply the acquired data to the existing design. The direct comparison of windshield film thicknesses between the current model and our optimization model, conducted over time, revealed



substantial improvements in defogging performance. Region A witnessed an 8.2% reduction in the average film thickness, while region B displayed a remarkable 48.1% decrease.

In summation, this study not only contributes to the advancement of truck windshield defogging systems but also underscores the potential for substantial energy conservation. Our findings hold the promise of safer and more energy-efficient driving experiences, underscoring the importance of continuous research and innovation in addressing critical issues affecting the automotive industry. This research paves the way for future studies and practical applications in the realm of vehicle safety and energy efficiency.

## APENDIX A

Calculate the vapor mass fraction from relative humidity

Inlet Conditions:

P inlet = 101325 Pa, T inlet = 288 K and RH = 40 %

Equation 28 shows that August–Roche–Magnus formula.

$$P_{sat}(kPa) = 0.61094 \times \exp\left(\frac{17.625T(^{\circ}C)}{T(^{\circ}C) + 243.04}\right) \quad (28)$$

P sat = 1701.98 Pa

Equation 29 shows that partial pressure of water vapor at inlet conditions.

$$P_{vap} = RH \times P_{sat} \quad (29)$$

P vapor = 680.792 Pa

Equation 30 shows that partial pressure of dry air.

$$P_{air} = P_{inlet} - P_{sat} \quad (30)$$

P air = 99623.02 Pa

Equation 31 shows that specific humidity.

$$w = \frac{M_{water}}{M_{air}} \left(\frac{P_{vap}}{P_{air}}\right) \quad (31)$$

Water (H<sub>2</sub>O): Molar mass = (2 × atomic mass of H) + atomic mass of O)

= (2 × 1.008 g/mol) + 15.999 g/mol

M water = 18.015 g/mol

Nitrogen (N<sub>2</sub>): Molar mass = 28.0134 g/mol, Mole fraction = 0.7808

Oxygen (O<sub>2</sub>): Molar mass = 31.9988 g/mol, Mole fraction = 0.2095

Carbon Dioxide (CO<sub>2</sub>): Molar mass = 44.01 g/mol, Mole fraction = 0.0004

M air = (28.0134 × 0.7808) + (31.9988 × 0.2095) + (44.01 × 0.0004)

$M_{air} \approx 28.965 \text{ g/mol}$

$w = 0.00425 \text{ kg moisture/ kg dry air}$

Equation 32 shows that vapor mass fraction.

$$Y_{vapor} = \frac{w}{1 + w} \quad (32)$$

$Y_{vapor} \approx 0.0042$

Second Option: We can easily determine the specific humidity using a psychrometric chart.

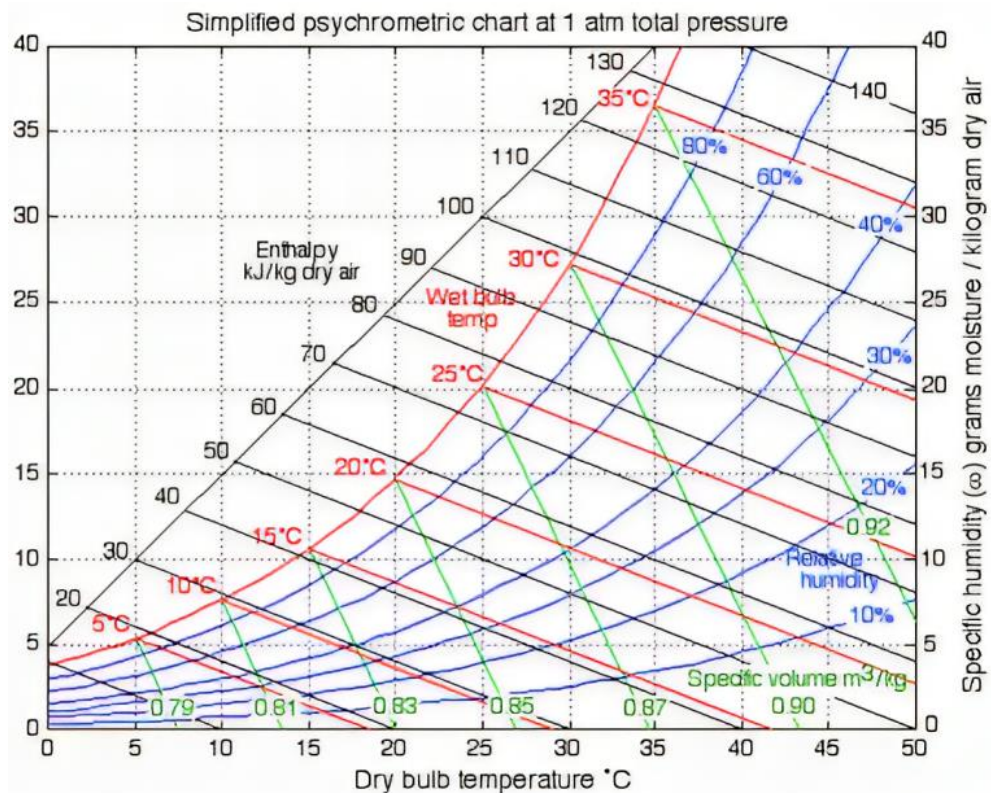


Figure 63. Psychometrics chart Source: (Shamshiri 2014)

$w \approx 4 \text{ g moisture/ kg dry air} \approx 0.004 \text{ kg moisture/ kg dry air}$

Use the Equation 32 for vapor mass fraction

$Y_{vapor} \approx 0.0042$

Note:

$T_{initial} = 270 \text{ K}$  and  $RH = 50 \%$

$Y_{vapor} \approx 0.0015$

## REFERENCES

- 78/317/EEC. 1978. "On the approximation of the laws of the member states relating to the defrosting and demisting systems of glazed surfaces of motor vehicles, Council Directive 78/317/EEC of 21 December 1977." *Official Journal L* 081: 27-48.
- A.Bhatia. 2023. "HVAC System for Cars and Automotive Vehicles." *Continuing Education and Development, Inc (CED Engineering)*. Continuing Education and Development, Inc. <https://www.cedengineering.com/>.
- ANSYS Inc. 2011. *ANSYS FLUENT User Guide-Theory Guide*. Release 14. Canonsburg, PA, November.
- ANSYS Inc. 2013. *Tutorial: Windshield Defogging Analysis Using EWF Model*. May 16.
- Ariyaratne, W.K. Hiromi, E.V.P.J. Manjula, Chandana Ratnayake, and Morten C. Melaaen. 2016. "CFD Approaches for Modeling Gas-Solids Multiphase Flows – A Review." *The 9th EUROSIM & the 57th SIMS 682 September 12th-16th*. IEEE (Institute of Electrical and Electronics Engineers). 629 - 634. doi:10.3384/ecp17142680.
- ASHRAE® HANDBOOK. 2008. *Heating, Ventilating, and Air-Conditioning Systems And Equipment*. American Society of Heating, Refrigerating and Air-Conditioning Engineers, Inc.
- Chen, Xizhong, and Junwu Wang. 2014. "A comparison of two-fluid model, dense discrete particle model and CFD-DEM method for modeling impinging gas-solid flows." *Powder Technology* 254: 94–102. doi:10.1016/j.powtec.2013.12.056.
- Davis, L. I., G. A. Dage, and J. D. Hoeschele. 2001. "Conditions for Incipient Windshield Fogging and Anti-Fog Strategy for Automatic Climate Control." *SAE Transactions* (SAE International) 110: 537–45. doi:10.4271/2001-01-0583.
- Du, Xuzhi, Zhigang Yang, Hua Zhou, Qiliang Li, and Zheyang Jin. 2016. "Numerical Investigation of Geometry Effects on Flow Heat Transfer and Defrosting Characteristics of a Simplified Automobile Windshield with a Single Row of Impinging Jets." *SAE Technical Paper 2016-01-0208* 15. doi:10.4271/2016-01-0208.
- Ene, A, and C Teodosiu. 2021. "Studies dealing with defogging and de-icing phenomena on vehicles' windshield: a review." *The 7th Conference of the Sustainable Solutions for Energy and Environment*. Bucharest: IOP Conference Series: Earth and Environmental Science. doi:10.1088/1755-1315/664/1/012071.
- Fojtlína, Miloš, Michal Planka, Jan Fišer, Jan Pokorný, and Miroslav Jicha. 2016. "Airflow Measurement of the Car HVAC Unit Using Hot-wire Anemometry." *EPJ Web of Conferences*. Czech Republic: EFM15 – Experimental Fluid Mechanics 2015. 6. doi:10.1051/epjconf/201611402023.

- Ghani, A.G. Abdul, and M.M. Farid. 2006. "Using the computational fluid dynamics to analyze the thermal sterilization of solid–liquid food mixture in cans." *Innovative Food Science & Emerging Technologies* 7 (1-2): 55-61. doi:10.1016/j.ifset.2004.07.006.
- Goreham, John. 2020. *Traveling Safely In a Shared Vehicle During COVID-19 - Be Certain You Know What the Recirculation Button Does*. March 19. <https://www.torquenews.com/1083/traveling-safely-shared-vehicle-during-covid-19-be-certain-you-know-what-recirculation-button-does>.
- Guzej, Michal, and Martin Zachar. 2019. "CFD Simulation of Defogging Effectivity in Automotive Headlamp." *Energies* 12 (13). doi:10.3390/en12132609.
- Hassan, Moulay Bel, Christophe Petitjean, Jean C. Deffieux, and Philippe Gilotte. 1999. "Windshield Defogging Simulation with Comparison to Test Data." *SAE Technical Paper* 10. doi:10.4271/1999-01-1202.
- He, Zhilong, Xide Qu, Lantian Ji, Weifeng wu, and Xiaolin Wang. 2020. "Analysis and Optimization of Truck Windshield Defroster." *Applied Sciences* 10 (16): 5671. doi:10. 5671.10.3390/app10165671.
- Hermes, Christian J. L., Joel Boeng, Diogo Londero da Silva, Fernando T. Knabben, and Andrew D. Sommers. 2021. "Evaporator Frosting in Refrigerating Appliances: Fundamentals and Applications." *Energies* 14 (18): 5991. doi:10.3390/en14185991.
- Ko, Yohan, Chanyong Lee, Youbin Kim, Yechan Kim, Yong Ju Yun, and Yongseok Jun. 2018. "Dew point temperature as an invariant replacement for relative humidity for advanced perovskite solar cell fabrication systems." *Journal of Materials Chemistry A* (Royal Society of Chemistry ) (42): 6. doi:10.1039/c8ta06689b.
- Leasca, Stacey. 2022. "This Often-overlooked Button in Your Car Can Make Your Ride More Comfortable and Help You Save on Gas." *Traveland+Leisure*. 4 21. <https://www.travelandleisure.com/travel-tips/air-recirculation-button-in-car>.
- Link, Krystian J., and Nicholas A Pohlman. 2018. "CFD Windshield Deicing Simulations for Commercial Vehicle Applications." *SAE Int. J. Commer. Veh* 11 (1): 17-30. doi:11. 10.4271/02-11-01-0002.
- Mao, Hui, Zhengsong Qiu, Binqiang Xie, Zaiming Wang, Zhonghou Shen, and Weichao Hou. 2016. "Development and Application of Ultra-High Temperature Drilling Fluids in Offshore Oilfield Around Bohai Sea Bay Basin, China." *Paper presented at the Offshore Technology Conference Asia*. Kuala Lumpur. Accessed March 2016. doi:10.4043/26384-MS.
- Matthias, Müller Fischer, Pauly Mark, Gross Markus, Keiser Richard, and Wicke Martin. 2007. "Physics-Based Animation." Chap. 7 in *Point-Based Graphics*, edited by Hanspeter Pfister Markus Gross, 340-387. doi:10.1016/B978-012370604-1/50008-0.
- Michal, Guzej, and Martin Zachar. 2019. "CFD Simulation of Defogging Effectivity in Automotive Headlamp." *Energies* 12 (13): 2609. doi:10.3390/en12132609.

- Mulbah, Christian, Can Kang, Ning Mao, Wei Zhang, Ali Raza Shaikh, and Shuang Teng. 2022. "A review of VOF methods for simulating bubble dynamics." *Progress in Nuclear Energy (Progress in Nuclear Energy)* 154 (104478). doi:10.1016/j.pnucene.2022.104478.
- Nagano, Hideaki, Kenji Tomita, Yasuhiro Tanoue, Yuji Kobayashi, Itsuhei Kohri, and Shinsuke Kato. 2016. "Analysis of Defogging Pattern on Windshield and Ventilation Load Reduction based on Humidity Distribution Control." *SAE Technical Paper* 6. doi:10.4271/2016-01-0256.
- Nasr, Karim J., ve Bashar S. AbdulNour. 2000. «Defrosting of automotive windshields: progress and challenges.» *Int. J. of Vehicle Design* 23: 360-375. doi:10.1504/IJVD.2000.001901.
- Ono, Taro, Hideaki Nagano, Suguru Shiratori, Kenjiro Shimano, and Shinsuke Kato. 2019. "Analysis of Defogging Performance, Thermal Comfort, and Energy Saving for HVAC System Optimization in Passenger Vehicles." *E3S Web of Conferences* 111: 01033. doi:10.1051/e3sconf/201911101033.
- Panton, Ronald L. 2013. *Incompressible Flow*. New Jersey: John Wiley & Sons, Inc.
- Pinnacle Auto Glass. 2023. *Heated Windshield Replacement - What You Need to Know*. <https://www.pinnacleautoglass.com/heated-windshield.html>.
- Qiu, Gang, Sascha Henke, and Jürgen Grab. 2011. "Application of a Coupled Eulerian–Lagrangian approach on geomechanical problems involving large deformations." *Computers and Geotechnics* 38 (1): 30-39. doi:10.1016/j.compgeo.2010.09.002.
- Sadananda, Thejeshwar. 2016. "Improving the Accuracy of CFD Method for Windscreen Deicing." *Division of Fluid Dynamics*. Göteborg: Chalmers University of Technology.
- SAE J381. 2000. "Surface vehicle recommended practice, windshield defrosting systems test procedure and performance requirements, trucks, buses and multipurpose vehicles."
- SAE Standard J902A. 1967. "SAE J902A: Passenger Car Windshield Defrosting Systems."
- Santos, Rodrigo Borges, João Paulo Sabioni, César Abrahão Pereira Melo, and Alexandre Carlos Ramos. 2014. "Analysis of Vibro-Acoustic Propagation Generated by an Automotive Refrigeration System." *SAE Brasil International Noise and Vibration Colloquium 2014*. doi:10.4271/2014-36-0773.
- Schmidt, Jan-Simon, and Rainard Osebold. 2017. "Environmental management systems as a driver for sustainability: state of implementation, benefits and barriers in German construction companies." *Journal of Civil Engineering and Management* 150-162. doi:10.3846/13923730.2014.946441.
- Shamshiri, Redmond R. 2014. "A lecture note on Ideal levels of Vapor Pressure Deficit in Greenhouse Production." doi:10.13140/RG.2.1.2422.0566.



- Sjodin, Bjorn. 2016. "What's The Difference Between FEM, FDM, and FVM?" *Machine Design Web site*. April 18. <https://www.machinedesign.com/3d-printing-cad/fea-and-simulation/article/21832072/whats-the-difference-between-fem-fdm-and-fvm>.
- Stat-Ease. 2023. *Two-Level Factorial*. <https://www.statease.com>.
- TestingAutos. 2020. *Car heating system: how it works*. March 15. [https://www.testingautos.com/car\\_care/car-heating-system.html](https://www.testingautos.com/car_care/car-heating-system.html).
- Unverdi, alih Ozen, Hayri Eren, Vadi Erdem, Nilgun Sonmez, Alper Emre, and Volkan Bayraktar. 2010. "Technical note: Optimisation of the defroster ducts and windshield electric resistances of a city bus with CFD analysis." *International Journal of Vehicle Design* (INT J VEH DES.) 52. doi:10.1504/IJVD.2010.029644.
- Yin, Shangyi, Wenqi Zhong, Baosheng Jin, and Jianren Fan. 2014. "Modeling on the hydrodynamics of pressurized high-flux circulating fluidized beds (PHFCFBs) by Eulerian–Lagrangian approach." *Powder Technology* 259: 52–64. doi:10.1016/j.powtec.2014.03.059.
- Zhang, Elaine, Xingying Lan, and Jinsen Gao. 2012. "Modeling of gas-solid flow in a CFB riser based on computational particle fluid dynamics." *Petroleum Science* 9: 535-543. doi:10.1007/s12182-012-0240-7.
- Zolet, T. Luis, G. Fonseca de Freitas Maia, G. Gusmao Dutra, and L. Vinicius Mendes Pereira. 2010. "CFD Methodology to Correlate the Defrost Flow and Passenger Car's Windshield Defogging." *SAE Technical Paper 2010-36-0335*. 11. doi:10.4271/2010-36-0335.